Development of Biomaterials for Chimeric Antigen Receptor (CAR) T Cell Therapy

Brynn Riann Olden

A dissertation

submitted in partial fulfillment of the

requirements for the degree of

Doctor of Philosophy

University of Washington

2018

Reading Committee:

Suzie H. Pun, Chair

Hao Yuan Kueh

Wayne R. Gombotz

Program Authorized to Offer Degree:

Bioengineering

University of Washington

Abstract

Development of Biomaterials for
Chimeric Antigen Receptor (CAR) T Cell Therapy

Brynn Riann Olden

Chair of the Supervisory Committee:

Suzie H. Pun

Department of Bioengineering

Chimeric antigen receptor (CAR) T cell therapy has emerged as an effective new cancer treatment that genetically reprograms a patient's T cells to recognize an epitope specifically expressed on the surface of cancer cells and trigger cytotoxic action against those cancer cells. This therapy has been especially effective in the treatment of $CD19^+$ hematologic malignancies. However, the manufacturing of these autologous cell therapies requires laborious processing steps that present multiple challenges and opportunities for innovation, described in Chapter 1. The current manufacturing system requires extensive use of biologic reagents including antibody-coated magnetic beads for manipulation and expansion, and retroviruses for genetic modification of *ex vivo* cultured T cells. In this work, three classes of synthetic biomaterials are developed to improve and study the *ex vivo* expansion and genetic modification of primary human T cells. In Chapter 2, we describe the development of cell-templated supported lipid

bilayers as a platform for studying the effect of activation particle design on polyclonal T cell expansion and differentiation. Chapter 3 describes work towards identifying synthetic peptide and aptamer targeting ligands for T cell activation through library screening techniques. In Chapters 4 and 5, we report the use of cationic polymers of defined architecture for non-viral gene delivery to T cells and study the underlying barriers to improved gene delivery in T cells. The major findings from this work are summarized in Chapter 6 where we also make recommendations for future applications and directions of this work.

TABLE OF CONTENTS

LIST OF FIGURES

LIST OF TABLES

ACKNOWLEDGEMENTS

Completing my PhD has been one of the most challenging and rewarding pursuits of my life. It truly takes a village of support to achieve this milestone. I have the best village of family, friends, mentors, co-workers, and collaborators who made this thesis possible.

I would like to begin by thanking my advisor, Suzie Pun, for her endless support and encouragement throughout my five years in her research group. Throughout my PhD, Suzie has matched her mentoring style to foster my growth: encouraging when experiments didn't work, generous with her time when I had questions, selfless in allowing me to pursue career development opportunities, challenging when I needed someone to question my assumptions, and hands-off when I finally knew what I was doing. She truly epitomizes a superb graduate mentor.

I also want to thank my committee members, Hao Yuan Kueh, Michael Jensen, Wayne Gombotz, and James Carothers, whose genuine interest, enthusiasm, and expertise contributed greatly to this research.

The Jensen lab has been an instrumental collaborator to my work and understanding of T cells. I want to specifically thank Dr. Joshua Gustaftson who was generous with his time and resources to aid in many of the studies presented in this thesis.

The Pun lab has been a phenomenal place to work, in large part due to the people who contributed both scientifically and personally to my development in graduate school:

- Maryelise Cieslewicz: As a senior graduate student and my rotation mentor, you taught me most of the lab techniques I know. Thank you for your encouragement when I was in way over my head and for becoming a true friend and confidant.
- Yilong Cheng: As a highly talented polymer chemist, you contributed significantly to this work through your creative and innovative polymer systems.
- Nataly Kacherovsky: Thank you for your patience and perseverance in teaching me and many other graduate students molecular biology techniques and SELEX, you truly have magical hands.
- Heather Gustafson: Your enthusiasm for science is contagious, and your creativity and expertise contributed greatly to this work. Thank you for always making time to talk science and life with me.

- Bob Lamm & Gary Liu: The statement I made during our first year of graduate school remains true: I could not have chosen better guys to do science with. Going through graduate school together has made all the difference. Thank you for encouraging me when imposter syndrome flared up, dancing to "Shake it Off" in lab when science wasn't going our way, being "good little spoons" at Kate's Pub trivia night, and drinking so much bubble tea at our "engineering meetings". Graduate school wasn't always easy, but it was made much more enjoyable by your friendship.
- David Peeler: I am so glad we shared an office and a love for all things PNW. Your passion and perseverance for research and adventure is inspiring, thanks for sharing it with me.
- The rest of the Punions (Albert Yen, Meilyn Sylvestre, Ian Cardle, Alex Prossnitz, Emmeline Cheng, Dan Lee, and Audrey Olshefsky): Thank you for your eagerness to learn, asking good questions, and your dedication to cultivating a positive and supportive work environment. I know I am leaving the lab in capable and caring hands.
- Emi Lutz and Caleb Perez, my undergraduate mentees: Thank you for your hard work and dedication to balancing high-caliber research with your demanding school work, you both contributed significantly to this work. I am proud of the scientists you have become and know you will continue to do great things as you advance in your careers.

I would like to thank my many friends who made these last five years in Seattle so much fun. Thank you to "You Shall Not Pass" volleyball team members past and present who made sure I exercised at least once a week and always exhibited exemplary teamsmanship. Thank you to my large family of friends at Bethany Ballard Community Church who always had an encouraging word for me and wisdom to help me see the big picture.

I would especially like to thank my family. My parents Jim and Marcia Livesay have been so supportive of my academic pursuits, making sure I knew I was loved and supported through each stage of my education. Thank you for raising me to be a strong, independent, and compassionate woman. You, as well as the rest of my extended family in Oregon, made sure I knew I had a large cheering squad in my corner that made the impossible feel possible.

Finally, I would like to thank my husband, Jeff Olden, for his love and support. You have done a fantastic job of encouraging me to work hard while also reminding me to take time to enjoy life. I'm excited to see where the next chapter in life takes us!

DEDICATION

To my mom, Marcia, and my father-in-law, Carl:
the cancer fighting warriors who encourage and inspire me to do this work.

Chapter 1. BACKGROUND AND SIGNIFICANCE

1.1 Adaptive Immune Response to Cancer

Cancer is the second leading cause of death in the United States after cardiovascular disease.[1] Traditional approaches to cancer treatment try to specifically eliminate cancer cells without harming healthy tissue either through surgery, chemotherapy drugs and radiation that target rapidly dividing cells, and targeted therapies that rely on a genetic or hormonal difference in cancer cells. However, these treatments do not have the same elegant specificity that our immune system has against foreign pathogens. In the last decade, it has been demonstrated that there are effective ways to engage the immune system in the clearance of cancer that lead to a more persistent anti-cancer response.[2]

The adaptive immune system plays an active role in cancer detection, elimination, but also progression. The interactions between tumor cells and the immune system can generally be described in three phases: elimination, equilibrium, and escape (Figure 1.1).[3] In the elimination phase, cancer cells are recognized by the immune system and eliminated. However, in the equilibrium phase cancer cells undergo mutations that aid in survival by evading the immune system. In the last phase of escape, cancer cells actively evade the immune system by expressing immunosuppressive receptors like PDL-1, and recruiting inhibitory cell populations like regulatory T cells, and tumor associated macrophages.[4,5]

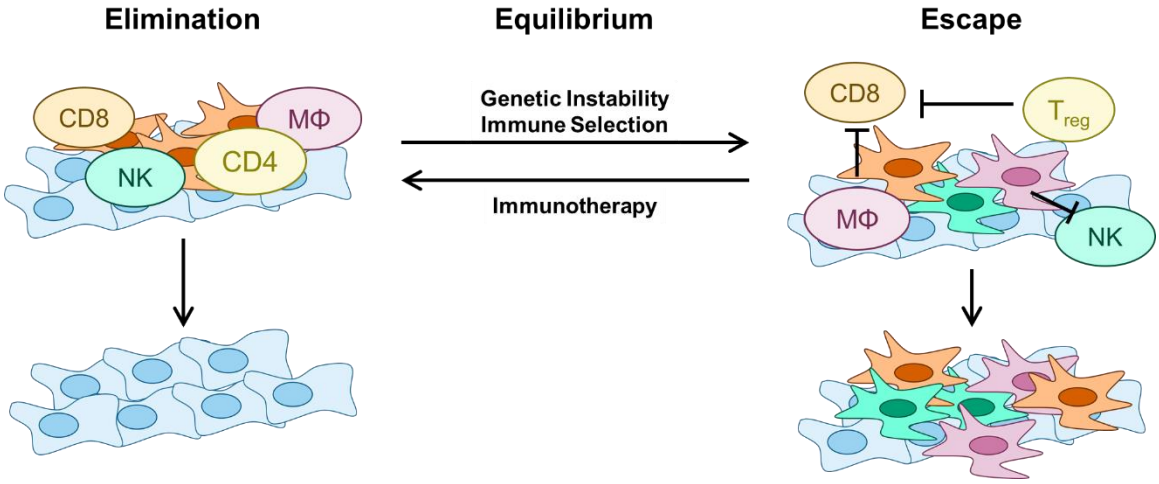

Figure 1.1. Three phases of cancer immunoediting.

As our understanding of the immune system has improved, cancer immunotherapies have been developed that aim to push the immune system back towards the Elimination phase.[2] Immune checkpoint inhibitors are monoclonal antibodies that block the binding sites of CTLA-4 and PD-1 on T cells, preventing T cell exhaustion or anergy in the tumor microenvironment.[6] Naked antibodies and antibody-drug-conjugates promote antibody-dependent cell-mediated cytotoxicity of cancer cells and deliver cytotoxic drugs intracellularly.[7,8] Building off the success of bone marrow and stem cell transplants for many blood cancers, treatments have been developed that specifically expand or genetically modify the immune cells responsible for mounting an attack on cancer.[9,10]

1.2 Chimeric Antigen Receptor (CAR) T Cell Immunotherapy

One such cellular therapy relies on genetically reprogramming T cells with a receptor that recognizes a surface epitope differentially expressed on cancer cells and triggers cancer cell killing (Figure 1.2). These chimeric antigen receptor (CAR) proteins contain an extracellular component comprised of a single-chain variable fragment (scFv) region derived from an antibody connected to a linker, transmembrane, and intracellular signaling units. The signaling unit contains the stimulatory zeta chain of the native t cell receptor (TCR) and a costimulatory domain from either CD28, 4-1BB, or both.

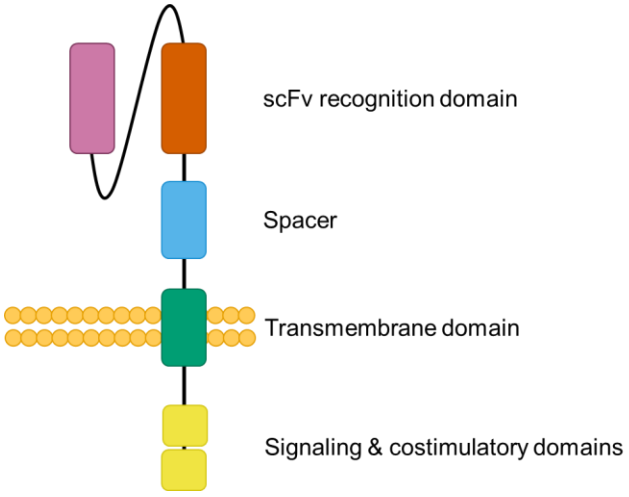

Figure 1.2. Chimeric Antigen Receptor (CAR) Design. The extracellular portion is comprised of a single-chain variable fragment (scFv) for recognition and spacer to allow for target binding. The intracellular signaling domain contains the CD3ζ chain of the TCR and often costimulatory signaling domains for either CD28, 4-1BB, or both. Adapted from Cheadle et al.[11]

CAR T cells are most commonly manufactured using autologous cells collected from the cancer patient by apheresis (Figure 1.3). Generally, T cells are isolated from the bulk peripheral blood mononuclear cells by magnetic activated cell sorting. They are subsequently activated using an artificial antigen presenting cell to stimulate proliferation prior to being genetically modified to stably express the CAR protein by viral transduction or non-viral transfection. Cells are cultured with activation reagents to induce T cell growth until the clinical dose is reached. Patient cells are cryopreserved, transported, and then reinfused into the cancer patient. This process takes from 10-28 days to manufacture one patient dose.

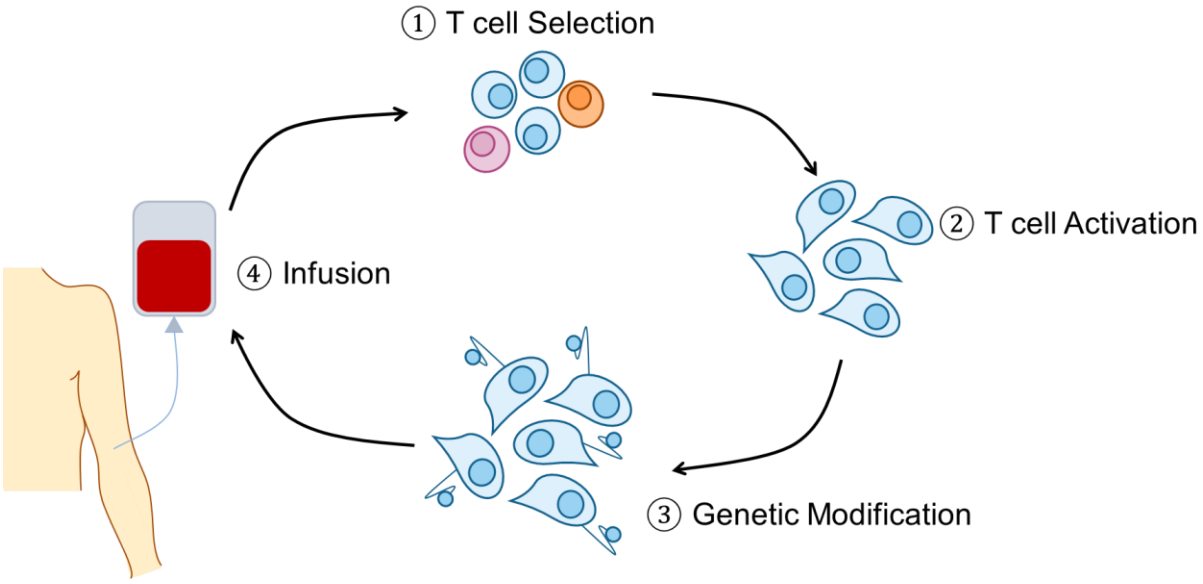

Figure 1.3. Overview of CAR T Cell Manufacturing Process. Cells are collected from the patient via apheresis. (1) T cells are selected from the bulk white blood cells. (2) T cells are activated to stimulate proliferation. (3) T cells are genetically modified to express the CAR protein. (4) CAR T cells are infused back into the patient.

Results of CAR T cell therapies have shown early success in treating hematologic cancers, with CD19-directed CARs making up the earliest clinical trials and first FDA approved CAR T cell products.[12–15] The CD19 scFv fragment allows these re-directed CAR T cells to be used in the treatment of B cell acute lymphoblastic leukemia (B-ALL), non-Hodgkin lymphoma (NHL), and chronic lymphocytic leukemia (CLL). Notably, both pediatric and adult clinical trials in B-ALL have shown impressive complete response rates of >90%.[16,17] New CAR designs are under development to treat other kinds of cancer including glioblastoma, multiple myeloma, prostate cancer, breast cancer, and lung cancer.

1.3 Opportunities for Innovation in CAR T Cell Therapy

As cellular therapy, there is a complex manufacturing process for generating CAR T cells from patient blood samples. Many of these manufacturing steps rely on special cell manipulation equipment and reagents. The current manufacturing process used for late-stage clinical trials and FDA approved products use equipment and reagents that were available "off-the-shelf" and oftentimes developed for alternative processes. While the current process works, there are many unit operations that are costly, time and labor intensive, or non-ideal solutions.

Currently, antibody-coated magnetic beads are used for both the T cell selection and activation/expansion processes. These reagents are expensive and can vary in activity lot-to-lot, due to the biological nature of antibody production. This can have a large impact on critical process steps, especially since T cell expansion is often triggered by magnetic beads coated with activating antibodies. In addition, removing these magnetic beads from cells at the end of each unit process is challenging, as antibody binding does not have a built-in release mechanism. An opportunity for innovation is to develop selection and activation reagents that are chemically well-defined and result in cells exiting the unit operation without any reagent carry-over.

The genetic reprogramming of T cells with the CAR protein is most often done using retroviral or lentiviral vectors. This often requires CAR T cell manufacturers to have a parallel processing stream for generating clinical grade viruses in-house. Lot-to-lot variability is even higher in viral products compared to antibodies and the potential for vector persistence requires adhering to strict regulatory requirements to comply with the FDA. This significantly increases the cost of CAR T cell manufacturing. An opportunity for innovation is to develop a highly efficient alternative gene delivery method that is chemically or mechanically based and does not rely on highly-regulated reagents like viruses.

1.4 REFERENCES

1. Heron, M., Ph, D., Anderson, R. N. & Ph, D. Changes in the Leading Cause of Death: Recent Patterns in Heart Disease and Cancer Mortality. *NCHS Data Brief* **254,** 1–8 (2016).
2. Ira Mellman, George Coukos, G. D. Cancer immunotherapy comes of age. *Nature* **480,** 480–489 (2011).
3. Strausberg, R. L. Tumor microenvironments, the immune system and cancer survival. *Genome Biol.* **6,** 211 (2005).
4. Gajewski, T., Meng, Y. & Harlin, H. Immune suppression in the tumor microenvironment. *J Immunother* **29,** 233–240 (2006).
5. Gallimore, A. & Godkin, A. Regulatory T cells and tumour immunity - Observations in mice and men. *Immunology* **123,** 157–163 (2008).
6. Weber, J. Immune checkpoint proteins: A new therapeutic paradigm for cancer - preclinical background: CTLA-4 and PD-1 blockade. *Semin. Oncol.* **37,** 430–439 (2010).
7. Ryan, M. C. *et al.* Antibody targeting of B-cell maturation antigen on malignant plasma cells. *Mol. Cancer Ther.* **6,** 3009–3018 (2007).
8. Tai, Y. T. *et al.* Novel anti-B-cell maturation antigen antibody-drug conjugate (GSK2857916) selectively induces killing of multiple myeloma. *Blood* **123,** 3128–3138 (2014).
9. Banchereau, J. & Palucka, A. K. Dendritic cells as therapeutic vaccines against cancer. *Nat. Rev. Immunol.* **5,** 296–306 (2005).
10. Kalos, M. *et al.* T cells with chimeric antigen receptors have potent antitumor effects and can establish memory in patients with advanced leukemia. *Sci. Transl. Med.* **3,** 95ra73 (2011).
11. Cheadle, E. J. *et al.* CAR T cells: Driving the road from the laboratory to the clinic. *Immunol. Rev.* **257,** 91–106 (2014).
12. Turtle, C. J. & Maloney, D. G. Clinical trials of CD19-targeted CAR-modified T cell therapy; a complex and varied landscape. *Expert Rev. Hematol.* **4086,** 17474086.2016.1203251 (2016).
13. Singh, H. *et al.* Manufacture of Clinical-Grade CD19-Specific T Cells Stably Expressing Chimeric Antigen Receptor Using Sleeping Beauty System and Artificial Antigen Presenting Cells. *PLoS One* **8,** 1–11 (2013).
14. Brentjens, R. J. *et al.* CD19-targeted T cells rapidly induce molecular remissions in adults with chemotherapy-refractory acute lymphoblastic leukemia. *Sci. Transl. Med.* **5,** 177ra38 (2013).
15. Davila, M. L. *et al.* Efficacy and toxicity management of 19-28z CAR T cell therapy in B cell acute lymphoblastic leukemia. *Sci. Transl. Med.* **6,** 224ra25 (2014).
16. Turtle, C. J. *et al.* CD19 CAR – T cells of defined CD4 + : CD8 + composition in adult B cell ALL patients. *J Clin Invest* **1,** 1–16 (2016).
17. Gardner, R. *et al.* CD19CAR T Cell Products of Defined CD4:CD8 Composition and Transgene Expression Show Prolonged Persistence and Durable MRD-Negative Remission in Pediatric and Young Adult B-Cell ALL. *Blood* **128,** 219 LP-219 (2016).

Chapter 2. CELL-TEMPLATED SUPPORTED LIPID BILAYERS FOR T CELL ACTIVATION

Brynn R. Olden, Caleb R. Perez, Ashley L. Wilson, Ian I. Cardle, Yu-Shen Lin, Bryan Kaehr, Joshua A. Gustafson, Michael C. Jensen, Suzie H. Pun

Abstract

Biomaterial properties that modulate T cell activation, growth, and differentiation are of significant interest in the field of cellular immunotherapy manufacturing. In this work, we develop a new platform technology that allows for the modulation of various activation particle design parameters important for polyclonal T cell activation. We successfully create artificial antigen presenting cells (aAPCs) using supported lipid bilayers on various cell-templated silica microparticles with defined membrane fluidity and stimulating antibody density. We use this panel of aAPCs to probe the importance of activation particle shape, size, membrane fluidity, and stimulation antibody density on T cell outgrowth and differentiation. All aAPC formulations were able to stimulate T cell growth, and preferentially promoted $CD8^+$ T cell growth over $CD4^+$ T cell growth when compared to commercially available pendant antibody-conjugated particles. $CD8^+$ T cells cultured with HeLa and red blood cell templated aAPCs had a less differentiated phenotype than those cultured with spherical aAPCs with matched membrane coatings when cultured for 14 days. Future work will investigate how these differences in particle shape and resulting T cell differentiation state impact cytotoxic action of chimeric antigen receptor (CAR) redirected $CD8^+$ T cells against target cancer cell lines.

2.1 INTRODUCTION

In the native immune system, naïve T cells are activated by antigen presenting cells (APCs) to elicit an adaptive immune response towards an antigen. This process requires multiple binding events, and mechanotransduction through the TCR to trigger T cell activation.[1] Synthetic *ex vivo* platforms for activation of T cells have been widely studied and developed both for basic biology understanding of T cell activation, as well as for clinical use in expanding patient T cells for various cellular therapies.[2–7] Typically, signals 1 and 2 (TCR & costimulatory receptor binding) are delivered on a solid substrate called an artificial APC (aAPC) with signal 3 provided by soluble cytokines either encapsulated in the aAPC or added to the culture medium. More recently, mesopourous silica scaffolds have been loaded with cytokines and coated with lipid membranes to result in paracrine cytokine release from the activating substrate.[7]

When activated *in vivo*, T cells form a micro-scale interaction structure with APCs called the immune synapse.[8] Quiescent TCRs reside in 15-30 nm nano-clusters, but begin to form larger clusters upon activation that reach a micron in diameter.[9] Not surprisingly, studies have shown that signaling molecules attached to planar lipid membranes with high fluidity activate T cells better than membranes with low fluidity due to the improved ability to facilitate receptor clustering.[10]

Size, shape, rigidity, and antigen density of the scaffold have independently been shown to impact T cell activation.[11] Particles with a higher aspect ratio, larger diameter, and made with softer material have all been shown to improve T cell activation and proliferation.[5,12,13] However, the relative importance of these different aAPC design parameters has not been evaluated in a comprehensive platform. This is of special interest in the context of the manufacturing of chimeric antigen receptor (CAR) T cell therapies, as T cell growth, differentiation, and function are all important parameters to control for successful *in vivo* anti-tumor efficacy.[14]

Supported lipid bilayers on cell-templated silica scaffolds is a flexible platform that allows individual control of many of these parameters including particle size & shape, membrane fluidity, and antigen density (Figure 2.1). Particle size and shape can be controlled by templating silica microparticles off of various cell suspensions that faithfully capture cell size, surface roughness, and morphology.[15,16] Membrane fluidity can be controlled by using lipids with transition temperatures (T_m) above and below physiological temperature (37 °C) in the composition of the supported lipid bilayer.[17,18]

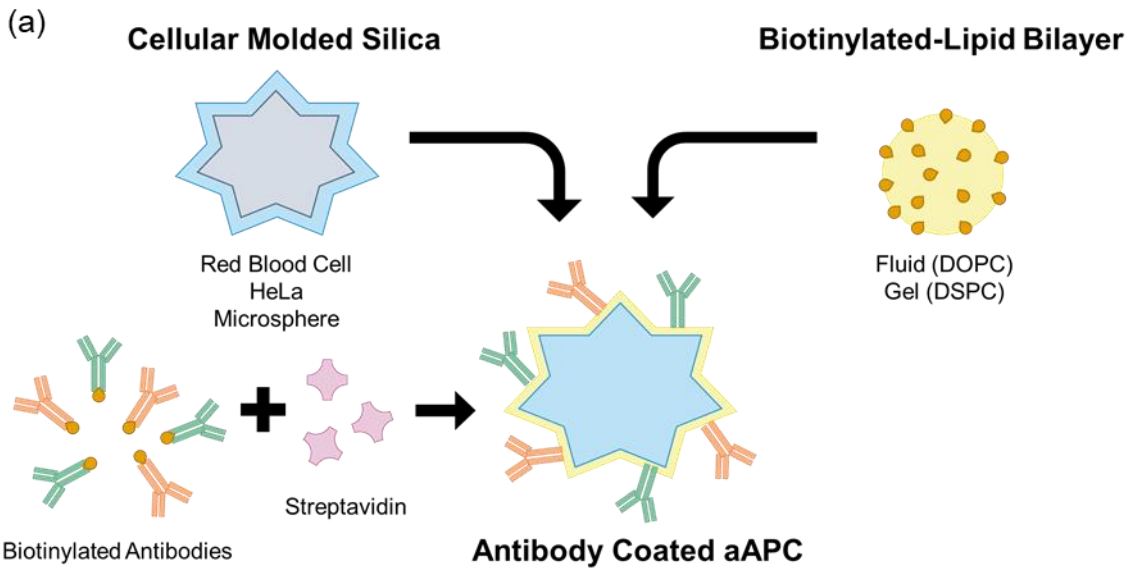

(b)

	"Fluid" DOPC			"Gel" DSPC		
Molar Loading	0.02%	0.2%	2%	0.02%	0.2%	2%
RBC (4.5 μm)						
Microsphere (8 μm)						
HeLa (16 μm)						

Figure 2.1. Platform technology for cell-templated supported lipid bilayer activation particles. (a) Schematic of aAPC synthesis and design parameters. (b) 18 particle formulations used in T cell outgrowth and differentiation studies.

In this work, we develop an artificial antigen presenting cell (aAPC) T cell activation platform to evaluate the influence of particle shape and size, membrane fluidity, and antigen density on T cell outgrowth, and differentiation (Figure 2.1 a). We successfully assemble and characterize a panel of 18 aAPCs (Figure 2.1 b) and demonstrate their ability to induce polyclonal T cell proliferation. We then use this panel of particles to probe other important parameters for T cell manufacturing: ratio of $CD4^+$ vs $CD8^+$ T cell growth, and T cell differentiation state.

2.2 MATERIALS AND METHODS

2.2.1 *Materials*

Lipids (DOPC, DSPC, cholesterol, 18:1 PEG-2000 PE, 18:0 PEG-2000 PE, and DSPE-PEG(2000) Biotin) were purchased from Avanti Polar Lipids in chloroform. Silica microspheres (6.0-8.0 μm diameter) were purchased from Spherotech.

2.2.2 *Silicified cell synthesis and characterization*

Silicified cells were prepared as described previously.[15,16] Briefly, cultured HeLa cells and red blood cells from healthy donors were fixed in 4% formaldehyde in phosphate buffered saline for 16-24 hours, rinsed in phosphate buffered saline (PBS) and 0.9% saline solution, and reacted in 0.1 M TMOS in 0.9% saline and 1.0 mM HCl (pH 3) and incubated at 37 °C for 16-24 hours. The organic templates were removed by calcination in air at 550 to 600 °C for 3-4 hours. For imaging, calcined particles were sputter-coated with gold/palladium to a thickness of ~10 nm, and imaged with an FEI XL830 dual beam focused ion beam/scanning electron microscope.

2.2.3 *Small unilamellar vesicle (SUV) formation, synthesis, and characterizatoin*

Lipid-chloroform suspensions (cholesterol, DSPE-PEG(2000)-biotin, either 18:1 PEG-2000 PE or 18:0 PEG-2000 PE, and either DOPC or DSPC) were mixed at defined compositions (Supplemental Table 2.1). Chloroform was removed by evaporation in a vacuum desiccator overnight. Dry lipid films were hydrated by addition of PBS to a concentration of 4 mg/mL. Monodisperse suspensions of SUVs were then generated from the hydrated lipid films via sonication (Branson 2800 bath sonicator). DOPC lipid films were sonicated for approximately 15 minutes in a room temperature water bath, while DSPC lipid films were sonicated for 45-60 minutes in a warm water bath. Biotinylated SUV suspensions were stored at 4 °C.

Liposomes were diluted to a final concentration of 10 μg/mL in Nanopure H_2O and dynamic light scattering (DLS) measurements were made on a Zetasizer Nano ZS (Malvern Instruments) (Supplemental Table 2.2).

2.2.4 *Supported lipid bilayer synthesis and characterization*

Dry silica RBC and HeLa microparticles were suspended in methanol and dried by SpeedVac for weighing, then subsequently mixed with the SUV suspensions at a 1:1 mass ratio. Spherical microspheres (Spherotec) were directly mixed with the SUV suspensions at a 1:1 mass ratio and

fused at room temperature for 1 hour with intermittent mixing by inversion. Excess lipids were removed by centrifugation and PBS washes (500×g for 5 minutes).

Supported lipid bilayers were characterized by fluorescent microscopy and flow cytometry. Lipid fusion was confirmed by staining with Vibrant DiD Cell-Labeling Solution (ThermoFisher) and FITC-labeled neutravidin (ThermoFisher) which was subsequently visualized by fluorescent microscopy on a Nikon Eclipse Ti inverted microscope. To quantify biotin content, supported lipid bilayers were labeled with FITC-neutravidin and the resulting fluorescence was measured on an Attune NxT Flow Cytometer (ThermoFisher).

2.2.5 *Antibody attachment and characterization*

Biotinylated human anti-CD3ε (clone: OKT3) and anti-CD28 (clone: CD28.2) antibodies (Biolegend) were conjugated to the biotinylated supported lipid bilayers via a neutravidin linker at a 1:5 anti-CD3ε-to-anti-CD28 molar ratio.[3] Briefly, each biotinylated antibody was mixed with neutravidin at a 1:1 molar ratio in separate reactions, and allowed to bind at 4 °C for 10 minutes. Neutravidin-linked antibodies were combined, briefly mixed, and then added to lipid-coated particles diluted in PBS resulting in a 41.5 nM reaction of total antibodies (6.92 nM anti-CD3ε and 34.63 nM anti-CD28). Binding occurred for 30 minutes at 4 °C. Unbound antibodies were removed by centrifugation (500×g for 5 minutes) and PBS washes. Antibody-loaded aAPCs were stored at 4 °C up to 1-2 weeks before use in T cell activation experiments. Antibody conjugation was characterized by flow cytometry and total protein quantification. Relative loading of anti-CD3ε and anti-CD28 was assessed by loading into microsphere-supported lipid bilayers, but anti-CD3ε was conjugated via a FITC-labeled neutravidin and anti-CD28 was conjugated via a DyLight 633-labeled neutravidin. The relative fluorescence of the two different neutravidin linkers was measured on an Attune NxT Flow Cytometer as the anti-CD3ε-to-anti-CD28 molar ratio was varied (0:1, 1:5, 1:1, 5:1, and 1:0).

2.2.6 *T cell isolation and culture*

Leukapheresis products were obtained from health donors (Bloodworks Northwest). Primary $CD4^+$ and $CD8^+$ T cells were isolated serially using the CliniMACS System (Miltenyi) and cryopreserved for later use in activation studies. Cells were cultured in RPMI 1640 (Corning) supplemented with 10% fetal bovine serum (FBS) (ThermoFisher), recombinant human IL-2 (50

U/mL), and recombinant human IL-15 (0.5 U/mL) (Miltenyi). Cells were maintained in a 37 °C and 5% CO_2 humidified incubator.

2.2.7 *Cell activation and analysis*

$CD4^+$ and $CD8^+$ T cells from 3 independent donors were thawed, mixed at a 1:1 ratio, and rested for 3-4 hours in basal media (RPMI supplemented with 10% FBS) before activation. 3×10^5 cells were seeded in a U-bottom 96-well plate at a density of 1.5×10^6 cells/mL. Supported lipid bilayer formulations (aAPCs) and CD3/CD28 Human T Activator Beads (DynaBeads, Gibco) were suspended in complete T cell medium and cocultured with T cells at defined aAPC-to-cell ratios based on equivalent particle surface area (1:3 microsphere-to-cell, 1:10 HeLa-to-cell, 1:1 RBC-to-cell, and 1:1 DynaBead-to-cell). For outgrowth experiments, media was exchanged for fresh cytokine-supplemented medium every 3 days following activation. On days 6, 9, 12, and 14 post-activation, all aAPC-stimulated cells were counted by hemocytometer. Cells were passaged into larger culture vessels once reaching densities of 1-1.25 $\times 10^6$/mL.

2.2.8 *Intracellular cytokine staining (ICCS)*

T cells were treated with Protein Inhibitor Cocktail (ThermoFisher) for 4 hours to block cytokine release prior to staining 3 days post-activation. Positive controls were also treated with Cell Stimulation Cocktail containing phorbol myristate acetate (PMA) and Ionomycin (ThermoFisher) for 1 hour prior to protein transport inhibition. Surface staining was performed, followed by permeabilization during fixation with Cytofix/Cytoperm solution (BD Biosciences). Permeabilized cells were then stained for intracellular markers and analyzed on a BD LSR Fortessa (Supplemental Table 2.3). Data analysis was performed using FlowJo software (FlowJo, LLC), with serial or boolean gating (Supplemental Figure 2.1).

2.2.9 *Surface marker flow cytometry analysis*

On days 9 and 14 post-activation, samples of each treatment were stained for CD4 and CD8 expression and analyzed on an Attune NxT flow cytometer (ThermoFisher) (Supplemental Table 2.4). On day 12 post-activation, samples of each treatment were stained with a differentiation panel (Supplemental Table 2.5) and analyzed on a BD LSR Fortessa. Data analysis was performed using FlowJo software (FlowJo, LLC), with serial or boolean gating (Supplemental Figure 2.2 & Supplemental Figure 2.3).

2.2.10 *Statistical analysis*

Results are presented as mean ± standard deviation (SD). All statistical analysis was performed in GraphPad Prism software (Graph Pad Software). Analysis of variance (ANOVA) was used for statistical analysis, with paired hypothesis testing to account for donor-to-donor variability. One-way ANOVA with Dunnett's multiple comparisons posthoc analysis was performed in the analysis of fold expansion and CD4-to-CD8 ratios. Two-way ANOVA with Bonferonni's multiple comparisons was performed in the analysis of T cell differentiation.

2.3 RESULTS AND DISCUSSION

2.3.1 *Cell-templated supported lipid bilayer platform for T cell activation*

We formulated aAPCs with varying physical properties (size, shape, and surface roughness), membrane fluidity, and anti-CD3/anti-CD28 densities using silica microparticles coated with a lipid bilayer following methods developed previously by Brinker and coworkers.[17,19] Roughness and shape variations were attained using silica microparticles templated from HeLa cells or human red blood cells. These microparticles were successfully synthesized using dilute silicic acid solutions and retained the expected cell morphology and size after calcination to remove the biological template (Figure 2.2 a). Commercially available spherical and smooth silica microspheres were also used; in total we formulated particles that cover a range of sizes (average diameter from 4.5 to 16 μm), sphericities (red blood cells ≈ 0.63 to microspheres ≈ 1), and surface textures.[20] Biotinylated lipid bilayers were fused on to the particle surfaces from small unilamellar vesicles (SUVs) (Supplemental Table 2.2), a method previously reported to create supported lipid bilayers on solid and mesoporous silica microspheres.[21,22]

We formulated lipid bilayers with two different lipid compositions and three different biotin loading ratios (0.02, 0.2, and 2% molar loading) to control membrane fluidity and antigen density (Supplemental Table 2.1). The lipid DOPC has a melting temperature below 37 °C (T_m= -17 °C) and is in a fluid-like state at physiological temperatures, whereas DSPC has a melting temperature above 37 °C (T_m= 55 °C) and is in a gel-like state at physiological temperatures. Previous studies have demonstrated that more fluid lipid membranes exhibit improved ligand clustering capabilities, important for early immune synapse formation.[10,23] Fluorescent microscopy images of lipid-fused microparticles stained with neutravidin-FITC and Vibrant DiD membrane dye show that all three particle shapes were successfully coated with lipids and biotin is well-dispersed

throughout the particle surface (Figure 2.2 b). Quantitative flow cytometry experiments confirm that the molar loading of biotin into the SUVs correlates to fluorescent intensity of neutravidin-FITC labeling, and that two different antibodies can be loaded at defined stoichiometric ratios (Figure 2.2 c & d).

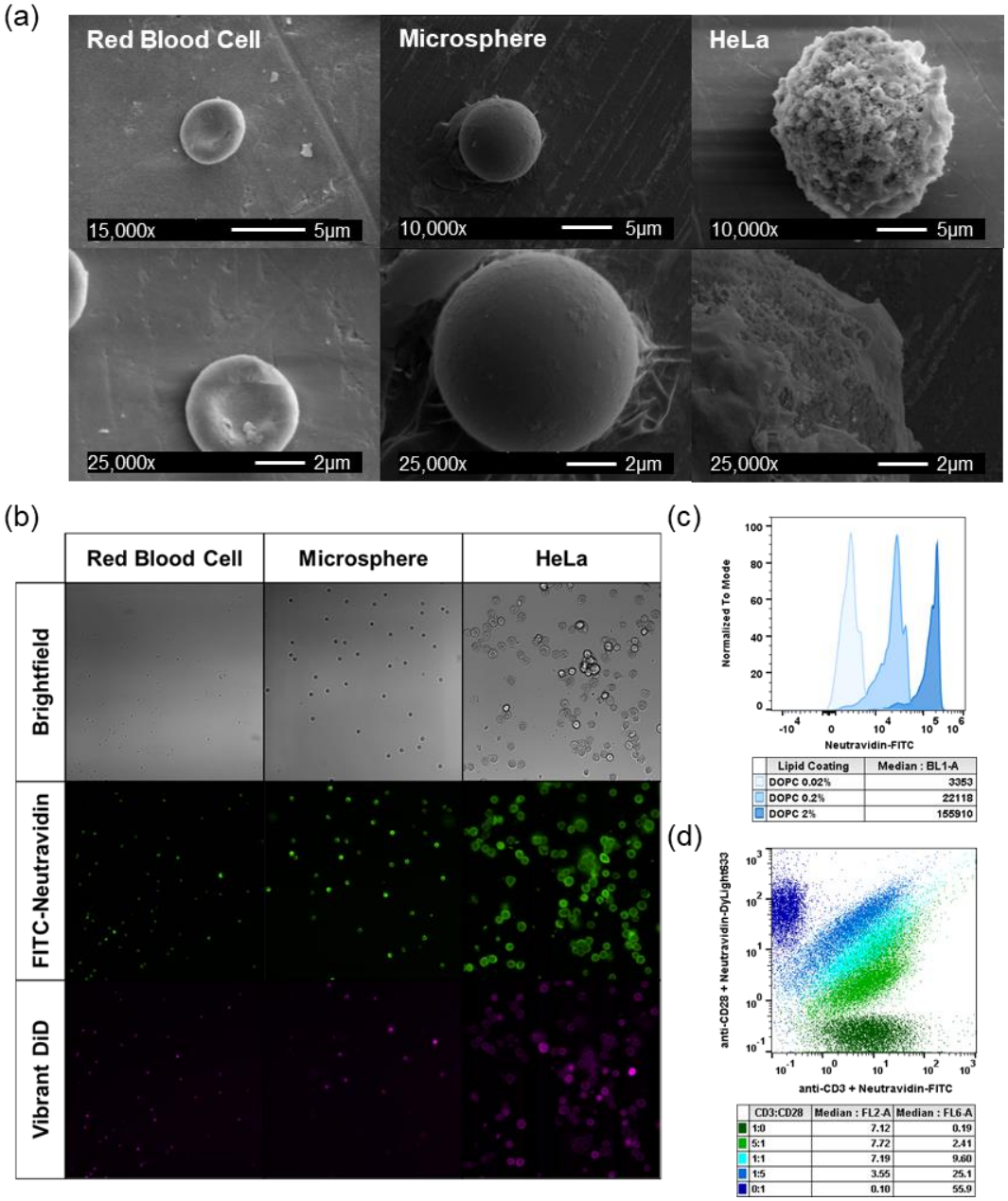

Figure 2.2. Activation particle characterization. (a) Scanning electron microscope (SEM) images of red blood cell, microsphere, and HeLa silica microparticles. (b) Fluorescent and brightfield microscope images of activation particles at 20× magnification. (c) Biotin loading on activation particles quantified by FITC-neutravidin and flow cytometry. (d) Ratiometric loading of anti-CD3ε and anti-CD28 antibodies with fluorescently labeled neutravidin and flow cytometry.

We performed an initial proof-of-concept study using microsphere supported lipid bilayers to confirm that these particles could activate primary human T cells. Cells were co-cultured with particles for 72-hours and assessed for cytokine production and expression of the activation marker 4-1BB (Figure 2.3). Uncoated microspheres and lipid-coated microspheres with no activating antibody did not elicit T cell activation or cytokine production, suggesting that the activating antibodies are the only stimulation cues in the platform. All particle formulations induced a Th1 response in T cells as expected from polyclonal T cell expansion, characterized by the expression of IFN-γ, IL-2, and TNF-α.[24] An antibody dose-dependence was observed for both 4-1BB expression and cytokine production, which was more pronounced in the DSPC lipid coated particles than the DOPC coated particles. Commercially available Human T-Activator CD3/CD28 bead (Dynabead) activated T cells had the highest 4-1BB expression and cytokine production, suggesting a rapid and robust activation. To investigate if these differences in early activation translate to differences in longer-term T cell expansion and *in vitro* differentiation, we performed 14-day outgrowth studies using all 18 aAPC formulations.

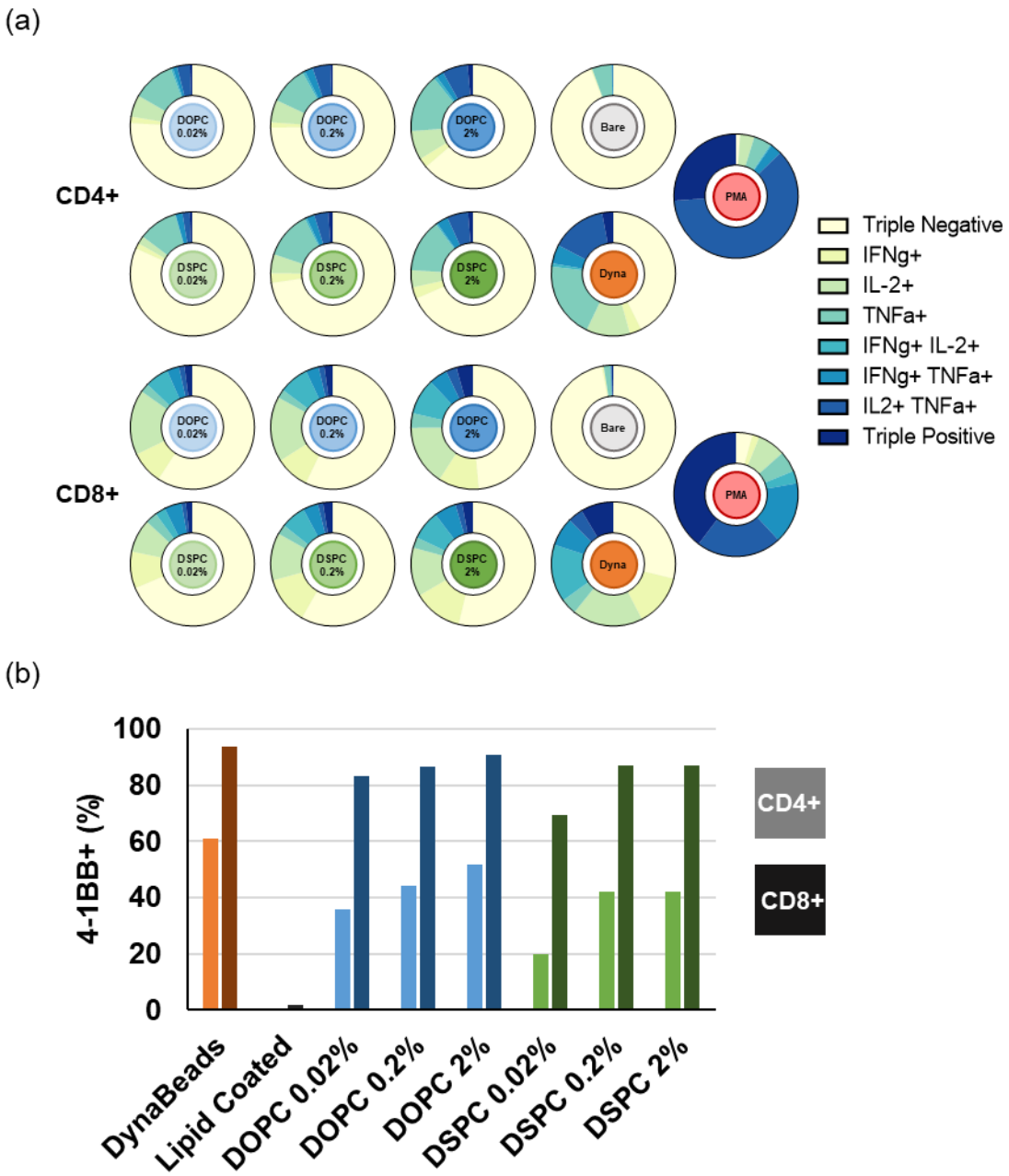

Figure 2.3. 72-hour microsphere particle activation. (a) Basal cytokine production and (b) 4-1BB expression in $CD4^+$ and $CD8^+$ T cells co-cultured with microsphere activation particles (n=1).

2.3.2 *Lipid membrane coated activation particles promote $CD8^+$ T cell growth*

All 18 aAPC formulations were tested in a 14-day polyclonal outgrowth study of healthy donor primary human T cells seeded at a 1:1 $CD4^+$:$CD8^+$ ratio. Due in part to the large donor-to-donor variability ($p < 0.0001$ for donor-to-donor residual variation), there was no significant difference

in fold expansion over 14 days between the aAPC treatment groups and DynaBead activated T cells (Figure 2.4). Qualitatively, there does seem to be a trend of greater T cell expansion at higher antigen densities (2% and 0.2%) and membrane fluidity (DOPC).

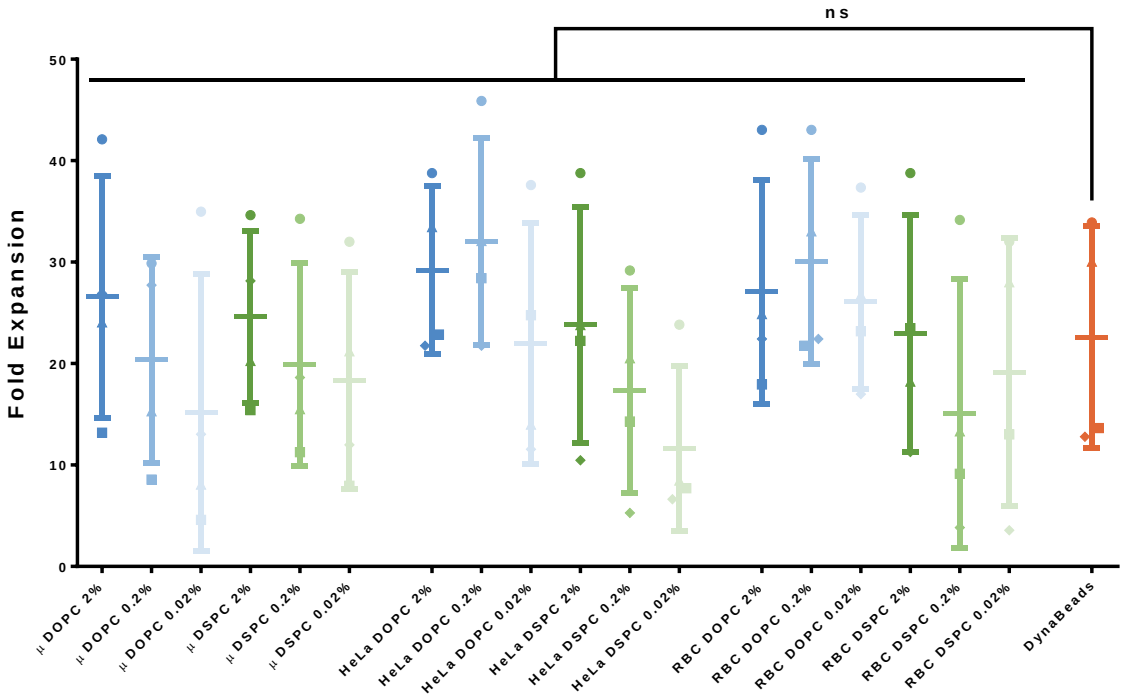

Figure 2.4. 14-day T cell outgrowth. Fold expansion of T cells co-cultured with panel of aAPCs for 14 days. Data represented as mean ± SD (n=4 biological replicates; paired one-way ANOVA with Dunnett's multiple comparisons test, ns = not significant, p=0.0648).

The outgrowth of $CD4^+$ versus $CD8^+$ T cells was monitored by flow cytometry staining on days 9 and 14 of T cell culture. On day 9, the 0.02% molar antibody loaded DSPC coated HeLa and red blood cell particle activated T cells had significantly reduced $CD4^+$ to $CD8^+$ ratio compared to DynaBeads control (Supplemental Figure 2.4). By day 14, all the lipid-coated particle treatment groups had a reduced $CD4^+$ to $CD8^+$ ratio compared to DynaBeads control, and many promoted equal growth of $CD4^+$ and $CD8^+$ T cells (Figure 2.5).

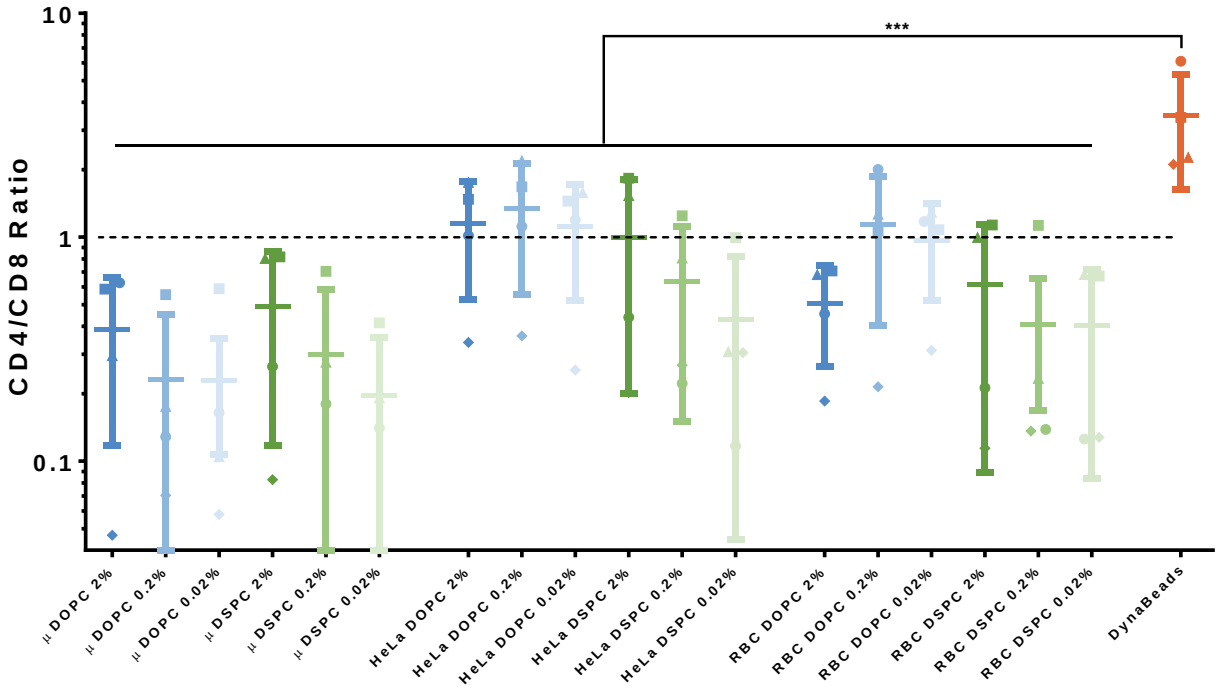

Figure 2.5. Ratio of $CD4^+$ to $CD8^+$ T cells after 14-day outgrowth. Data represented as mean ± SD (n=4 biological replicates; paired one-way ANOVA with Dunnett's multiple comparisons test, *** $p<0.001$).

The ability to control the outgrowth of specific subsets of T cells is of interest in CAR T cell manufacturing. Previous studies have shown that CAR T cell products of defined $CD4^+$:$CD8^+$ T cell ratios have better *in vivo* anti-tumor function.[25] Currently, $CD4^+$ and $CD8^+$ T cells must be expanded separately and then combined in a 1:1 ratio prior to infusion, doubling the amount of consumables and machinery required for manufacturing.[26] An activation platform that could maintain a nearly 1:1 ratio while culturing $CD4^+$ and $CD8^+$ T cells together could generate a large cost savings to CAR T cell manufacturing without compromising product quality and predictability. HeLa and red blood cell templated particles fused with 0.2% and 0.02% molar antibody loaded DOPC membranes show the most consistent equal expansion of $CD4^+$ and $CD8^+$ T cells. Additional studies with patient-derived T cells would be required to confirm that these specific aAPCs promote equal $CD4^+$ and $CD8^+$ outgrowth even from patient samples, which often have a very different T cell population than healthy subjects.

2.3.3 *Fluid lipid membranes on non-spherical support reduces T cell differentiation in culture*

In addition to $CD4^+$:$CD8^+$ T cell ratio, T cell differentiation is an important parameter that impacts *in vivo* anti-tumor function. Animal studies using CAR T cells generated from different T cell subsets show that naïve ($CD45RA^+/CD62L^+$) and central memory ($CD45RA^-/CD62L^+$) T cells have better *in vivo* efficacy than CAR T cells generated from effector memory ($CD45RA^-/CD62L^-$) T cells.[25] We were interested to see if any of our aAPCs promoted a larger population of less-differentiated cells. To test this, we stained T cells from the outgrowth studies with surface markers of T cell differentiation and exhaustion after 12 days of polyclonal expansion. There were no statistical differences in the percent of least-differentiated ($CD45RA^+/CD62L^+$) cells between aAPC treatments on $CD4^+$ T cells (Supplemental Figure 2.5). There was also no statistical difference in PD-1 expression, a marker of exhaustion in prolonged T cell growth, between the aAPC treatment groups for either $CD4^+$ or $CD8^+$ T cells (Supplemental Figure 2.6 & Supplemental Figure 2.7).

There were some interesting differences in $CD8^+$ T cell differentiation between aAPC treatment groups (Figure 2.6). Comparing between different membrane coatings on the same particle shape, reduced activating antibody density in DOPC and DSPC coated microspheres and DSPC coated HeLa particles resulted in an increase in differentiated $CD8^+$ T cell populations. None of the aAPC particles had a significantly larger population of "naïve-like" $CD45RA^+/CD62L^+$ T cells compared to DynaBeads. At two lipid coatings (0.2% and 0.02% DOPC), T cells activated with HeLa or red blood cell particles had reduced differentiation compared to microsphere particles.

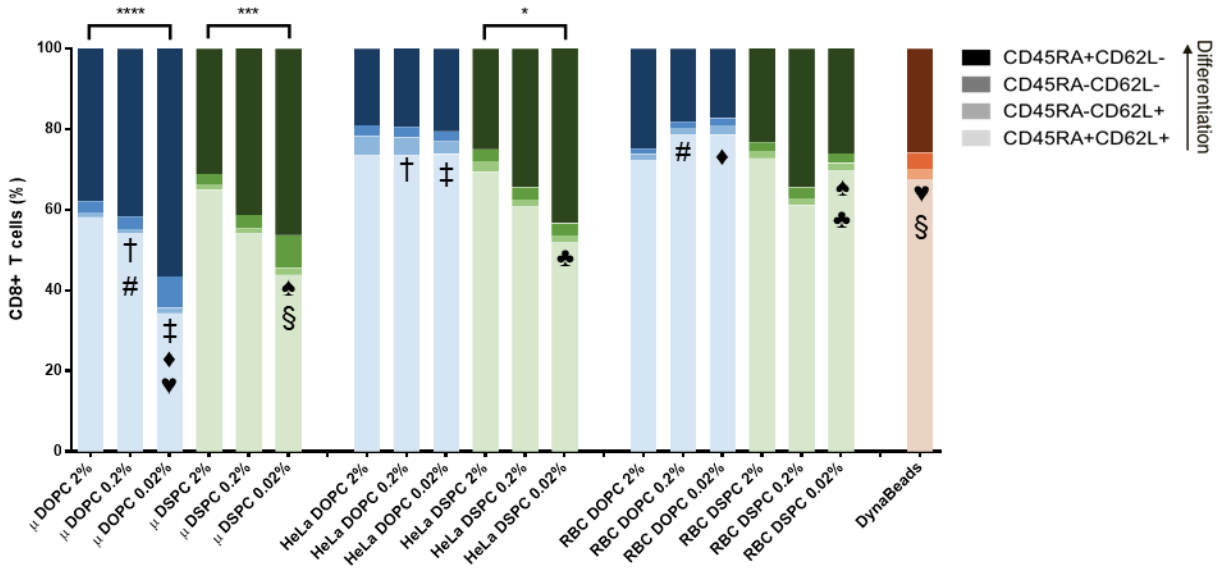

Figure 2.6. Differentiation state of $CD8^+$ T cells after 12-day outgrowth. Data represented as mean, SD omitted for legibility (n=3 biological replicates; two-way repeated measures ANOVA with Bonferroni's multiple comparisons test). Statistical significance between least-differentiated subpopulations within morphology groups are represented by brackets (* $p<0.05$, *** $p < 0.0001$, **** $p < 0.0001$). Matching symbols indicate statistical significance between least-differentiated subpopulations of treatments across different morphologies: † = μSpheres DOPC 0.2% vs. HeLa DOPC 0.2% ($p < 0.01$); # = μSpheres DOPC 0.2% vs. RBC DOPC 0.2% ($p < 0.0001$); ‡ = μSpheres DOPC 0.02% vs. HeLa DOPC 0.02% ($p < 0.0001$); ♦ = μSpheres DOPC 0.02% vs. RBC DOPC 0.02% ($p <0.0001$); ♠ = μSpheres DSPC 0.02% vs. RBC DSPC 0.02% ($p <0.0001$); ♣ = HeLa DSPC 0.02% vs. RBC DSPC 0.02% ($p <0.05$); ♥ = μSpheres DOPC 0.02% vs. DynaBeads ($p < 0.0001$); § = μSpheres DSPC 0.02% vs. DynaBeads ($p < 0.0001$).

2.4 Conclusion

Understanding how biomaterial design parameters translate to functional performance is important for the design of next-generation artificial antigen presenting cells for T cell therapy manufacturing. Specifically, in the field of CAR T cell therapies, there is specific interest in aAPCs that promote polyclonal expansion of T cells while maintaining a less-differentiated phenotype.

In this work, we develop a platform technology for evaluating aAPC design parameters. We successfully synthesized a library of 18 aAPC membrane-coated particles that vary in particle

shape and size, membrane fluidity, and activating antibody density. These particles can induce polyclonal T cell activation and proliferation, and promote $CD8^+$ T cell outgrowth compared to commercially available DynaBeads. Many of the aAPC particles with more fluid membranes (DOPC) on non-spherical supports (HeLa or red blood cell particle) promoted equal expansion of $CD4^+$ and $CD8^+$ T cells while maintaining a less-differentiated $CD8^+$ phenotype.

This platform technology allowed us to make some general observations about aAPC design parameters and how they contribute to T cell growth and differentiation. Trends in outgrowth data suggest that increased activating antibody density and membrane fluidity are more important than particle shape in promoting greater T cell expansion. Particle shape was a more important design parameter for modulating differentiation of $CD8^+$ T cells. We observed that $CD8^+$ T cells activated with non-spherical aAPCs had a less differentiated phenotype. In the future, this facile supported lipid bilayer technology platform could be expanded to evaluate a wider range of design parameters and applications including nano-sized particles, magnetic particles, and antigen-specific T cell expansion.

2.5 ACKNOWLEDGEMENTS

Part of this work was conducted at the Molecular Analysis Facility, a National Nanotechnology Coordinated Infrastructure site at the University of Washington which is supported in part by the National Science Foundation (grant ECC-1542101), the University of Washington, the Molecular Engineering & Sciences Institute, and the Clean Energy Institute. This work was supported by the National Institutes of Health [1R01CA177272, 2R01NS064404]. This work was supported by a National Science Foundation Graduate Research Fellowship to B.R.O [DGE-1256082] and a Washington Research Foundation Fellowship to C.R.P.

2.6 REFERENCES

1. Malissen, B. & Bongrand, P. Early T Cell Activation: Integrating Biochemical, Structural, and Biophysical Cues. *Annu. Rev. Immunol.* **33,** 539–561 (2015).
2. Bashour, K. T. *et al.* CD28 and CD3 have complementary roles in T-cell traction forces. *Proc. Natl. Acad. Sci. U. S. A.* **111,** 2241–6 (2014).
3. Trickett, A. & Kwan, Y. L. T cell stimulation and expansion using anti-CD3/CD28 beads. *J. Immunol. Methods* (2003). doi:10.1016/S0022-1759(03)00010-3
4. Steenblock, E. R. & Fahmy, T. M. A comprehensive platform for ex vivo T-cell expansion based on biodegradable polymeric artificial antigen-presenting cells. *Mol. Ther.* **16,** 765–72 (2008).
5. Sunshine, J. C., Perica, K., Schneck, J. P. & Green, J. J. Particle shape dependence of CD8+ T cell activation by artificial antigen presenting cells. *Biomaterials* **35,** 269–277 (2014).
6. Meyer, R. A. *et al.* Biodegradable Nanoellipsoidal Artificial Antigen Presenting Cells for Antigen Specific T-Cell Activation. *Small* **11,** 1519–1525 (2015).
7. Cheung, A. S., Zhang, D. K. Y., Koshy, S. T. & Mooney, D. J. Scaffolds that mimic antigen-presenting cells enable ex vivo expansion of primary T cells. *Nat. Biotechnol.* **36,** 160–169 (2018).
8. Martín-Cófreces, N. B., Baixauli, F. & Sánchez-Madrid, F. Immune synapse: Conductor of orchestrated organelle movement. *Trends Cell Biol.* **24,** 61–72 (2014).
9. Hu, Y. S., Cang, H. & Lillemeier, B. F. Superresolution imaging reveals nanometer- and micrometer-scale spatial distributions of T-cell receptors in lymph nodes. *Proc. Natl. Acad. Sci.* **113,** 7201–7206 (2016).
10. Hsu, C. J. *et al.* Ligand mobility modulates immunological synapse formation and T cell activation. *PLoS One* **7,** e32398 (2012).
11. Perica, K., Kosmides, A. K. & Schneck, J. P. Linking form to function: Biophysical aspects of artificial antigen presenting cell design. *Biochimica et Biophysica Acta - Molecular Cell Research* **1853,** 781–790 (2015).
12. Mescher, M. F. Surface Contact Requirements for Activation of Cytotoxic T Lymphocytes. *J Immunol* **149,** 2402–2405 (1992).
13. O'Connor, R. S. *et al.* Substrate rigidity regulates human T cell activation and proliferation. *J. Immunol.* **189,** 1330–9 (2012).
14. Berger, C. *et al.* Adoptive transfer of effector CD8+ T cells derived from central memory cells establishes persistent T cell memory in primates. *J. Clin. Invest.* **118,** 294–305 (2008).
15. Kaehr, B. *et al.* Cellular complexity captured in durable silica biocomposites. *Proc. Natl. Acad. Sci. U. S. A.* **109,** 17336–41 (2012).
16. Meyer, K. C., Coker, E. N., Bolintineanu, D. S. & Kaehr, B. Mechanically encoded cellular shapes for synthesis of anisotropic mesoporous particles. *J. Am. Chem. Soc.* **136,** 13138–13141 (2014).
17. Ashley, C. E. *et al.* The targeted delivery of multicomponent cargos to cancer cells by nanoporous particle-supported lipid bilayers. *Nat. Mater.* **10,** 389–397 (2011).
18. Liu, J., Jiang, X., Ashley, C. & Brinker, C. J. Electrostatically mediated liposome fusion and lipid exchange with a nanoparticle-supported bilayer for control of surface charge, drug containment, and delivery. *J. Am. Chem. Soc.* (2009). doi:10.1021/ja902039y

19. Durfee, P. N. *et al.* Mesoporous Silica Nanoparticle-Supported Lipid Bilayers (Protocells) for Active Targeting and Delivery to Individual Leukemia Cells. *ACS Nano* **10,** 8325–8345 (2016).
20. Park, H. *et al.* Measuring cell surface area and deformability of individual human red blood cells over blood storage using quantitative phase imaging. *Sci. Rep.* **6,** 1–10 (2016).
21. Bayerl, T. M. & Bloom, M. Physical properties of single phospholipid bilayers adsorbed to micro glass beads. *Biophys. J.* **58,** 357–362 (1990).
22. Buranda, T. *et al.* Biomimetic molecular assemblies on glass and mesoporous silica microbeads for biotechnology. *Langmuir* **19,** 1654–1663 (2003).
23. Ashley, C. E. *et al.* The Targeted Delivery of Multicomponent Cargos to Cancer Cells via Nanoporous Particle-Supported Lipid Bilayers. doi:10.1038/nmat2992
24. Raphael, I., Nalawade, S., Eagar, T. N. & Forsthuber, T. G. T cell subsets and their signature cytokines in autoimmune and inflammatory diseases. *Cytokine* **74,** 5–17 (2015).
25. Sommermeyer, D. *et al.* Chimeric antigen receptor-modified T cells derived from defined CD8+ and CD4+ subsets confer superior antitumor reactivity in vivo. *Leukemia* **30,** 492–500 (2016).
26. Turtle, C. J. *et al.* CD19 CAR – T cells of defined CD4 + : CD8 + composition in adult B cell ALL patients. *J Clin Invest* **1,** 1–16 (2016).

2.7 SUPPLEMENTARY INFORMATION

2.7.1 *Supplementary tables*

Supplemental Table 2.1. Molar composition of lipid bilayers

Molar %	**Liquid Crystalline (Fluid)**	**Ordered Gel (Stationary)**
77.5	DOPC (***T_m*** **= -17°C**)	DSPC (***T_m*** **= 55°C**)
20	Cholesterol	Cholesterol
0.02-2	DSPE-PEG-Biotin	DSPE-PEG-Biotin
0.5-2.48	18:1 PEG-2000 PE	18:0 PEG-2000 PE

Supplemental Table 2.2. Size and polydispersity of liposomes

Formulation	**Z-average diameter (nm)**	**PDI**
DOPC 2%	86.91	0.251
DOPC 0.2%	104.7	0.361
DOPC 0.02%	87.61	0.337
DSPC 2%	81.13	0.172
DSPC 0.2%	81.22	0.161
DSPC 0.02%	93.74	0.213

Supplemental Table 2.3. Antibody clones and vendors for intracellular cytokine staining (ICCS) panel

Panel: ICCS	**Clone**	**Dye**	**Vendor**
Live/Dead	N/A	BD Horizon Fixable Viability Stain 520	BD Biosciences
CD4	SK3	APC	Biolegend
CD8	SK1	PacBlue	Biolegend
4-1BB	4B4-1	PE	Biolegend
TNFa	MAb11	BUV395	BD Biosciences
IFNg	4S.B3	BV786	BD Biosciences
IL-2	MQ1-17H12	PE-Cy7	Biolegend

Supplemental Table 2.4. Antibody clones and vendors for outgrowth panel

Panel: Outgrowth	**Clone**	**Dye**	**Vendor**
Live/Dead	N/A	Zombie NIR Fixable Viability Stain	Biolegend
CD3	HIT3a	PE	Biolegend
CD4	RPA-T4	APC	Biolegend
CD8	RPA-T8	FITC	Biolegend

Supplemental Table 2.5. Antibody clones and vendors for differentiation panel

Panel: Differentiation	**Clone**	**Dye**	**Vendor**
Live/Dead	N/A	BD Horizon Fixable Viability Stain 520	BD Biosciences
CD4	OKT4	PE-Dazzle594	Biolegend
CD8	SK1	PacBlue	Biolegend
CD45RA	HI100	BV785	Biolegend
CD45RO	UCHL1	APC	Biolegend
CCR7	150503	BUV395	BD Biosciences
CD62L	DREG-56	PE	Biolegend
PD-1	EH12.2H7	BV711	Biolegend

2.7.2 *Supplementary figures*

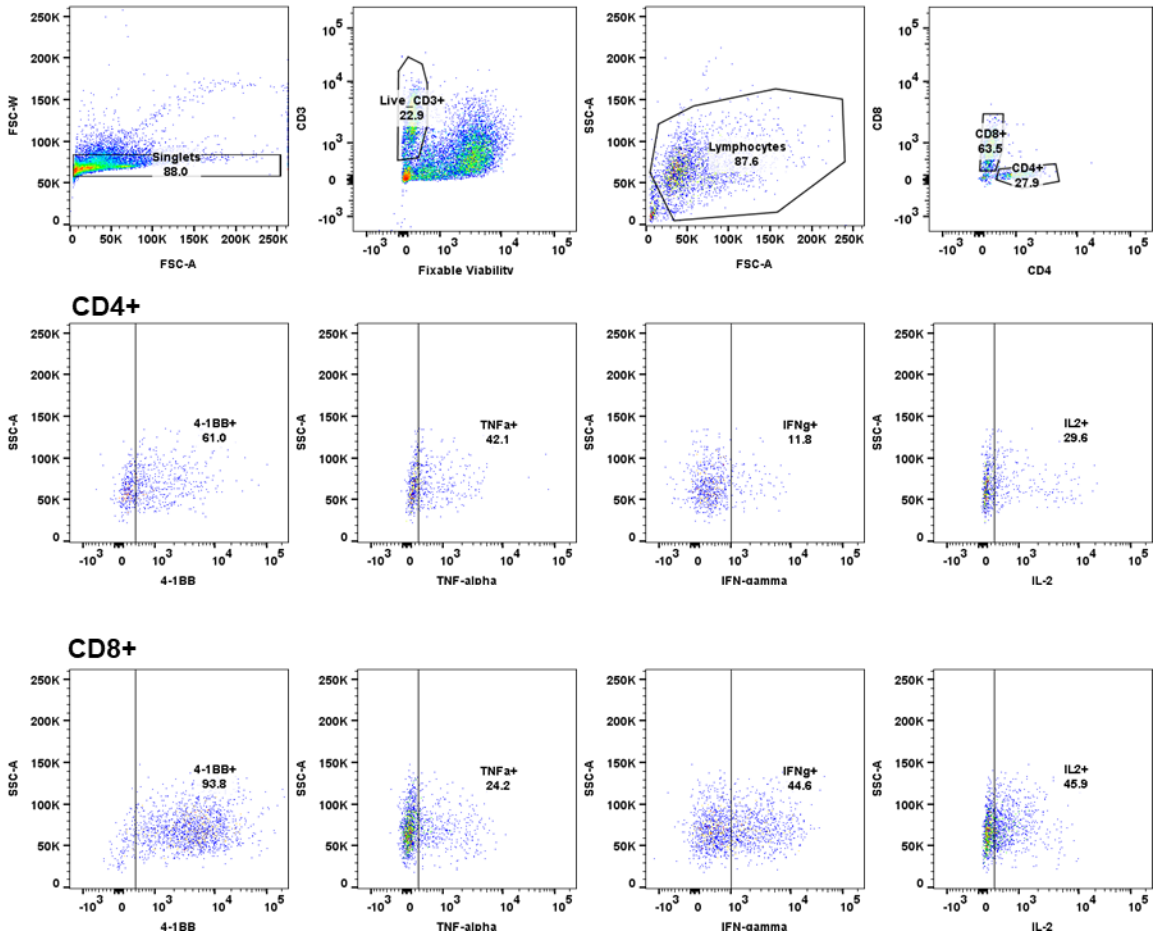

Supplemental Figure 2.1. Gating strategy for ICCS flow analysis

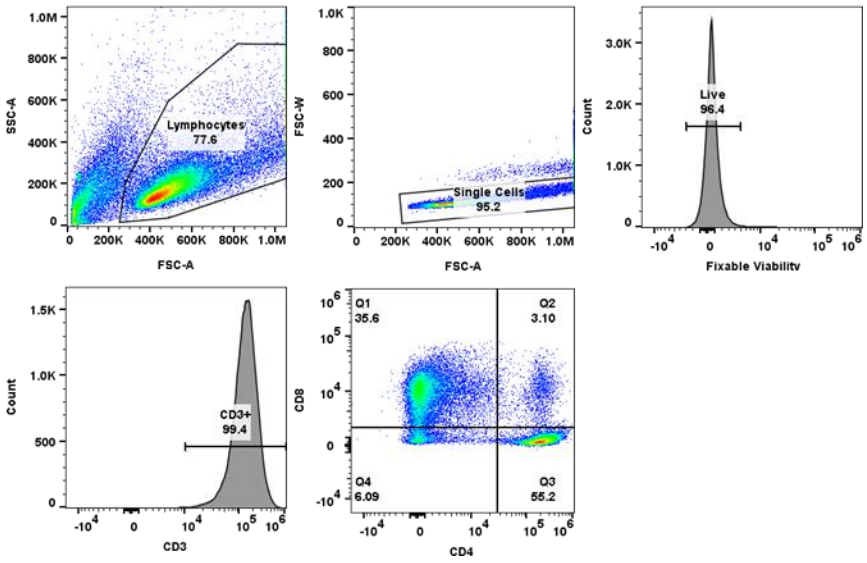

Supplemental Figure 2.2. Gating strategy for outgrowth flow analysis

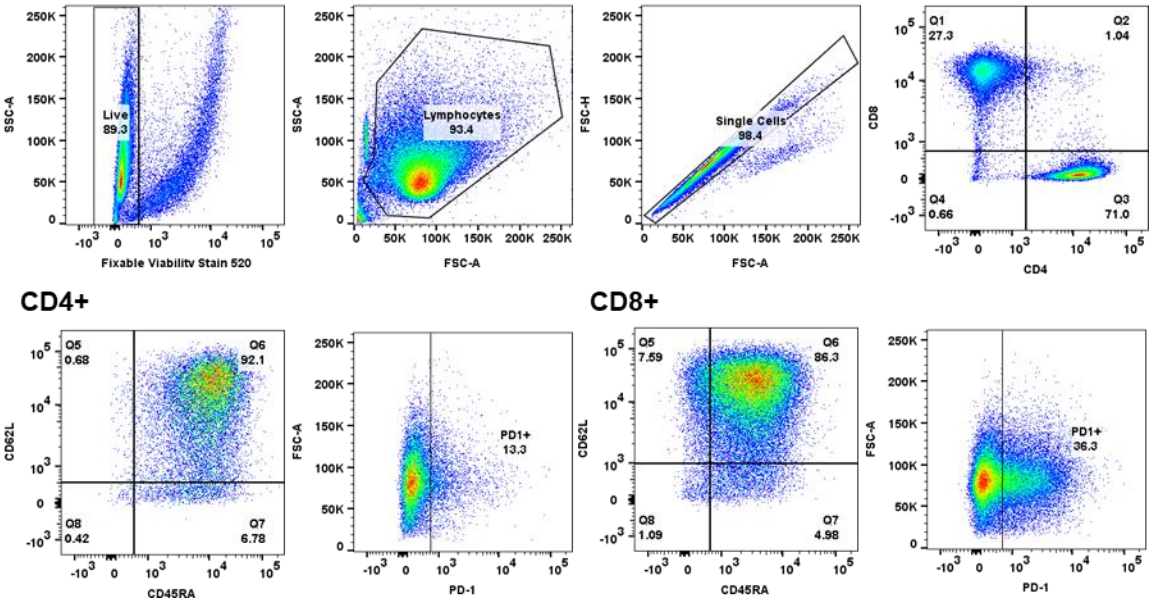

Supplemental Figure 2.3. Gating strategy for differentiation flow analysis

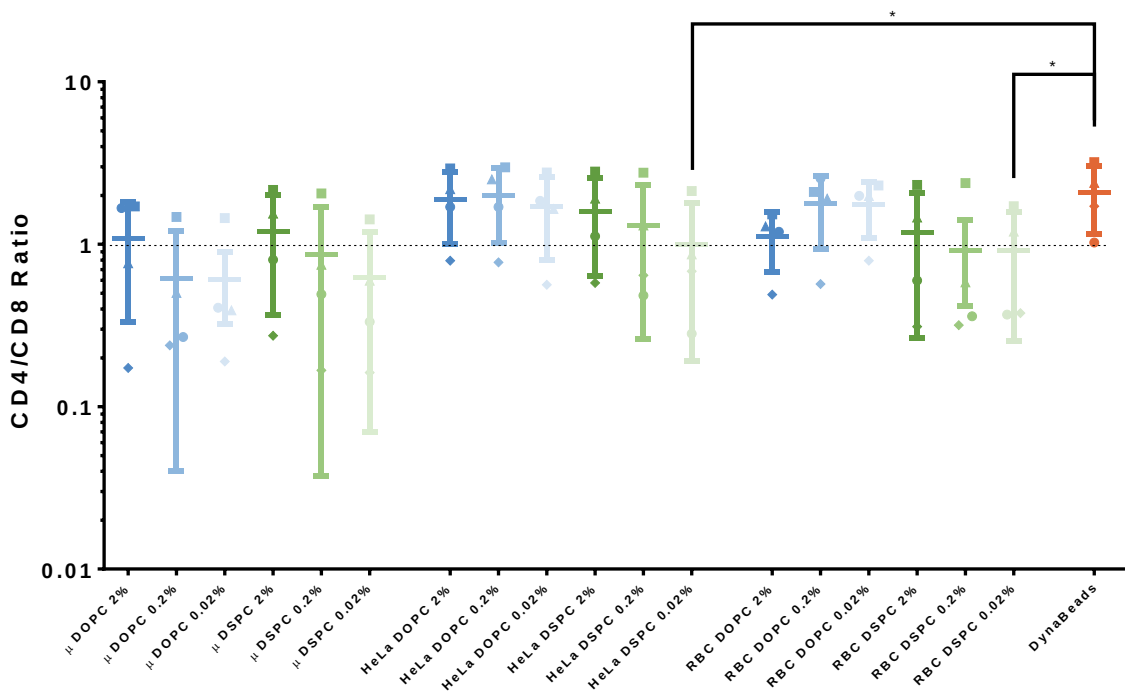

Supplemental Figure 2.4. Ratio of $CD4^+$ to $CD8^+$ T cells after 9-day outgrowth. Data represented as mean ± SD (n=4 biological replicates; paired one-way ANOVA with Dunnett's multiple comparisons test, *p<0.05).

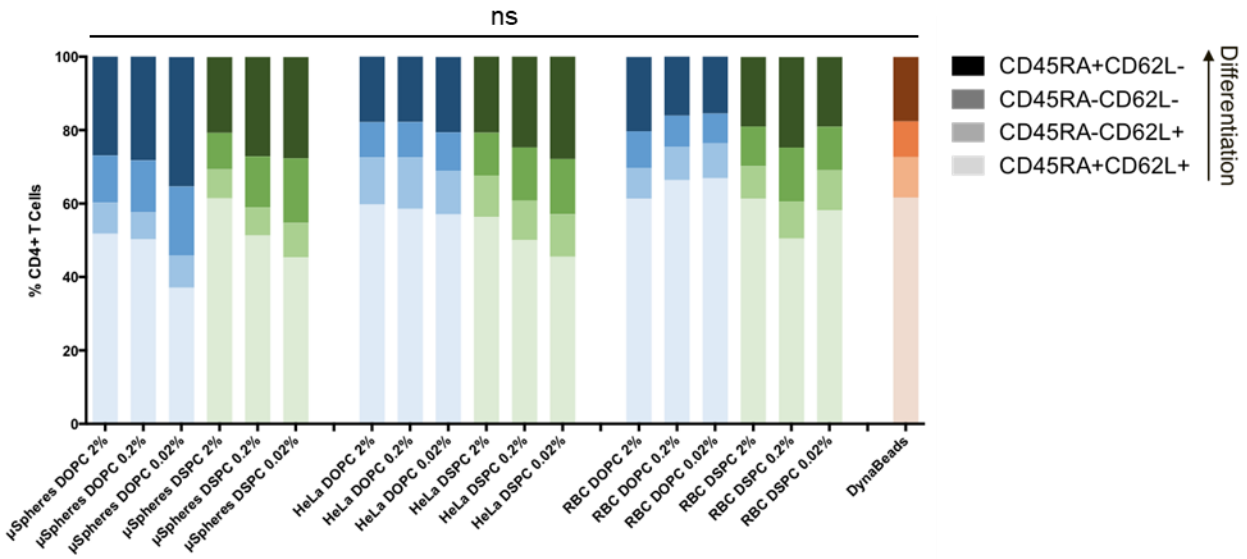

Supplemental Figure 2.5. $CD4^+$ T cell differentiation at day 12 post-stimulation. Data are shown as mean of 3 independent experiments with cells from 3 donors (error bars omitted for legibility, paired two-way ANOVA with Bonferroni's multiple comparisons test, ns = not significant).

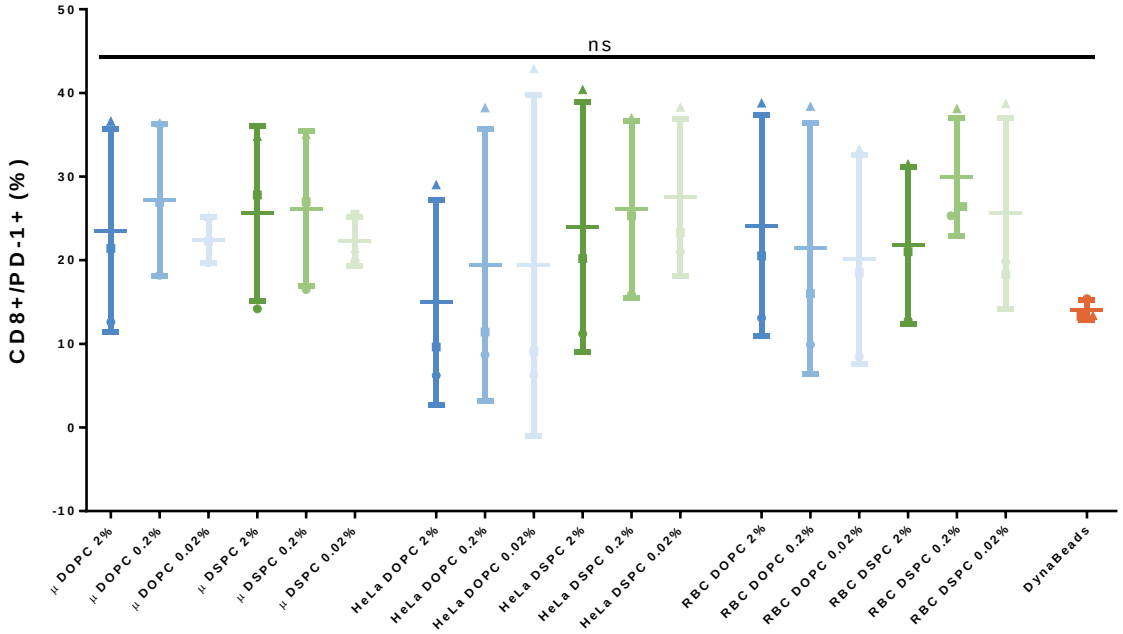

Supplemental Figure 2.6. $CD8^+$ T cell PD-1 expression at day 12 post-stimulation. Data are shown as mean of 3 independent experiments with cells from 3 donors (Paired one-way ANOVA with Tukey's multiple comparisons test, p=0.3342).

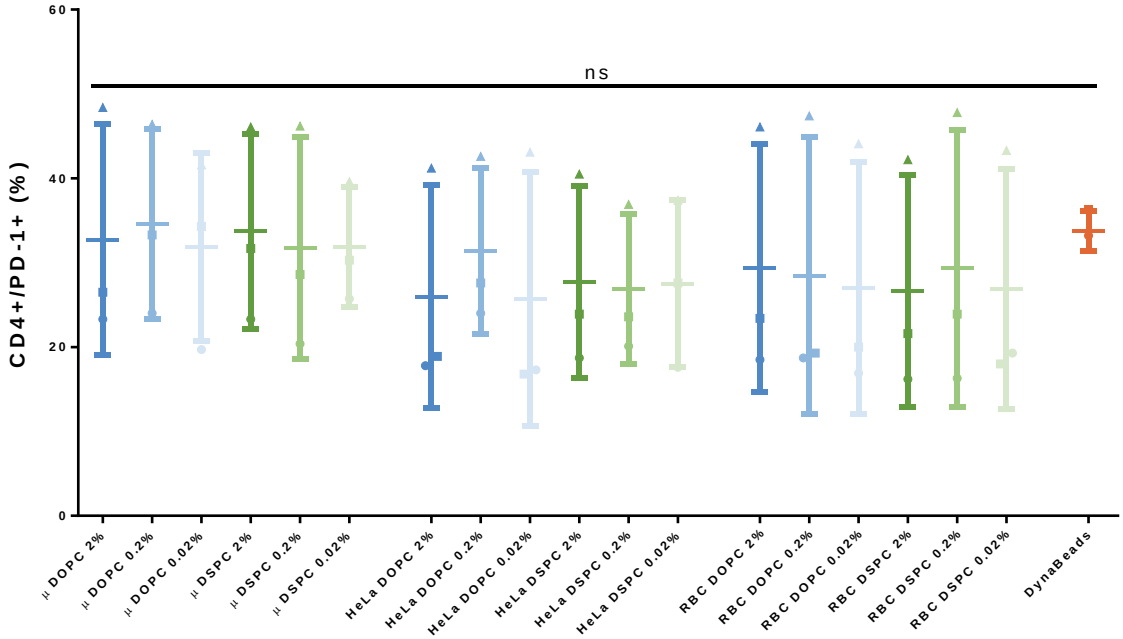

Supplemental Figure 2.7. $CD4^+$ T cell PD-1 expression at day 12 post-stimulation. Data are shown as mean of 3 independent experiments with cells from 3 donors (Paired one-way ANOVA with Tukey's multiple comparisons test, ns = not significant, p=0.3975).

Chapter 3. TOWARDS IDENTIFICATION OF HUMAN CD28 AND CD3E BINDING LIGANDS

Brynn R. Olden, Emi Lutz, Gary W. Liu, Nataly Kacherovsky, and Suzie H. Pun

Abstract

T cells must be expanded *ex vivo* to reach clinical doses for cell therapy applications. In the native immune system, T cells interact with antigen presenting cells (APCs) to receive three chemical signals that induce an immune response: (1) Antigen and MHC interaction with T cell receptor (TCR); (2) Co-stimulatory signals through CD28 receptor; and (3) Soluble co-stimulatory and inflammatory cytokines. Current *ex vivo* expansion reagents combine signals 1 and 2 via anti-CD3ε and anti-CD28 antibodies anchored to magnetic beads and supplement media with cytokines for signal 3. An opportunity for process improvement and cost reduction lies in the development of a synthetic material that can achieve similar rapid *ex vivo* expansion of T cells and be synthesized chemically under cGMP conditions. In this work, directed evolution techniques paired with high throughput sequencing were used in attempts to identify peptide and aptamer ligands that bind to CD3ε and CD28 as alternative stimulation reagents. While no ligands with high affinity and specificity were identified, the techniques developed in this chapter will inform future efforts for novel ligand identification.

3.1 INTRODUCTION

3.1.1 *T cell activation*

T cell activation and division is required for CAR T cell manufacturing to reach the desired cell dose and genetically modify T cells with retroviruses or lentiviruses.[1] Within the native immune system, T cells require three signals from an antigen presenting cell (APC) to become activated against a target antigen (Figure 3.1 a). The first signal is received through the T-cell receptor/CD3 complex that binds to peptide antigen presentation within the MHC complex: MHC-II and MHC-I for CD4+ and CD8+ T cells, respectively.[2] If T cells only receive signal 1, they enter a non-responsive state of anergy, do not proliferate, and cannot be restimulated.[3] The second signal required for successful activation is a co-stimulatory signal. The most robust costimulatory molecule is CD28, which is engaged by CD80 or CD86 on APCs. When engaged at the same time as the TCR, CD28 triggers production of the inflammatory cytokines and induces cell proliferation. OX-40 and 4-1BB are additional co-stimulatory receptors that are upregulated later in activated T cells. The final signal required for T cell activation *in vivo* is inflammatory cytokines.[4] Variation in cytokine signals directs the differentiation of T cells into various phenotypes.[5]

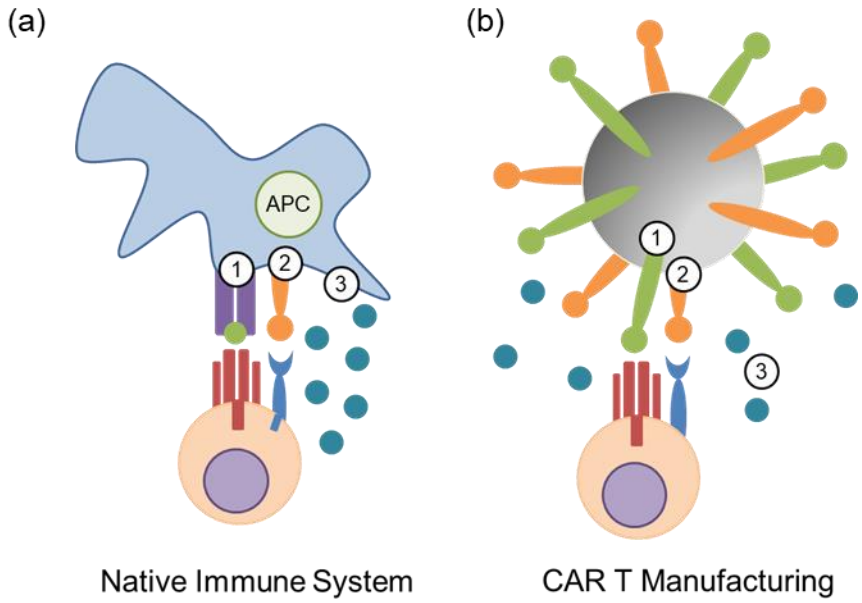

Figure 3.1. Native and synthetic methods for T cell activation. Activation of T cells in the (a) native immune system and (b) current CAR T manufacturing both rely on 3 signals for T cell activation: (1) TCR stimulation, (2) co-stimulatory receptor stimulation, and (3) cytokine signals.

In CAR T cell manufacturing, polyclonal T cell activation and expansion, rather than antigen-specific T cell expansion, is often desired. This is achieved using artificial antigen presenting cells (aAPCs). Both cell and bead-based aAPCs have been developed and used in CAR T cell manufacturing.[1] For example, K562 cell lines have been genetically modified to express costimulatory molecules, and act as aAPCs after being irradiated.[6] More commonly, synthetic reagents like micro- and nanometer sized magnetic beads are covalently attached to antibodies for T cell activation.[7,8] Stimulation of the CD3ε side chain of the TCR/CD3 complex with a monoclonal anti-CD3ε antibody can independently elicit an antigen non-specific "signal 1".[9] Multi-valent engagement of the CD3ε receptor triggers receptor clustering and intracellular ITAM (immune receptor tyrpsine based activation motif) phosphorylation similar to a TCR binding event. Including an anti-CD28 antibody can simultaneously deliver the co-stimulatory "signal 2" (Figure 3.1 b). Soluble cytokines are supplemented in the culture medium to deliver "signal 3".

3.1.2 *Library evolution and screening for unique targeting ligands*

Targeting ligands are biomolecules that facilitate cell recognition and are key technologies in targeted drug delivery, molecular imaging, and immunotherapy. Three common classes of targeting ligands are antibodies, peptides, and aptamers. Monoclonal antibodies are the most widely used, but have many properties that make them less ideal for certain applications. In addition, generation of new antibodies requires animal immunization and generation of hybridoma cell lines, a costly and time-intensive process.[10]

Aptamers and peptides are emerging classes of ligands due to their smaller sizes, identification through library screening, and ease of chemical synthesis (Table 3.1).[11–13] Aptamers are single stranded oligonucleotide sequences, typically made from chemically modified RNA or single stranded DNA, that form defined three-dimensional structures.[13,14] Peptides are short polypeptides (<20 amino acids) with defined secondary structure. Due to their synthesis by solid-phase chemistry, peptides and aptamers are both amenable to site-specific conjugation chemistries attractive for cGMP manufacturing.[15] Peptides and aptamer targeting ligands are most commonly identified through library evolution technologies.

Table 3.1. Comparison of various targeting ligand properties. Adapted from Aptamer Group, University of York.

Characteristic	Antibodies	Peptides	Aptamers
Development Time	Several months	Several weeks	Several weeks
Targets	Immunogenic materials	Small molecules & proteins	Small molecules & proteins
Stability	Poor, irreversible denaturation	Good, but still prone to irreversible denaturation	Good, withstand repeated rounds of denaturation without loss of function
Shelf Life	Limited (~ 2 years)	Long (years)	Long (years)
Affinity	High (nM-pM)	Moderate (μM-nM)	High (nM-pM)
Specificity	Good, but variable between clones	Great, built into selection method	Great, built into selection method
Size	140-160 kDa	1-3 kDa	10-30 kDa
Synthesis	Cellular protein expression	Solid phase chemical	Solid phase chemical

Phage display is a well-established method to screen up to 10^9 unique peptide sequences for binding to a desired target. A commonly used commercial system (Ph.D. Phage Display Peptide Library, New England Biolabs) modifies the pIII minor coat protein of the M13 filamentous bacetriophage to display five copies of a single peptide.[16] In a typical phage display experiment, the starting library is mixed with a target of interest (positive selection), after which a partitioning event isolates bound phage. Bound phage are eluted and amplified in E coli and subjected to further rounds of selection. Selectivity can be built into phage display experiments by removing phage that bind to an off-target control (negative selection). After 3-5 rounds of selection, the evolved library is sequenced either by Sanger sequencing of individual phage clones, or bulk library sequencing by next generation sequencing.[17] Phage display has been used successfully to identify peptides by *in vitro* and *in vivo* methods that bind to specific cell types, proteins, organs, and small molecules.[18–21]

SELEX is an equivalent technique for aptamer discovery, with a much larger diversity, upwards of 10^{14} unique aptamer sequences, in the starting library.[13] Figure 3.2 shows the general methods of phage display and SELEX. In SELEX, the amplification step between each round of selection is performed using polymerase chain reaction (PCR) and either transcription for RNA aptamers, or single strand displacement for ssDNA aptamers.[22,23]

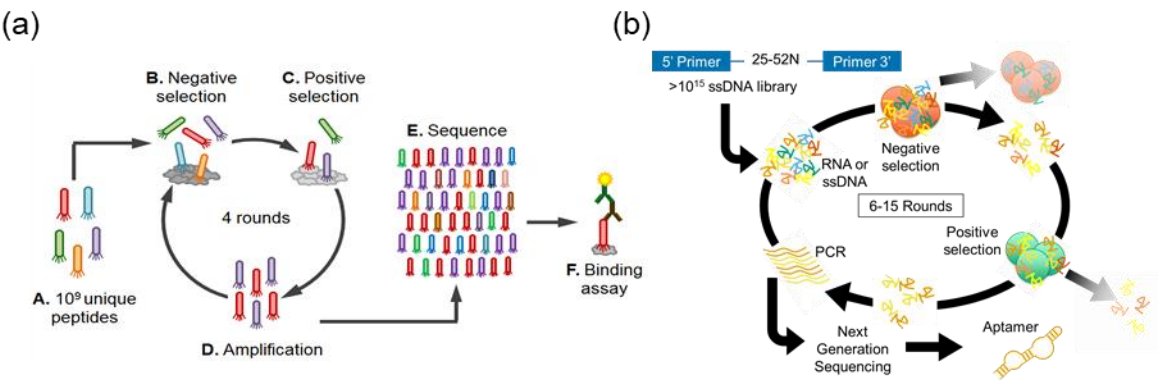

Figure 3.2. Library evolution methods for ligand identification. (a) Phage display for peptide screening and (b) SELEX for RNA or ssDNA aptamer screening.

3.1.3 *T cell specific aptamers identified by SELEX*

Aptamers have been identified that bind to other T cell surface receptors by protein SELEX including murine CD28, murine and human 4-1BB, murine CTLA-4, murine and human OX-40, and human CD4.[24,25] Aptamers can elicit antagonistic and agonistic responses when bound to target receptors. A murine CD28 aptamer acted as an antagonist in monomeric form by blocking B7 protein binding and inhibiting T cell activation, but also displayed agonistic T cell activation in a dimeric form.[26] Similarly, a dimerized murine OX40 aptamer was used to improve T cell expansion and IFN-γ production in an *in vitro* T cell activation assay, and enhanced tumor immunity in a dendritic cell tumor vaccine model.[25,27]

3.1.4 *Next-generation sequencing (NGS) methods for ligand identification*

In recent years, advances in high-throughput sequencing technology has increased the number of sequencing reads researchers can obtain for an evolved ligand library by many orders of magnitude (from 10^2 with Sanger sequencing to 10^7 with Illumina sequencing) for roughly the same price.[28] Both Ion Torrent and Illumina sequencing platforms have been explored extensively for improving data analysis in library evolution experiments. Both sequencing methods use spatial separation of individual DNA strands on a detection surface and sequencing-by-synthesis to sequence many DNA strands in parallel.

In phage display, both sequencing platforms have been used to better understand the hallmarks of binding sequences in a phage library.[29] Notably, these techniques allow researchers to eliminate "parasitic" phage sequences that preferentially amplify in E. coli, and track enrichment of specific sequences through each round of selection.[17,30–32]

Similar advancements have been made in analyzing data from SELEX experiments, leading to the hypothesis that the fold-enrichment of aptamers throughout rounds is a better predictor for target binding sequences than bulk frequency.[33] High throughput sequencing can also decrease the number of rounds of SELEX needed before a high affinity aptamer can be identified. The Gilboa group was able to identify a murine IL-10 aptamer within 5 rounds of SELEX, compared to the convention of 9-16 rounds required prior to Sanger sequencing.[34] In this study the authors also noted that performing too many rounds of SELEX can deplete high affinity aptamers, allowing lower affinity aptamers with better PCR amplification properties to dominate the library.

In this work, we employ both phage display and SELEX in attempts to identify novel binding ligands to the human CD3ε and CD28 receptors on T cells.

3.2 MATERIALS AND METHODS

3.2.1 *Materials*

PhD-C7 and PhD-12 Phage Libraries (New England Biolabs); Jurkat cell line (Generously given by Jensen Lab, Seattle Children's Research Hospital); RPMI 1640 medium with L-glutamine (Gibco); fetal bovine serum (FBS), (Seradigm); human anti-CD3-PE, OKT3 clone (Biolegend); human anti-CD28-APC, CD28.2 clone (Biolegend); human anti-CD3-biotin, OKT3 clone (Biolegend); human anti-CD28-biotin, CD28.2 clone (Biolegend); recombinant human CD28-Fc protein (AcroBiosystems); recombinant human CD3ε-Fc protein (AcroBiosystems); human IgG1 kappa (Sigma); phosphate buffered saline (PBS, pH 7.4), (Sigma); bovine serum albumin (BSA), (Miltenyi Biotech); tween-20 (Sigma); Protein G coated plates (Pierce); Protein G magnetic beads (ThermoFisher); mouse anti-M13 phage-HRP (GE Healthcare); ABTS substrate (Sigma); Acc65I enzyme (NEB); EagI enzyme (NEB); R&DNA T7 polymerase (EpicentreBio); 2'-fluoro-CTP (TriLink); 2'-flouro-UTP (TriLink); ATP (Roche); GTP (Roche); dNTPs (Invitrogen); Platinum Taq DNA polymerase (LifeTechnologies); Reverse transcriptase AMV (LifeTechnologies); Klenow DNA polymerase (NEB); 5'-biotin-GMP (TriLink); Protein G magnetic beads (LifeTechnologies); miRNeasy clean-up kit (Qiagen); DNA clean-up kit (Qiagen); MiSeq reagent kit v2 300 cycles (Illumina); streptavidin-FITC (eBioscience).

3.2.2 *Generation of CD28 and CD3ε knockdown Jurkat cell lines*

Jurkat cells were maintained per ATCC guidelines in RPMI + L-glutamine and 10% FBS in a humidified incubator at 37°C and 5% CO_2. Knockdown was generated using the CRISPR-Cas9 system. Guide RNAs were designed by collaborators in the Jensen Lab using the MIT CRISPR design web tool (http://crispr.mit.edu/) to target either CD3ε or CD28.[35,36] The guide RNA sequence (CD28: GCT TGT AGC GTA CGA CAA TGC GG; CD3ε: AGA TGC AGT CGG GCA CTC ACT GG) was cloned into the Cas9 expression plasmid and Nucleofected into Jurkat cells.

Cells containing the knockdown were isolated using magnetic-activated cell sorting. Individual clones were isolated by serial dilution cultures with irradiated feeder cells. Successful knockdown of CD3ε and CD28 were confirmed at the genomic level by PCR around the gRNA site and Sanger sequencing (Genewiz), and at the protein level by flow cytometry staining with CD3-PE and CD28-APC antibodies. Flow cytometry data was collected on a MacsQuant flow cytometer (Miltenyi Biotech) and analyzed using FlowJo software.

3.2.3 *Subtractive panning phage display*

Four separate phage display experiments were performed following the general phage tittering, amplification, and DNA sequencing protocols outlined in the NEB Phage Display Manual. For the first round, 2×10^{11} PFU of the Ph.D. library was used as input; for each subsequent round, 2×10^{11} PFU of the amplified eluate from the previous round was used as the input. All experiments used one positive selection round followed by 2-4 additional rounds of positive and negative selection. The variations in each experiment are outlined in Table 3.2.

Table 3.2. Phage display experimental design parameters for selection and sequencing

Experiment Step	Iteration	Phage Display Experiment			
		1	**2**	**3**	**4**
Phage library	Cyclic 7-mer peptide	X	X		
	Linear 12-mer peptide	X	X	X	X
Negative selection for plastic	None	X			
	1-hour negative incubation		X		
	Transfer to new tube before elution			X	X
Positive selection	Surface-immobilized-protein	X	X		
	Protein displayed on Jurkat cells			X	X
	Protein in solution				X
Selection temperature	4˚C	X	X	X	X
	21˚C				X
Washing	PBS-Tween	X	X	X	X
	BRASIL				X
Elution	General elution with Gly-HCl	X	X	X	X
	Specific elution with antibodies				X
Sequencing	Sanger sequencing	X	X		
	NGS		X	X	X
Sequencing Analysis	Manual search for motifs	X	X		
	MEME		X	X	X
	Amino acid prevalence code		X		
	False positive code				X

In experiments 1 and 2, recombinant CD3ε-Fc or CD28-Fc were immobilized on Protein G coated plastic 96-well plates for the positive selection and immobilized human IgG was used for negative selection. Protein solutions in PBS with 1% BSA (1% PBSA) were incubated in Protein G plates for 1 hour at room temperature with rotation followed by washing 3x with 1% PBSA to remove unbound protein prior to phage binding. In experiment 2, a negative selection against plastic was included. In experiments 3 & 4, the wildtype Jurkat cell line that express CD3ε and CD28 was used for positive selection, and knockout Jurkat cell lines were used for negative selection. Experiment 4 included selection against proteins in solution followed by collecting bound phage using Protein G coated magnetic beads.

Stringency was applied throughout the rounds by increasing the Tween-20 content (0.1, 0.3, 0.5%) in wash steps or using the bio-panning and rapid analysis of selective interactive ligands (BRASIL) washing method in experiment 4.[37] In all experiments, bound phage were eluted non-specifically with Glycine-HCl. In experiment 4, specific elution using antibodies against CD3ε or CD28 was also employed.

3.2.4 *Sanger sequencing of selected phage clones*

The amplified output library from the last round of each phage display experiment (experiments 1 & 2) were infected into log-growth phase E. Coli and plated for colony growth using the serial dilution tittering method outline in the NEB Phage Display Manual. 10-20 individual clonal plaques were randomly selected, amplified, and the genomic DNA was submitted for Sanger sequencing of the peptide-encoding region.

3.2.5 *Next generation sequencing of selected phage libraries*

DNA amplicons were prepared as previously described with some modifications.[32] Single-stranded DNA (ssDNA) was isolated from 1×10^{11} PFU of the amplified phage eluate from each round of peptide phage display using QIAprep Spin M13 Kit (QIAGEN), and 50 ng of ssDNA was amplified by PCR using primers containing Illumina-compatible sequencing adaptors and sample-specific barcodes. For each library sample, the PCR reaction (50 μL) contained 500 nM of both the forward primer and reverse barcode primer unique to that sample, 250 μM dNTP, 1 U Phusion High Fidelity DNA Polymerase and 1× Phusion High Fidelity buffer. Thirteen PCR cycles (10 s at 98 °C, 30 s at 59 °C, 30 s at 72 °C) were performed and PCR products were purified from a 2% agarose gel using QIAquick Gel Extraction Kit (QIAGEN). The concentration of DNA was determined by a quantitation assay using a Qubit 3.0 Fluorometer (Life Technologies). Purified PCR products prepared from the unselected and selected phage libraries were combined in an equimolar ratio prior to sequencing.

Sequencing and data processing was performed as previously described with some modifications.[30] Sequencing was performed on an Illumina MiSeq system in the presence of 7% PhiX control, using 150 bp single ended sequencing chemistries and custom sequencing primers (Read_1_primer, 5'-GCTCGACCTGTTCCTTTAGTGGTACCTTTCTAT TCTCACTCT-3'; Index_read_primer, 5'- AGCAAAATCCCATACAGAAA ATTCATTTACCGCAGGTCGCTCC -3') according to manufacturer instructions.

3.2.6 *Generation of phage clones*

Oligonucleotides encoding the peptides of interest were designed with 5' overhangs and an overlap region with T_m ~55-60 °C and synthesized by IDT. Oligonucleotide pairs were annealed, filled in with Klenow (New England BioLabs), digested with Acc65I/EagI (New England BioLabs), and cloned into M13KE dsDNA vector per the New England BioLabs Ph.D. manual.

The resulting plaques were used for amplification and production of phage. Peptide sequences were confirmed by DNA sequencing.

3.2.7 *Enzyme-linked immunoabsorbent assay (ELISA) phage binding*

Target and non-target proteins were immobilized on Protein G plates as described in section 2.2.3.1. 5×10^9 PFU of phage clones and an instertless phage (control phage that does not display peptides) were added to designated wells and allowed to bind for 1-2 hours at room temperature. Plates were washed 6× with PBS + 0.1% Tween prior to addition of anti-M13-HRP for 1 hour at room temperature. An additional 6 washes were performed before ABTS substrate was added, developed, & quenched. Absorbance at 450 nm and 540 nm was read on a Safire^2 plate reader (Tecan).

3.2.8 *Flow cytometry phage binding*

5×10^{10}-5×10^{11} PFU of phage clones were incubated with 10^5 target or non-target Jurkat cells for 30 minutes on ice. Cells were washed twice with PBSA and fixed for 15 minutes on ice in 4% PFA. Bound phage was probed using a 1:2000 dilution of a primary rabbit anti-M13 antibody followed by a 1:80 dilution of the secondary goat anti-rabbit-FITC antibody, with 2 PBSA washes after each antibody incubation. Cells were analyzed using by a MacsQuant flow cytometer (Miltenyi).

3.2.9 *2'-fluoropyrimidine RNA SELEX for CD28 binding aptamer*

A template ssDNA library with 25-nucleotide random region flanked by constant regions of 22 nucleotides at the 5' end and 49 nucleotides at the 3' end, and containing a T7 RNA polymerase promoter was purchased (IDT). The library was transcribed into the initial 2'-fluoropyrimidine (2'-F) RNA library (~10^{14} diversity), as described previously. [26] Nine rounds of SELEX with increasing stringency, shown in Table 3.3, were performed using human CD28 extracellular domain/human IgG Fc fusion protein and human IgG1 immobilized at saturating concentrations on protein G magnetic beads as positive and negative selection targets, respectively. The selection buffer was 150 mM NaCl, 2 mM $CaCl_2$, 20 mM HEPES (pH 7.4), 0.01% BSA, and 0.001% Tween 20.

Table 3.3. Concentrations of RNA aptamers, CD28-Fc, and IgG1 in each round of SELEX

Round	RNA (μM)	CD28-Fc (nM)	IgG1 (nM)
1	3.2	250	250
2	3.2	125	125
3	1.6	125	125
4	0.8	125	125
5	0.4	125	125
6	0.2	62.5	62.5
7	0.1	62.5	62.5
8	0.05	62.5	62.5
9	0.05	62.5	62.5

After each round of selection, the pool of RNA was reverse transcribed, amplified by PCR, and transcribed into 2'-F RNA for the starting library of the next round. After 9 rounds of selection, the last round of SELEX was prepared for sequencing.

3.2.10 *Next-generation sequencing*

Reverse transcribed dsDNA of round 9 aptamer library were ligated to Illumina sequencing adaptors as described previously, and sequenced using 150 single-end reads on an Illumina Miseq.[38] Aptamer sequences were extracted from sequence reads containing the expected flanking sequences at the proper positions. Counts were made for the occurrence of each unique sequence, and the phylogenetic relationships relating them were inferred using a neighbor-joining tree. Phylogenetic trees were generated with FigTree v1.4 software (University of Edinburgh) and sequence alignments were generated using Chimera software (University of California San Francisco).

3.2.11 *T cell binding via flow cytometry*

2'F RNA aptamers were transcribed and purified as described (section 2.2.4.3) with the addition of biotinylated GMP in the transcription reaction. Aptamers were annealed at 80°C for 5 minutes and slow cooled before dimerization with streptavidin-FITC. Wildtype Jurkat cells and the CD28 knockout Jurkat cell line (clone 3H10) were incubated in 100 nM of aptamer dimers (200 nM total aptamer) for 30 minutes at 37°C in binding buffer. Then washed twice with binding buffer before analyzed using a MACSQuant flow cytometer (Miltenyi). Flow cytometry data was analyzed using FlowJo software.

3.2.12 *Protein binding via biolayer interferometry*

Oligos for promising aptamer sequences were designed as two strands with overlapping complementary sequence, filled in by Klenow, and transcribed into 2'F RNA with T7 R&DNA. Aptamers were DNase treated and purified using a miRNeasy mini kit and quantified by NanoDrop. Binding kinetics to CD28-Fc were quantified using the Octet RED96 biolayer interferometry system (fortéBIO) using the Protein G sensors. CD28-Fc was loaded on to the sensors and washed briefly in binding buffer. After a stable baseline was established in binding buffer, the sensors were inserted into solutions of aptamer at varying concentrations (2 nM – 2 μM) for 30 minutes to measure association and then returned binding buffer for 30 minutes to measure dissociation. Binding curves were baseline-corrected using the Octet software.

3.2.13 *Single stranded DNA (ssDNA) SELEX for CD3ε and CD28 binding aptamers*

A ssDNA library with a 52-nucleotide random region and 18-nucleotide constant regions on each side was used as the starting library (5'-ATCCAGAGTGACGCAGCA-52N-TGGACACGGTGGCTTAGT-3') with the same wash and binding buffers that were used in previously published cell-SELEX experiments.[22] This library underwent 6 rounds of recombinant protein SELEX using a FITC-labeled forward primer and biotinylated reverse primer for library amplification and streptavidin-mediated strand separation between rounds. All rounds included a negative selection to human IgG1 before positive selection to recombinant human CD28-Fc or human CD3ε-Fc (Table 3.4). Both negative and positive selection steps included a 30 minutes incubation with soluble protein at 37 °C, followed by a second 30 minute incubation at 37 °C with Protein G magnetic beads to partition protein-bound aptamers. Unbound aptamers from the negative selection step were transferred to positive selection. Stringency was increased throughout rounds by decreasing the target protein concentration and aptamer library concentration, while increasing the number and duration of washes.

Table 3.4. Conditions used in each round of ssDNA protein SELEX

Round	[DNA] (μM)	[CD-Fc] (nM)	[IgG1] (nM)	Protein G Beads (μL)	Volume (μL)	Wash
1	10	1	1	10	1000	2x, 30s
2	1	1	1	5	200	3x, 1 min
3	1	0.8	1	5	200	3x, 1 min
4	0.5	0.4	1	5	200	3x, 2 min
5	0.25	0.4	1	5	200	3x, 3 min
6	0.125	0.2	1	5	200	3x, 3 min

Libraries from each round were amplified and ssDNA was generated by strand separation prior to use in binding studies.

3.2.14 *Protein binding via flow cytometry*

Recombinant and biotinylated CD3ε, CD3εδ heterodimer, and CD28 (AcroBiosystems) were attached to streptavidin coated magnetic beads (Spherotech) for binding studies. Protein attachment and conformation were confirmed using fluorescently labeled anti-CD3 PE (clone: HIT3a) and anti-CD28 APC (clone: CD28.2) antibodies (Biolegend) analyzed on an Attune NxT flow cytometer (ThermoFisher).

In SELEX round binding studies, recombinant proteins were attached to streptavidin coated magnetic beads and then incubated with 250 nM FITC-labeled ssDNA libraries from each round for 30 minutes at 37 °C followed by two washes in wash buffer. A FITC-labeled random aptamer from the naïve library (RANL, sequence: ATC CAG AGT GAC GCA GCA AAT TCC AAA CTC GAG TAA GCG TAG AGC CTC TCA TCG CCT CAA TAA-TGG ACA CGG TGG CTT AGT) was used at the same concentration as a negative control.

Aptamer binding was assessed by measuring the fluorescent intensity of protein-coated magnetic beads via flow cytometry on an Attune NxT flow cytometer (ThermoFisher). Data was analyzed using FlowJo software.

3.2.15 *Primary human T cell binding via flow cytometry*

Cryopreserved primary human T cells isolated by magnetic-activated cell sorting were generously gifted by Juno Therapeutics. Cells were thawed and rested in RPMI-1640 media supplemented with 10% FBS for at least 1 hour prior to binding studies. Cells were stained with Zombie Violet fixable viability stain (Biolegend) at a 1:500 dilution in PBS for 10 minutes at room temperature prior to FITC-labeled aptamer binding in binding buffer for 30 minutes at 37 °C. As a positive control, cells were stained with fluorescently labeled anti-CD3ε PE (clone: HIT3a) and anti-CD28 APC (clone: CD28.2) antibodies to confirm protein expression. Cells were washed twice in wash buffer and analyzed using an Attune NxT flow cytometer (ThermoFisher). Data was analyzed using FlowJo software.

3.3 RESULTS AND DISCUSSION

3.3.1 *Knockout cell lines for CD28 and CD3ε genes established in Jurkat cells using CRISPR/Cas9 system*

The Jurkat cell line is an immortalized human CD4+ T cell leukemia line. The wildtype cell line has consistent CD28 expression (100%) and variable CD3ε expression. Cell lines with depleted CD28 or CD3ε expression were generated using CRISPR/Cas9 technology for use as negative controls in selection experiments. Of the sixteen CD28 clones, 15 showed reduced or ablated CD28 expression by flow cytometry (Figure 3.3 a). From the 47 screened CD3ε clones, 16 showed reduced or ablated CD3ε expression by flow cytometry (Figure 3.3 b).

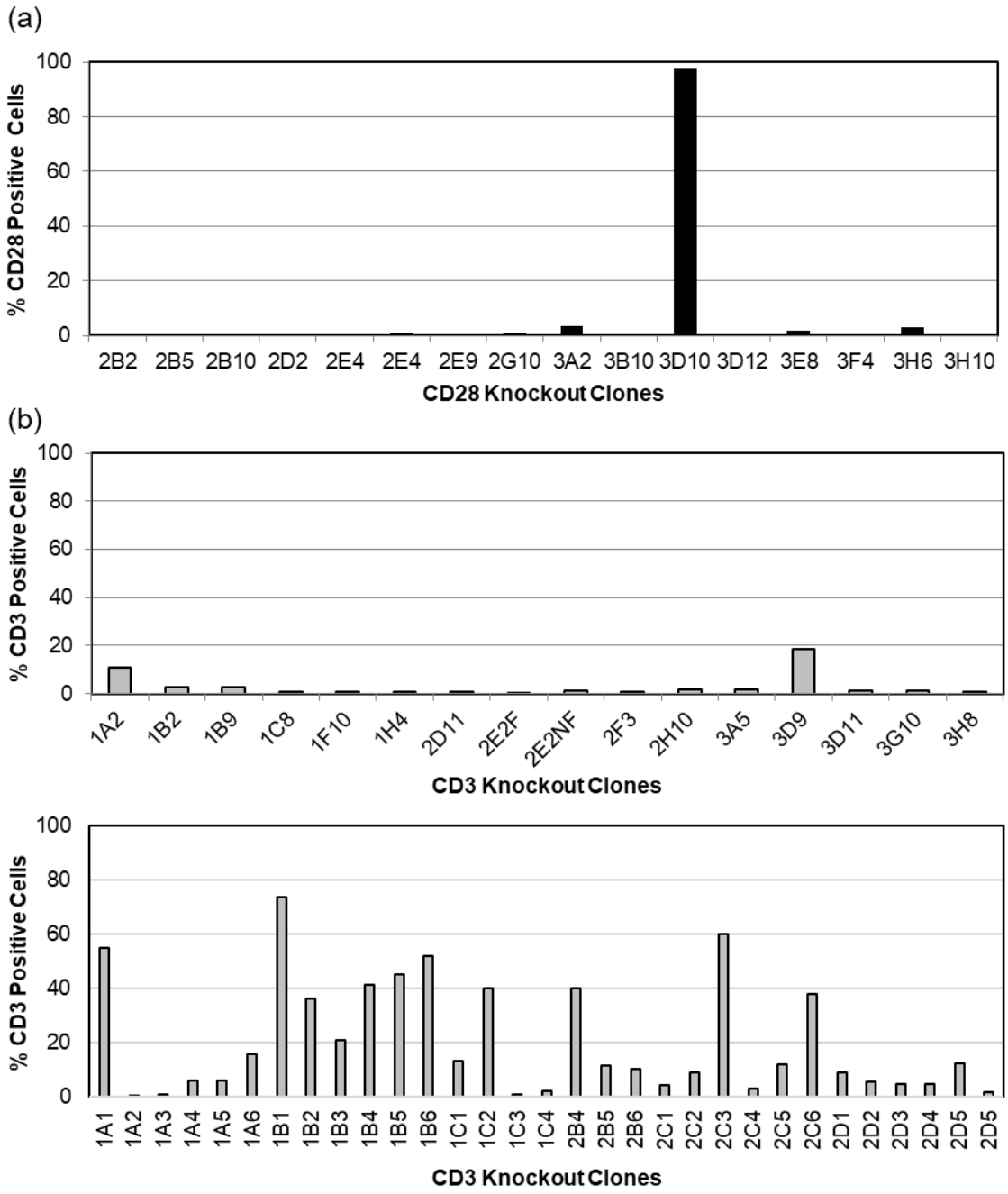

Figure 3.3. CD3ε and CD28 expression of Jurkat clonal cell lines. (a) 15/16 CD28 clones showed ablated CD28 expression by flow cytometry. (b) 16/47 CD3ε clones showed ablated CD3ε expression by flow cytometry.

Genomic DNA was isolated from 18 clones (13 CD3ε, 5 CD28), and amplified with primers designed to excise an ~500 bp region around the gRNA cut site. Gel-purified samples were submitted for Sanger sequencing and analyzed for disruptive Non-Homologous End Joining

(NHEJ) on each allele using 4Peaks software. One CD28 clone (2D2) and one CD3ε clone (1A2) were confirmed knockouts. Clone 1A2 has a clean frame shift mutation on both alleles, with a one base deletion on allele A and a 4 base deletion on allele B. Clone 2D2 has a clean frame shift mutation, with a 1 base deletion in each allele.

3.3.2 *Immobilized protein phage display selections for CD28 and CD3ε binding peptides yield no candidate peptide sequences*

Two phage display experiments were performed in series to identify peptide sequences that show preferential binding to the extracellular domain of human CD28 or CD3ε using recombinant proteins with an Fc tag for immobilization on Protein G plates. Experimental design improvements were made after the first experiment to increase likelihood of enriching for binding peptides.

The first phage display experiment used immobilized IgG as a negative selection, to remove any phage that preferentially bind to the Fc portion of the recombinant proteins or the Protein G plates. However, upon sequencing, a large majority (18% of round 4 and 55% of round 5) of the selected phage contained the plastic-binding motif "WXXW".[39] The phage display protocol was likely exerting strong selective pressure for affinity to plastic plates and tubes.

In the second experiment, the phage library was incubated in an empty plastic well for 1-hour prior to negative and positive selection steps to remove plastic-binding peptides. This successfully reduced the prevalence of the "WXXW" motif to 0%.

Phage clones from each experiment were evaluated for binding to immobilized CD3ε and CD28 proteins, as well as uncoated Protein G plates. All phage clones tested from the first two phage display experiments exhibited higher binding to plastic wells than protein-coated wells and none showed significantly higher binding to either protein compared to insertless phage (Figure 3.4 a & b). Next generation sequencing (NGS) was used to re-analyze the final round of enriched phage clones from the second protein immobilized phage display experiment. These sequences were compared to a phage library that was amplified multiple times without selection pressure to eliminate preferentially amplified phage clones (parasitic sequences).[17] Six new sequences, three for each target, were chosen for cloning into the phage vector for binding studies based on frequency and dominant motif analysis.[40] Of the six sequences, three phage clones showed higher binding to targets over insertless phage (data not shown). An ELISA binding study was repeated

for the three phage clones and identified one peptide sequence with selected specificity towards CD28, clone CD28_B (Figure 3.4 c).

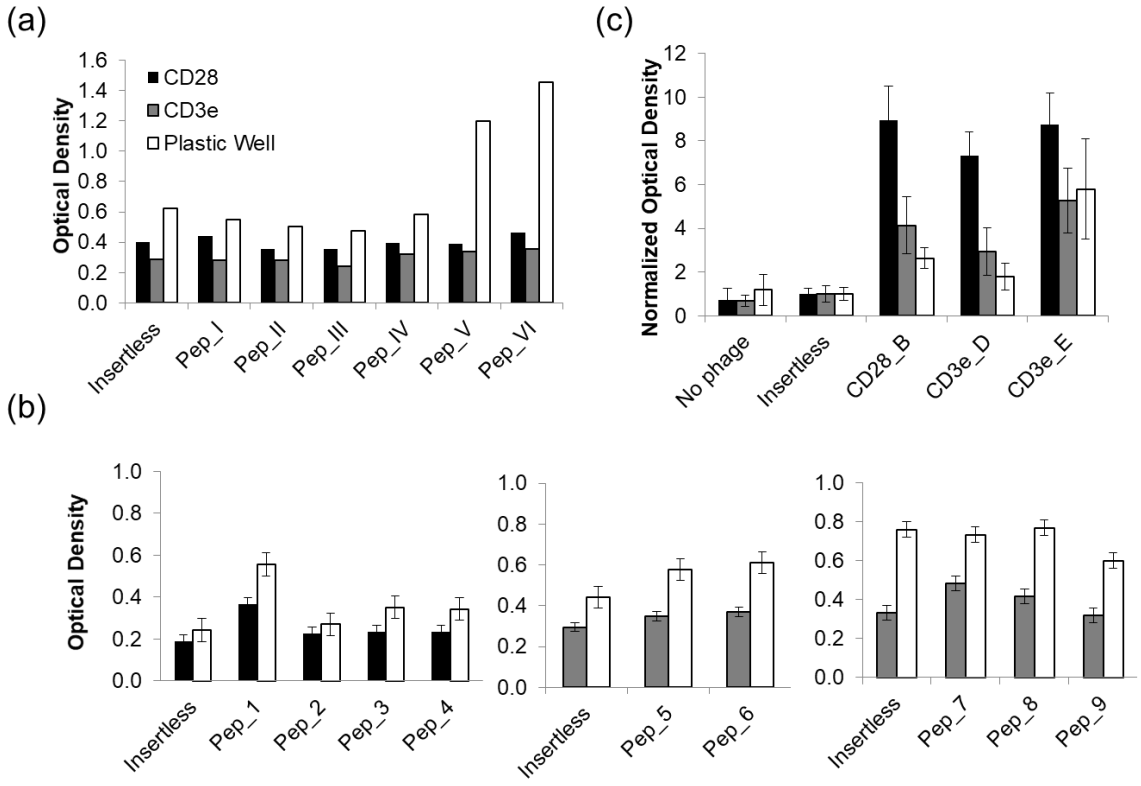

Figure 3.4. ELISA phage binding study results from immobilized protein experiments. (a) Six peptides from the first phage display experiment compared to insertless phage. Data taken in singlet. (b) Four promising CD28 binding phage and five promising CD3ε binding phage from the second experiment compared to the insertless phage. Mean of 3 replicates with standard deviation shown. (c) One promising CD28 binding phage and two promising CD3ε binding phage from second experiment after NGS sequencing, normalized to insertless phage binding. Data shown as mean ± SD (n=3). Representative of 3 independent experiments.

This phage displayed peptide (CD28_B) was characterized further for binding to CD28 in the native conformation using cell lines that express CD28 (Jurkat) or do not express CD28 (HeLa). The CD28_B peptide did not show preferential binding to Jurkat cells, or higher binding to either cell type over an insertless phage control (Figure 3.5).

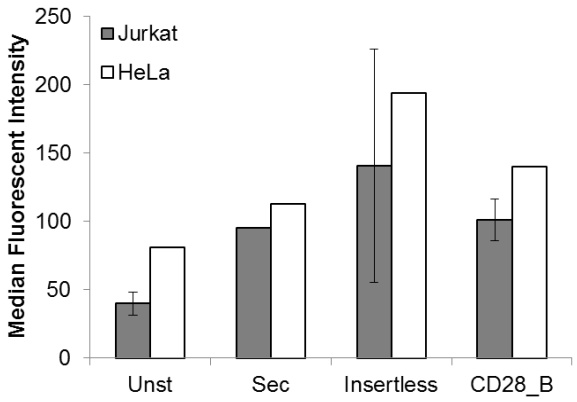

Figure 3.5. CD28_B Phage Clone Binding to Jurkat (CD28+) Cell Line and HeLa (CD28-) Cell Line. Data shown is mean ± SD (n=3).

We hypothesize that as a membrane-bound receptor, CD28 does not maintain its native conformation in the recombinant form and therefore peptides selected against the recombinant protein will not bind to the native receptor. CD28 is a membrane-bound receptor and may not be able to adopt the native conformation in a soluble, recombinant form.[41,42] Alternatively, the epitope CD28_B binds to on recombinant CD28 could be sterically blocked in the membrane bound form. Additional phage display experiments were conducted either solely on cell lines differentially expressing CD3ε and CD28, or in combination with recombinant proteins. In other binding studies a monoclonal anti-CD28 antibody was shown to be able to bind both the recombinant and cell-bound CD28 receptor, suggesting that a combinatorial selection approach is feasible (data not shown).

3.3.3 *Cell and combinatorial phage display selections for CD28 and CD3ε binding peptides yield nonspecific binder*

In the first cell-based phage display experiment, wildtype Jurkat cells were used for positive selection and the CD3ε and CD28 Jurkat knockout clones were used for negative selection. Rounds 3 and 4 from both the CD3ε and CD28 were sequences by NGS, with the top 5 from each round shown in Table 3.5. The top 5 sequences from both the CD3ε and CD28 phage display experiments contained very similar sequences, with one peptide family (variations of ARAEPEANLWLL, shown in blue) dominating both selections.

Table 3.5. Next generation sequencing results from first cell-based phage display experiment. Peptides with similar sequences indicated by color.

CD3ε		CD28	
Round 3	**Round 4**	**Round 3**	**Round 4**
ARAEPEANLWLL (57.4%)	ARAEPEANLWLL (98.9%)	ARAEPEANLWLL (55.5%)	ARAEPEANLWLL (98.9%)
GEPPPIALELPT (38.1%)	GEPPPIALELPT (0.33%)	GEPPPIALELPT (40.4%)	GEPPPIALELPT (0.33%)
FGKCCNMVGSAR	ACAEPEANLWLL	FGKCCNMVGSAR	DWSSWVYRDPQT
DWSSWVYRDPQT	DWSSWVYRDPQT	DWSSWVYRDPQT	ACAEPEANLWLL
ACAEPEANLWLL	ARTEPEANLWLL	ACAEPEANLWLL	ARAEPEANLRLL

These results suggest that the phage display experiment did not select for peptides with specificity to either CD3ε or CD28. In addition the peptide sequence "DWSSWVYRDPQT" was previously identified by our lab to be a preferentially amplifying phage clone during a cell phage display experiment for macrophage binding peptides.[17] To confirm our hypothesis, the other three peptides were cloned into the phage vector for further binding studies (Figure 3.6 a). None of the phage clones showed preferential binding, except for "GEPPPIALELPT" (denoted as GEP) that showed slight preferential binding and slightly higher binding to CD3ε+ cells. However, a second flow cytometry binding experiment concluded that the GEP phage displayed peptide did not show higher binding to any of the cell types tested over an insertless phage control (Figure 3.6 b).

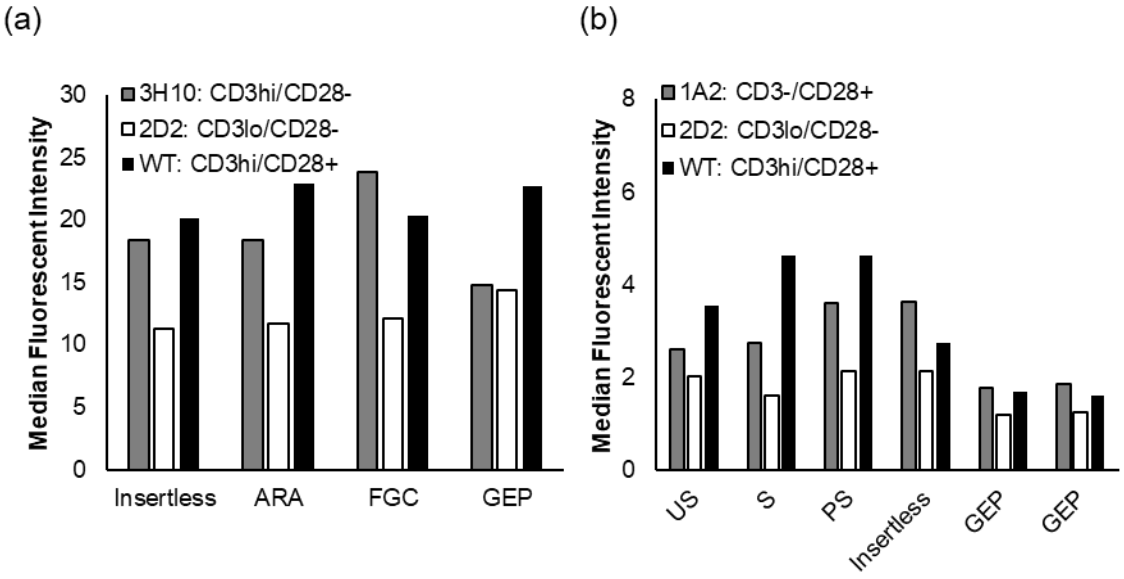

Figure 3.6. Flow cytometry binding studies of phage clones identified in the first cell-based phage display study. (a) Top 3 identified clones. Results are average of duplicates. (b) Repeat binding with GEP peptide. Results are average of duplicates.

Phage display with cells as targets enables exclusive targeting of extracellular protein regions. However, disadvantages of phage display with cells as targets include high target complexity, low target concentration, and low target accessibility.[43] We hypothesize that the low target concentration of CD3ε and CD28 on the surface of Jurkat cells reduced our ability to identify binding peptides.

Low target concentration limits the percent of peptide bound at equilibrium and can make phage display too stringent. Assuming one binding site per protein, equations 3.1 and 3.2 can be used to describe the binding reaction and dissociation constant (K_d) in a peptide and protein mixture, where *[Peptide]* is the concentration of free peptide, *[Protein]* is the concentration of unbound target protein, *[PeptideProtein]* is the concentration of peptide-bound protein. The percent of peptide bound at equilibrium can be estimated for peptides with hypothetical affinities to the target (Table 3.6). At a low target concentration, for example 1 nM, a peptide with strong target affinity (K_d = 1 nM) is 50% bound and has high probability of being selected. However, peptides with weaker affinities that could still be useful in a multivalent activation platform (K_d = 100 nM and K_d = 1 μM) are only ~1% and ~0.1% bound, respectively. The vast majority of these peptides would be unbound at equilibrium and discarded.

$$[Peptide] + [Protein] \leftrightarrow [PeptideProtein] \quad (3.1)$$

$$K_d = [Peptide][Protein] \div [PeptideProtein] \quad (3.2)$$

Table 3.6. Percent phage bound to target at equilibrium for three peptides with varying hypothetical K_d.

Selection Method	[Target]	% of peptide bound at equilibrium		
		K_d = 1 nM	K_d = 100 nM	K_d = 1 μM
Cells/immobilized protein	1 nM	50 %	1 %	0.1 %
Protein in solution	2 μM	99.95 %	95.2 %	66.7 %

To address this issue in our next phage display experiment, we increased the target concentration to 2 μM by panning against protein in solution and collecting them with Protein G magnetic beads for the first two rounds of selection. This approach increases the likelihood of capturing bound phage. In all rounds, positively selected phage were be transferred to a new microcentrifuge tube prior to elution to eliminate plastic binding phage.[44] In addition, an organic solvent partitioning method was employed to improve separation of bead-bound phage and unbound phage.[37] The libraries were split for the 3rd round between using protein in solution or

cells as the selection method. By round 3, the phage library has gone through 2 rounds of amplification, increasing the chances of capturing phage even if they have a lower affinity.

Significant wildtype phage contamination was a persistent issue in this phage display experiment, limiting the number of selection rounds prior to sequencing to 3, after which wildtype phage made up >30% of the entire phage library. Amplified phage libraries from each round 2, and unamplified libraries from round 3 were sequenced by NGS.

Data was analyzed by frequency and fidelity of peptide sequences for each target. Preferentially amplifying sequences were eliminated, and motifs were identified using the MEME suite web server.[45] The highest abundance peptide from each motif family was selected for binding experiments.

Three peptide sequences from the CD3ε and four peptide sequences from the CD28 phage display sequencing results were chosen to be cloned into phage vectors and tested in flow cytometry binding studies. Clone CD28_D with the peptide sequence "SLTHVSVNIAAS" was the only phage to show higher binding compared to insertless phage control (Figure 3.7). However, this phage did not have binding specificity to the CD28+ cell line over the CD28- cell line, it exhibited opposite binding behavior. Additional binding studies show that the binding of CD28_D increases with increasing CD3ε expression (WT Jurkats have moderate CD3ε expression while the 2D2 mutant has high CD3ε expression).

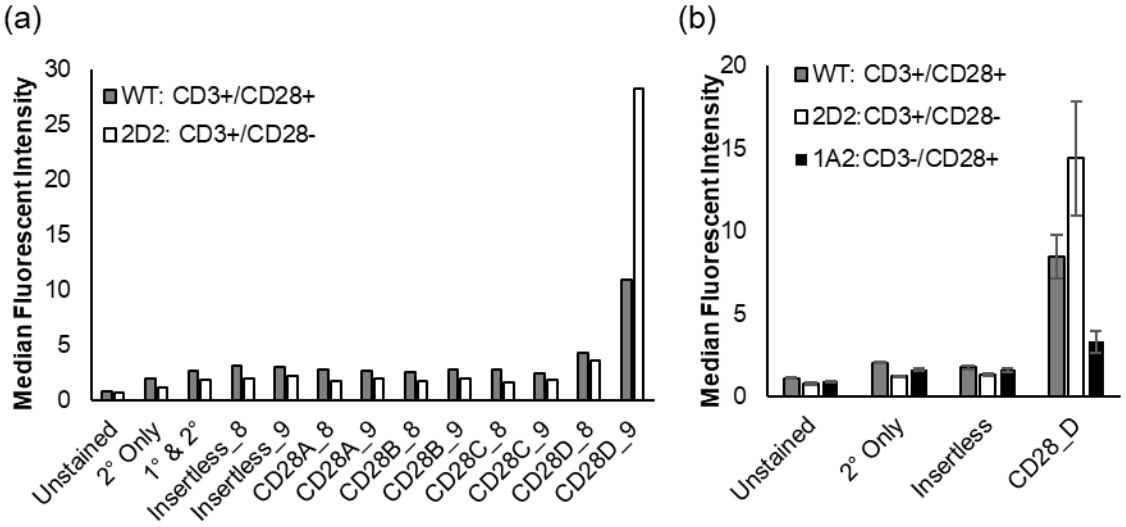

Figure 3.7. Binding results of CD28 sequences identified in combinatorial phage display. (a) Four phage clones at two different concentrations (5×10^8 or 5×10^9 PFU/μL). Data in singlet. (b) Clone CD28_D binding compared to insertless phage. Data are shown as mean ± SD (n=3).

The lack of specificity of the CD28_D phage displayed peptide for the CD28 receptor did not warrant additional development of the peptide sequence. Due to the lack of affinity and specificity for either receptor target after multiple iterations of phage display experiments, we moved to SELEX as an alternative library evolution technique with the potential for higher affinity and specificity binders. Peptides selected through phage display typically have moderate affinities (μM-nM), whereas aptamers selected through SELEX can have affinities in the pM-nM range. This increase in affinity and specificity is likely due to the increased complexity and size of aptamers that allow for tertiary structure formation similar to antibodies.

3.3.4 *2'-fluoropyrimidine RNA SELEX for CD28 binding aptamer yields two consensus motifs*

Next generation sequencing revealed 11,885 unique 25-nt sequences in the round 9 pool, with the 10 most frequent sequences and 60 most frequent sequences making up 63 and 87% of the sequencing reads, respectively. Phylogenetic tree analysis of the 25-nt random regions of the 60 most frequent sequences revealed three separate sequence clusters (Figure 3.8 a). Sequence alignment was performed for each cluster and identified two potential CD28 binding motifs "TTTCGAGTCTT--CA-G" and "GGGT-CAGGGC" (Figure 3.8 b). Over 80% of the sequences that passed quality control contained one of these two binding motifs, with nearly equal representation of each motif. The highest abundance aptamer from each cluster was selected for binding studies to human CD28.

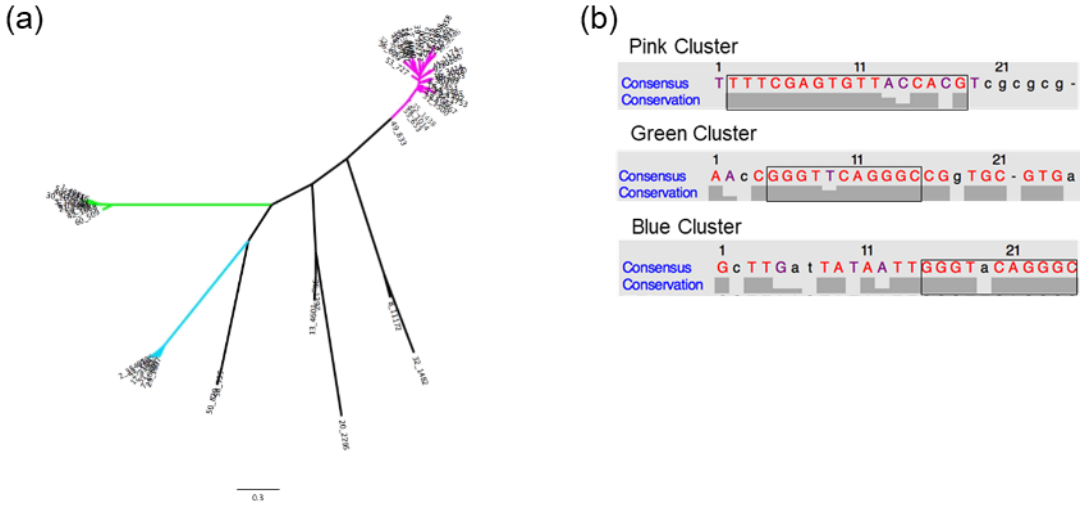

Figure 3.8. Sequence Alignment of 60 Most Frequent Sequences. (a) Phylogenetic tree of 60 most-frequent aptamer sequences with sequence clusters shown in magenta, green, and cyan; and (b) sequence alignment of random 25-nt region of the three sequence clusters reveals two independent sequences of possible CD28 binding sites, boxed in black.

3.3.5 *2'-fluoropyrimidine RNA aptamers do not exhibit binding to CD28 protein or CD28+ cells*

Three aptamers, one from each phylogenetic tree cluster, were chosen for evaluation in binding studies. Each individual aptamer as well as the bulk round 9 library was synthesized with biotinylated GMP spiked into the transcription reaction. Aptamers were dimerized using a fluorescently labeled streptavidin as reported previously in cell binding studies for a murine CD28 aptamer.[25] Binding to the wildtype (WT) Jurkat cell line as well as a CD28- mutant (3H10) were evaluated by flow cytometry. The aptamer with the highest frequency in the round 9 library (Green 1) showed moderate but preferential binding to WT cells compared to the CD28- cell line (Figure 3.9).

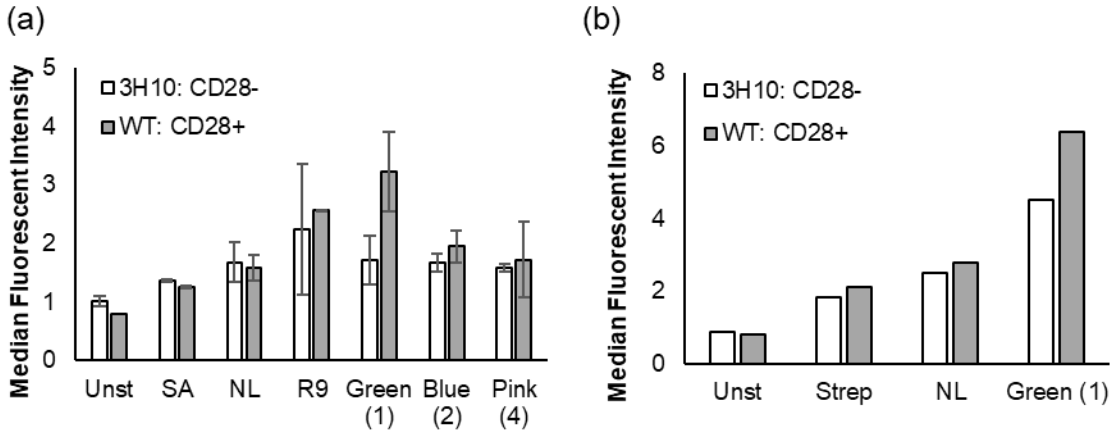

Figure 3.9. Flow Cytometry Binding Studies of 2'F RNA Aptamers. (a) Most frequent aptamer from each motif family. Data shown is mean ± SD (n=3). (b) Repeat binding study of highest frequency aptamer. Data shown is mean of duplicate.

The binding kinetics of this aptamer to recombinant CD28 protein was evaluated by OctetRed. No appreciable binding was observed at the range of concentrations tested (2 nM – 2 µM) (Figure 3.10).

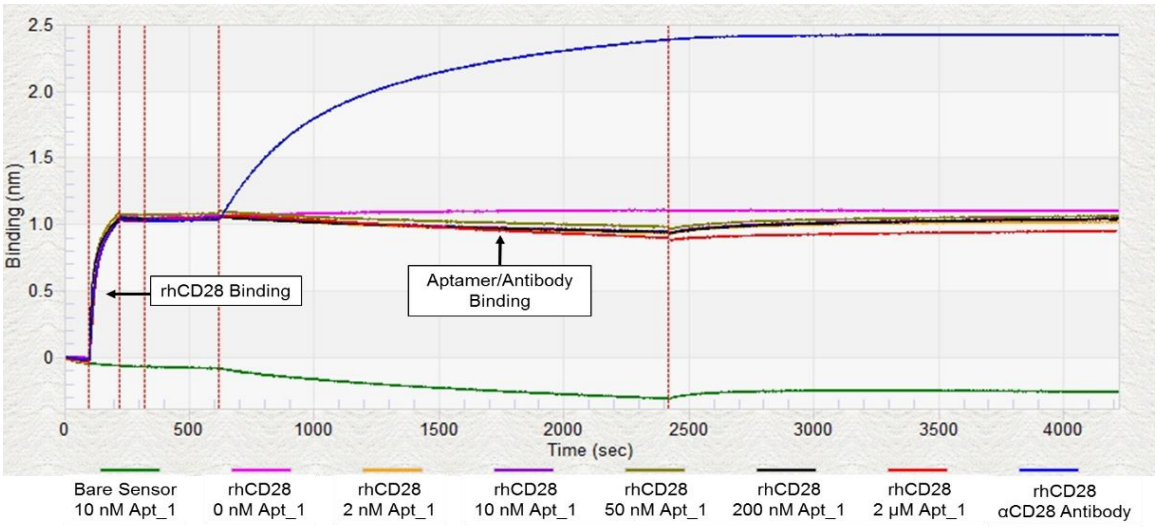

Figure 3.10. Octet Binding Study of Aptamer to Recombinant Human CD28. Binding of the "Green 1" aptamer to recombinant human CD28 at varying temperatures. Positive control was anti-CD28 monoclonal antibody clone 28.2 (blue).

These results suggest that this SELEX experiment did not converge on a human CD28 binding aptamer. The inability to monitor binding affinity of the bulk library throughout the rounds inhibited the tracking of enrichment and negated the option to modify selection parameters. These experimental limitations led to future SELEX experiments being performed using a ssDNA aptamer library rather than an RNA library. While ssDNA is less flexible than RNA (making it theoretically less likely to form tertiary structures) and unmodified DNA is more prone to nuclease degradation than modified RNA, ssDNA can more readily be tracked throughout rounds by synthesis with fluorescently labeled primer.[22]

3.3.6 *Recombinant protein ssDNA SELEX enriches for high affinity and low specificity aptamers*

Six rounds of recombinant protein SELEX were performed in parallel for human CD28 and human CD3ε using a ssDNA aptamer library with a 52-nucleotide random region. Stringency was applied throughout rounds by decreasing the concentration of target protein and aptamer library, and increasing the duration and number of washes. FITC-labeled output aptamers from rounds 2-6 were used in binding studies to recombinant proteins immobilized on magnetic beads and to primary human T cells. Fc labeled recombinant proteins were used with Protein G coated magnetic beads for selection. In order to ensure observed binding was not to the beads themselves,

biotinylated proteins and streptavidin magnetic beads were used in binding studies as an orthogonal protein display approach. Proper display of proteins was confirmed using anti-CD3 and anti-CD28 antibodies (Figure 3.11). The anti-CD3 antibody only recognizes CD3ε in the heterodimer form with CD3δ. The recombinant CD3εδ heterodimer was used in round binding studies so that the positive antibody control could be used.

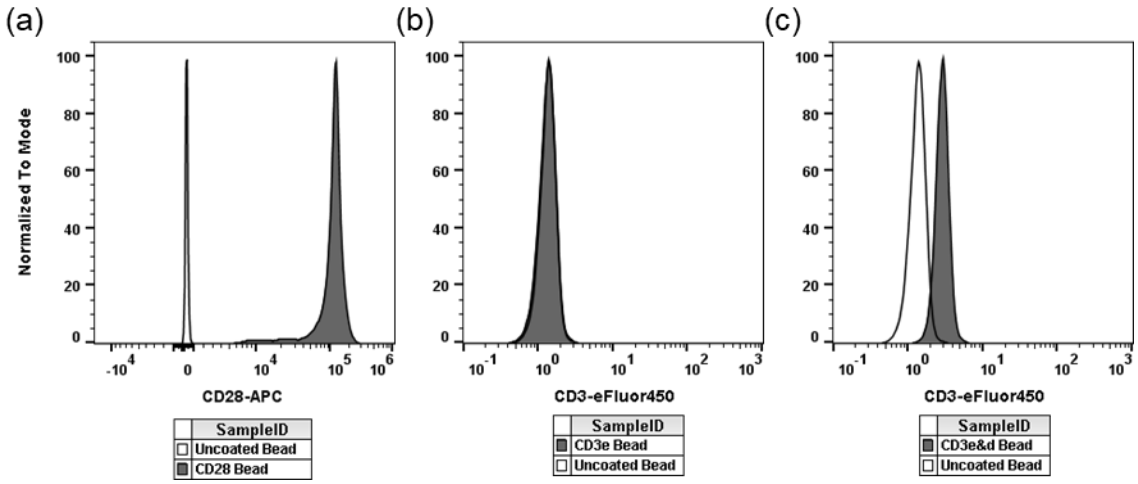

Figure 3.11. Antibody binding to recombinant protein coated beads. (a) Anti-CD3 binding to CD3εδ and CD3ε coated beads. (b) Anti-CD28 binding to CD28 coated beads.

In all rounds tested, the selected aptamer library pools bound to the recombinant protein coated beads more than the random control aptamer (Figure 3.12. a & b). However, when the rounds with the highest median fluorescent intensity (MFI) of binding to target protein (round 6 for CD3ε and round 5 for CD28) were incubated with their non-cognate receptor, they also demonstrated high binding (Figure 3.12 c & d). This suggests that the aptamer libraries did not enrich for specific binding ligands toward either of the recombinant proteins. These ligands could have evolved to bind the Fc domain that is conserved between the two recombinant proteins, though the human IgG1 negative selection was designed to remove Fc binding aptamers. Additional binding studies would be needed to confirm this hypothesis.

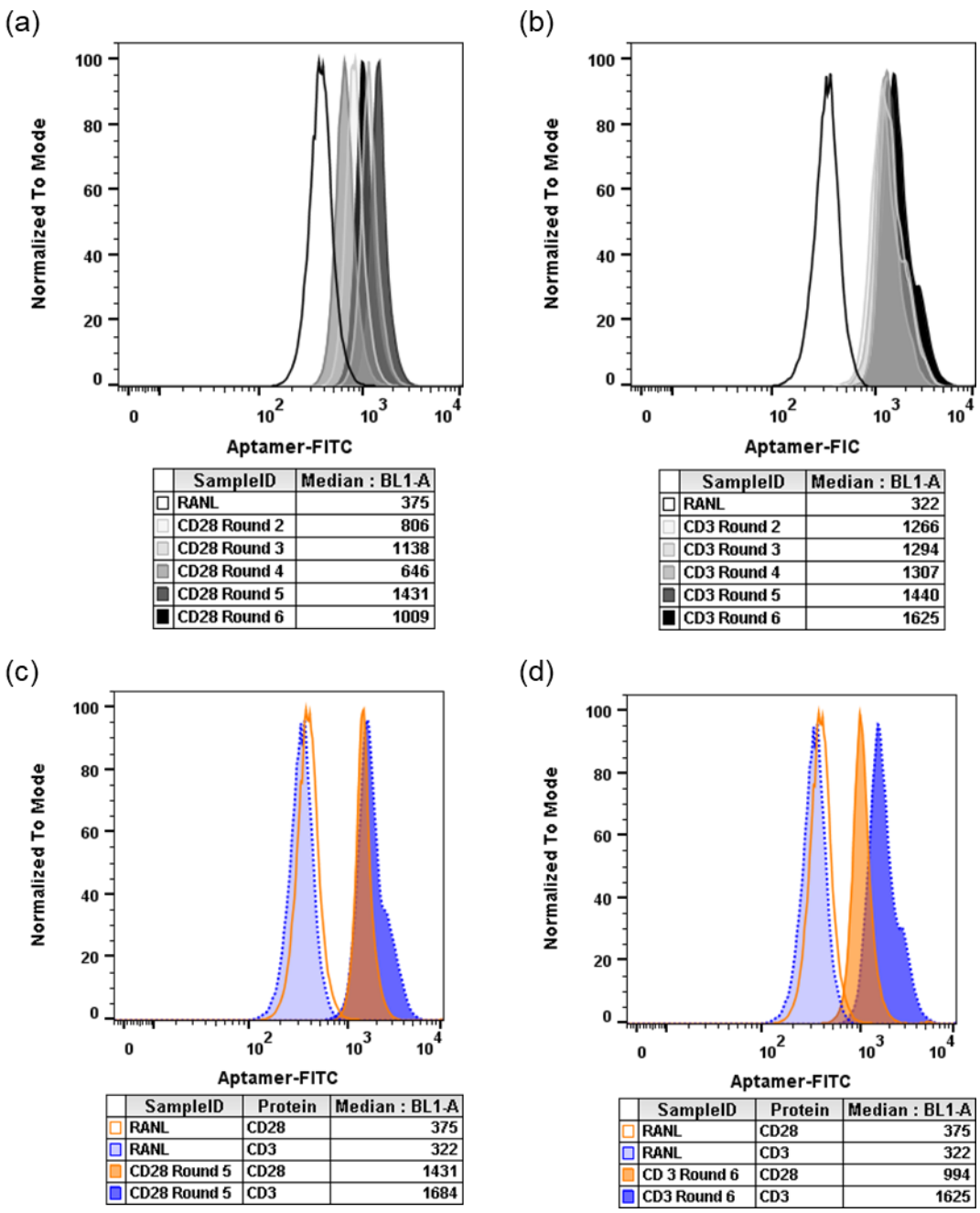

Figure 3.12. Aptamer round libraries binding to recombinant protein coated beads. (a) Round binding of CD3ε selected aptamers to CD3εδ coated beads.

Lastly, binding studies were performed on primary human T cells that express CD3ε and CD28 using the highest affinity round libraries from each selection. No observable binding above the random aptamer negative control was observed (Figure 3.13).

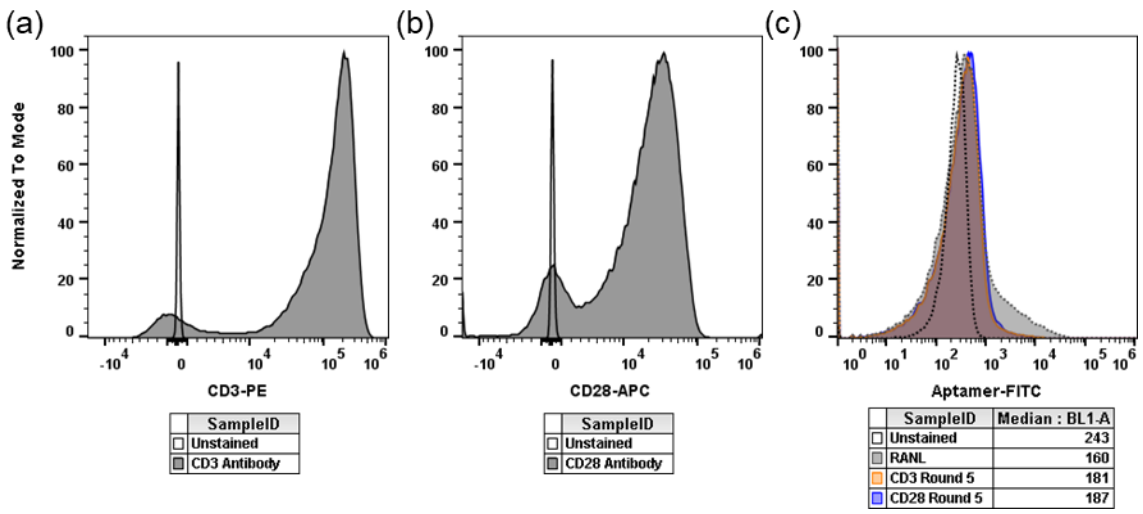

Figure 3.13. Aptamer libraries binding to primary human T cells. (a) CD3 expression and (b) CD28 expression on primary human T cells. (c) Binding of aptamer pools to primary T cells.

3.4 CONCLUSIONS AND FUTURE STUDIES

The objective of this work was to identify high affinity and high specificity ligands for targeting the stimulatory and co-stimulatory receptors CD3ε and CD28 on human T cells for use in a totally synthetic activation platform. Phage display and SELEX methods were employed in attempts to identify peptide or aptamer ligands against these targets, respectively. Methods were developed to sequence peptide and aptamer libraries using next-generation sequencing, and analysis pipelines were validated with a known binding pair.[17] Through multiple phage display experiments using both recombinant proteins and CRISPR knockout cell lines, no peptides with high affinity to either target were identified. In two SELEX experiments using 2'-fluoropyrimidine modified RNA aptamers or ssDNA aptamers and recombinant proteins for selection, no aptamer ligands with high specificity towards either protein were selected.

Recombinant protein SELEX using a FITC-labeled ssDNA aptamer library demonstrated that high affinity aptamers could be generated against targets, with binding observed at aptamer concentrations of 250 nM. Future selection experiments should use multiple protein target display and elution methods to specifically select for protein domain binding. For example, crossover-SELEX that alternates between recombinant proteins and protein expressing cells could be used to prevent the evolution of aptamers that bind to the non-native portions of recombinant proteins.[46] In addition, specific elution of aptamers with antibodies against the target receptor could be used

to elute only aptamers bound to the same epitope as the antibody.[47] Once these aptamer ligands are identified, there are promising applications in T cell selection via magnetic activated cell sorting and activation using multi-valent display of aptamers that can dimerize the T cell receptor and costimulatory receptors.

3.5 ACKNOWLEDGEMENTS

This work was supported by Juno Therapeutics, Inc. B.R.O. was supported by a National Science Foundation Graduate Research Fellowship [DGE-1256082].

3.6 REFERENCES

1. Wang, X. & Rivière, I. Clinical manufacturing of CAR T cells: foundation of a promising therapy. *Mol. Ther. oncolytics* **3,** 16015 (2016).
2. Malissen, B. & Bongrand, P. Early T Cell Activation: Integrating Biochemical, Structural, and Biophysical Cues. *Annu. Rev. Immunol.* **33,** 539–561 (2015).
3. Smith-Garvin, J. E., Koretzky, G. a & Jordan, M. S. T cell activation. *Annu. Rev. Immunol.* **27,** 591–619 (2009).
4. Curtsinger, J. M. & Mescher, M. F. Inflammatory cytokines as a third signal for T cell activation. *Curr. Opin. Immunol.* **22,** 333–340 (2010).
5. Schluns, K. S. & Lefrançois, L. Cytokine control of memory T-cell development and survival. *Nat. Rev. Immunol.* **3,** 269–279 (2003).
6. Singh, H., Huls, H. & Cooper, L. J. N. A new approach to gene therapy using Sleeping Beauty to genetically modify clinical-grade T cells to target CD19. *Immunol. Rev.* **257,** 181–190 (2014).
7. Trickett, A. & Kwan, Y. L. T cell stimulation and expansion using anti-CD3/CD28 beads. *J. Immunol. Methods* **275,** 251–255 (2003).
8. Kalamasz, D. *et al.* Optimization of human T-cell expansion ex vivo using magnetic beads conjugated with anti-CD3 and Anti-CD28 antibodies. *J. Immunother.* **27,** 405–418 (2004).
9. Letourneur, F. & Klausner, R. D. Activation of T Cells by a Tyrosine Kinase Activation Domain in the Cytoplasmic Tail of CD3 ε. *Science (80-.).* (1992).
10. Liu, J. K. H. The history of monoclonal antibody development - Progress, remaining challenges and future innovations. *Ann. Med. Surg.* **3,** 113–116 (2014).
11. Kedzierski, S., Khoshnejad, M. & Caltagirone, G. T. Synthetic Antibodies: The Emerging Field of Aptamers. *Bioprocess. J.* 46–49 (2013).
12. Bray, B. L. Innovation: Large-scale manufacture of peptide therapeutics by chemical synthesis. *Nat. Rev. Drug Discov.* **2,** 587–593 (2003).
13. Stoltenburg, R., Reinemann, C. & Strehlitz, B. SELEX--a (r)evolutionary method to generate high-affinity nucleic acid ligands. *Biomol. Eng.* **24,** 381–403 (2007).
14. Carothers, J. M., Oestreich, S. C., Davis, J. H. & Szostak, J. W. Informational Complexity and Functional Activity of RNA Structures Informational Complexity and Functional Activity of RNA Structures. *Science (80-.).* **126,** 5130–5137 (2004).
15. Carlson, R. The changing economics of DNA synthesis. *Nat. Biotechnol.* **27,** 1091–1094 (2009).
16. Molek, P., Strukelj, B. & Bratkovic, T. Peptide phage display as a tool for drug discovery: targeting membrane receptors. *Molecules* **16,** 857–87 (2011).
17. Liu, G. W. *et al.* Efficient Identification of Murine M2 Macrophage Peptide Targeting Ligands by Phage Display and Next-Generation Sequencing. *Bioconjug. Chem.* **26,** 1811–1817 (2015).
18. Cieslewicz, M. *et al.* Targeted delivery of proapoptotic peptides to tumor-associated macrophages improves survival. *Proc. Natl. Acad. Sci. U. S. A.* (2013). doi:10.1073/pnas.1312197110
19. Sellers, D. L. *et al.* Targeted axonal import (TAxI) peptide delivers functional proteins into spinal cord motor neurons after peripheral administration. *Proc. Natl. Acad. Sci. U. S. A.* **113,** 2514–2519 (2016).
20. Whaley, S. R., English, D. S., Hu, E. L., Barbara, P. F. & Belcher, A. M. Selection of

peptides with semiconductor binding specificity for directed nanocrystal assembly. *Nature* **405,** 665–8 (2000).
21. Hetian, L. *et al.* A novel peptide isolated from a phage display library inhibits tumor growth and metastasis by blocking the binding of vascular endothelial growth factor to its kinase domain receptor. *J. Biol. Chem.* **277,** 43137–43142 (2002).
22. Sefah, K., Shangguan, D., Xiong, X., O'Donoghue, M. B. & Tan, W. Development of DNA aptamers using Cell-SELEX. *Nat. Protoc.* **5,** 1169–1185 (2010).
23. Keefe, A. D. & Cload, S. T. SELEX with modified nucleotides. *Curr. Opin. Chem. Biol.* **12,** 448–456 (2008).
24. Dollins, C. M., Nair, S. & Sullenger, B. A. Aptamers in immunotherapy. *Hum. Gene Ther.* **19,** 443–50 (2008).
25. Pratico, E. D., Sullenger, B. a & Nair, S. K. Identification and characterization of an agonistic aptamer against the T cell costimulatory receptor, OX40. *Nucleic Acid Ther.* **23,** 35–43 (2013).
26. Pastor, F. *et al.* CD28 aptamers as powerful immune response modulators. *Mol. Ther. Nucleic Acids* **2,** e98 (2013).
27. Dollins, C. M. *et al.* Assembling OX40 aptamers on a molecular scaffold to create a receptor-activating aptamer. *Chem. Biol.* **15,** 675–82 (2008).
28. Shendure, J. & Ji, H. Next-generation DNA sequencing. *Nat. Biotechnol.* **26,** 1135–1145 (2008).
29. Matochko, W. L., Cory Li, S., Tang, S. K. Y. & Derda, R. Prospective identification of parasitic sequences in phage display screens. *Nucleic Acids Res.* **42,** 1784–98 (2014).
30. 't Hoen, P. a C. *et al.* Phage display screening without repetitious selection rounds. *Anal. Biochem.* **421,** 622–31 (2012).
31. Ngubane, N. a C. *et al.* High-throughput sequencing enhanced phage display identifies peptides that bind mycobacteria. *PLoS One* **8,** e77844 (2013).
32. Rentero Rebollo, I., Sabisz, M., Baeriswyl, V. & Heinis, C. Identification of target-binding peptide motifs by high-throughput sequencing of phage-selected peptides. *Nucleic Acids Res.* 1–12 (2014). doi:10.1093/nar/gku940
33. Cho, M. *et al.* Quantitative selection of DNA aptamers through microfluidic selection and high-throughput sequencing. *Proc. Natl. Acad. Sci. U. S. A.* **107,** 15373–15378 (2010).
34. Berezhnoy, A. *et al.* Isolation and Optimization of Murine IL-10 Receptor Blocking Oligonucleotide Aptamers Using High-throughput Sequencing. *Mol. Ther.* **20,** 1242–1250 (2012).
35. Cong, L. *et al.* Multiplex Genome Engineering Using CRISPR/Cas Systems. *Science (80-.).* **339,** (2013).
36. Ran, F. A. *et al.* Genome engineering using the CRISPR-Cas9 system. *Nat Protoc* **8,** 2281–2308 (2013).
37. Giordano, R. J., Cardó-Vila, M., Lahdenranta, J., Pasqualini, R. & Arap, W. Biopanning and rapid analysis of selective interactive ligands. *Nat. Med.* **7,** 1249–53 (2001).
38. Salipante, S. J. *et al.* Whole genome sequencing indicates Corynebacterium jeikeium comprises 4 separate genomospecies and identifies a dominant genomospecies among clinical isolates. *Int. J. Med. Microbiol.* **304,** 1001–1010 (2014).
39. Vodnik, M., Zager, U., Strukelj, B. & Lunder, M. Phage display: Selecting straws instead of a needle from a haystack. *Molecules* **16,** 790–817 (2011).
40. Bailey, T. L. & Elkan, C. Fitting a Mixture Model by Expectation Maximization to

Discover Motifs in Bipolymers. *Proc. Second Int. Conf. Intell. Syst. Mol. Biol.* 28–36 (1994). doi:citeulike-article-id:878292
41. Jones, M. L. *et al.* Targeting membrane proteins for antibody discovery using phage display. *Sci. Rep.* **6,** 26240 (2016).
42. Molek, P., Strukelj, B. & Bratkovic, T. Peptide phage display as a tool for drug discovery: Targeting membrane receptors. *Molecules* (2011). doi:10.3390/molecules16010857
43. Sui, J., Bai, J., Tallarico, A. S. C., Xu, C. & Marasco, W. A. Identification of CD4 and transferrin receptor antibodies by CXCR4 antibody-guided Pathfinder selection. *Eur. J. Biochem.* **270,** 4497–4506 (2003).
44. Watters, J. M., Telleman, P. & Junghans, R. P. An optimized method for cell-based phage display panning. *Immunotechnology* **3,** 21–9 (1997).
45. Bailey, T. L. *et al.* MEME Suite: Tools for motif discovery and searching. *Nucleic Acids Res.* **37,** 202–208 (2009).
46. Mallikaratchy, P. Evolution of complex target SELEX to identify aptamers against mammalian cell-surface antigens. *Molecules* **22,** 1–12 (2017).
47. Zumrut, H. E. *et al.* Ligand-guided selection of aptamers against T-cell Receptor-cluster of differentiation 3 (TCR-CD3) expressed on Jurkat.E6 cells. *Anal. Biochem.* (2016). doi:10.1016/j.ab.2016.08.007

Chapter 4. CATIONIC POLYMERS FOR NON-VIRAL GENE DELIVERY TO HUMAN T CELLS

Brynn R. Olden*, Yilong Cheng*, Jonathan L. Yu, Suzie H. Pun
**Equally contributing authors*

Abstract

The clinical success of chimeric antigen receptor (CAR) T cell immunotherapy in treating multiple blood cancers has created a need for efficient methods of *ex vivo* gene delivery to primary human T cells for cell engineering. Here, we synthesize and evaluate a panel of cationic polymers for gene delivery to both cultured and primary human T cells. We show that a subset of comb- and sunflower-shaped pHEMA-*g*-pDMAEMA polymers can mediate transfection with efficiencies up to 50% in the Jurkat human T cell line with minimal concomitant toxicity (>90% viability). We then optimize primary human T cell transfection conditions including activation time, cell density, DNA dose, culture media, and cytokine treatment. We demonstrate transfection of both $CD4^+$ and $CD8^+$ primary human T cells with messenger RNA and plasmid DNA at efficiencies up to 25 and 18%, respectively, with similarly high viability.[†]

[†] Reprint with permission from Olden, B.R., *et al. Journal of Controlled Release (2018)*.
doi: 10.1016/j.jconrel.2018.02.043.

4.1 INTRODUCTION

T lymphocytes are key cells of the adaptive immune system that facilitate recognition and clearance of disease. In cancer, T cells primed with cancer antigens can often effectively eliminate cancer cells.[1] However, tumors can hinder T cell activity by creating a poorly immunogenic environment and expressing anti-inflammatory cytokines and exhaustion signals that push T cells towards a regulatory or exhausted phenotype.[2] Over the last decade, scientists and clinicians have developed new immunotherapies that can overcome these barriers to allow T cells to better recognize and clear tumors.[3,4] One therapy that has shown remarkable promise, especially in hematologic cancers, is a cellular therapy using autologous, genetically-modified T cells that express a chimeric antigen receptor (CAR).[5] These CARs consist of an extracellular domain that recognizes a surface epitope on cancer cells, and an intracellular domain that contains co-stimulatory signals that trigger T cell expansion, inflammatory cytokine production, and cytotoxic action against cancer cells.[6]

To generate a CAR T cell product, primary human T cells must be genetically modified to express the CAR protein. Most clinical trials for CAR T cells use gammaretroviral and lentiviral methods for gene delivery.[7] These viruses are efficient at gene delivery, have low intrinsic immunogenicity, and integrate into the host genome, resulting in permanent CAR expression.[8]

However, viral vectors have important limitations: DNA cargo size, potential for insertional mutagenesis, cost and challenge of production, lot-to-lot variability, and increased regulatory requirements make them a costly choice for use in CAR T cell manufacturing.[9] Further, construction and production of viral vectors is time-intensive and often a limiting factor in screening CAR constructs at the research phase. In addition, lentiviral vectors are limited to a cargo size of ~10 kb, which could limit the future ability to introduce additional functionalities into CAR T cells including kill-switches, triggered cytokine production, and multiplexed gene delivery.[10] Non-viral gene delivery methods like electroporation and chemical transfection reagents are an attractive alternative due to their reduced cost, their easy adaptation to various cargo, and their improved safety profile compared to viral vectors but historically have low gene transfer efficiencies in T cells.[11,12]

Cationic lipid and polymer-based reagents have been developed extensively as gene delivery vehicles.[13] Unlike viruses, these materials are not limited to a size or type of genetic cargo they

can carry. This makes them attractive delivery vehicles, because they can deliver large plasmids (pDNA), as well as messenger RNA (mRNA) and small interfering RNA (siRNA). Polymer-based reagents are especially of interest due to their controllable chemical diversity and shelf stability. Polymers for gene delivery are typically made of cationic monomers that contain primary, secondary, and/or tertiary amine groups that can complex with negatively charged nucleic acid to form condensed polymer-nucleic acid nanoparticle complexes, called "polyplexes".[14] Polyethylenimine (PEI) and poly(2-dimethylaminoethyl methacrylate) (pDMAEMA) are two classes of cationic polymers that have been studied extensively.[15,16] Branched PEI contains primary, secondary, and tertiary amines at an approximate 1:2:1 ratio whereas pDMAEMA only contains tertiary amines. Polyplexes are formulated with an excess positive charge to promote electrostatic binding to the negative cell membrane.[17] Highly cationic polyplexes are taken up into cells by interaction with surface proteoglycans, followed by internalization via endocytosis.[18]

Very few polymers have been developed as gene delivery systems specifically for primary human T cells. Low molecular weight PEI (5 kDa) has been conjugated to transferrin to increase uptake of siRNA in activated primary T cells, which resulted in 50% gene silencing.[19,20] The Freitag group polymerized 20 "arms" of pDMAEMA off a silsesquioxane core and used this star polymer to deliver pDNA or siRNA, obtaining approximately 50% knockdown from siRNA delivery, and 10-50% transfection efficiency with 40-100% viability using pDNA.[21] This group also recently reported 13% transfection efficiency of primary T cells using this material with cell viability of 80%.[22] Most recently, the Stephan group reported a nanoparticle formulation with a poly(β-amino ester) core for DNA condensation and an antibody-conjugated polyglutamic acid shell for receptor-mediated uptake that was successfully used for *in vitro* and *in vivo* gene delivery to primary murine T cells, achieving ~3% transfection efficiency *in vitro* and ~1.5% *in vivo*.[23] This same nanoparticle system was able to achieve up to ~80% *in vitro* transfection efficiency of mRNA in primary human T cells.[24]

The advances in controlled radical polymerization techniques over the last decade have significantly increased the design space for gene delivery polymers.[25–27] Chemists can specifically tune molecular weight, create complex architectures, and build in environmentally-responsive components.[28,29] In our laboratory, we found that altering the architecture of a pDMAEMA polymer from linear-branched (comb) to cyclic-branched (sunflower) decreased the toxicity and increased the efficiency of gene delivery to multiple cancer cell lines.[30] Including an endosomal

lytic peptide in a pH sensitive block of a statistical co-polymer improved endosomal escape of polyplexes and increased subsequent gene expression in many cell lines.[31]

The aim of this study was to empirically evaluate a panel of polymer architectures developed recently by our group for efficacy as an *ex vivo* gene delivery agent to primary human T cells. Polymers identified in this study could hold potential for future applications in adoptive T cell therapy manufacturing. We were surprised to find that the trends in polymer gene transfer efficiency in our previous adherent cell line studies did not hold for either cultured (Jurkat) T cells or primary T cells. In this current work, we identified a specific architecture of comb pDMAEMA polymers that, combined with optimized transfection protocols, showed the highest gene transfer efficiency to cultured and primary human T cells.

4.2 Materials and Methods

4.2.1 *Synthesis of $pHEMA_{15}$-g-pDMAEMA*

$pHEMA_{15}$-g-pDMAEMA with different degrees of polymerization (DP) of DMAEMA was synthesized by three steps listed in Supplementary Information. Polymers were characterized by gel permeation chromatography (GPC) and nuclear magnetic resonance (1H NMR) (Supplemental Figure 4.1).

4.2.2 *Polymer preparation*

Branched polyethylenimine (Mw ~ 25,000) was purchased from Sigma and diluted to 65 µg/mL in sterile molecular grade H_2O for transfection studies. Linear $pDMAEMA_{290}$, comb and sunflower polymers with a core of $pHEMA_{25}$, and virus-inspired polymer for endosomal release (VIPER) were synthesized as reported previously by controlled living radical polymerization.[30,31] Polymers were diluted in sterile molecular grade H_2O to desired amine concentration for transfection studies.

4.2.3 *Antibodies and plasmids*

PE/Cy-7 anti-human CD4 (clone: RPA-T4), APC anti-human CD8 (clone: RPA-T8), and Zombie Violet fixable live-dead stain were purchased from Biolegend and titrated prior to use.

Plasmids were prepared using standard molecular biology techniques. XL10 Gold ultracompetent cells (Stratagene) were transformed with pmaxGFP plasmid (Lonza). A single colony was grown up in an overnight culture, lysed and purified using the NucleoBond Xtra Maxi

Endotoxin Free kit (Macherey-Nagel). Purity and concentration were quantified by Nanodrop and a diagnostic gel. Enhanced green fluorescent protein (eGFP) mRNA was purchased from TriLink and stored in aqueous stock solutions at -80 °C until use.

4.2.4 *Cell culture conditions*

Jurkat cells (human T lymphocyte line) were a kind gift from Dr. Michael Jensen (Seattle Children's Research Institute). Jurkat cells were cultured in RPMI-1640 supplemented with 10% fetal bovine serum (v/v). Cells were used in transfection studies 18-24 hours after passaging.

Cryopreserved vials of healthy donor primary human T lymphocytes, isolated by magnetic activated cell sorting, were generously provided by Juno Therapeutics. Thawed cells were washed once in basal X-VIVO 15 medium (Lonza) before being cultured in X-VIVO 15 supplemented with 2% KnockOut serum replacement (ThermoFisher) and either recombinant human IL-2 (200 IU/mL) or recombinant human IL-21 (10 ng/mL) (Miltenyi) at a density of 1.5×10^6/mL. Cells were rested for 2-16 hours before activation with CD3/CD28 Human T Activator beads (DynaBeads, Gibco) at the recommended 1:1 bead:cell ratio. Cells were activated for 0-72 hours prior to transfection. All cells were maintained in a 37 °C and 5% CO_2 humidified incubator.

4.2.5 *Polyplex formulation*

Polyplexes were formed immediately before transfection experiments. Plasmid DNA or mRNA (1.75 and 0.1 mg/mL, respectively) was diluted in a sterile filtered 150 mM NaCl solution (Sigma) after which cationic polymers were added at the desired amine-to-phosphate (N/P) ratio to a final volume of 45 µL. This mixture was vortexed for 10 seconds and incubated at room temperature for 20-30 minutes before transfection.

4.2.6 *Zeta potential and hydrodynamic diameters of polyplexes*

Polyplexes were formulated at N/P 3, 5 & 7 with CP-25-16 polymer and 2 µg pmaxGFP plasmid DNA in molecular grade H_2O. Polyplexes were diluted to a final volume of 800 µL in 10 mM NaCl and loaded into a DTS1070 Zetasizer cell (Malvern Instruments). Dynamic light scattering and zeta potential measurements were made on a Zetasizer Nano ZS (Malvern Instruments).

4.2.7 *Transfections*

The same transfection protocol was used for Jurkat cells and primary human T cells. Cells were washed once in phosphate buffered saline (PBS) via centrifugation at 300×g for 5 minutes and resuspended in transfection medium 30 minutes prior to transfection. OptiMEM (Gibco), Jurkat culture medium, and T cell culturing medium were all used as transfection media in various experiments. Cells were plated at various concentrations in 250 µL transfection medium in a 24-well TC treated plate and stored in a 37°C and 5% CO_2 humidified incubator until transfection. Jurkat cells were plated at 1×10^6/mL (250 K cells per well), and T cells were plated at 2×10^6/mL (500 K cells per well), unless otherwise noted in optimization experiments.

Unless specified otherwise, 1.5 µg of nucleic acid was used per well in Jurkat transfections, and 2 µg in primary T cells transfections. Polyplexes or a control 150 mM NaCl solution were added to designated wells dropwise. Plates were returned immediately to the 37 °C and 5% CO_2 humidified incubator. Cells were cultured for 48 hours prior to flow cytometry analysis.

4.2.8 *Flow cytometry*

Cells were transferred to a U-bottom 96-well plate by successive centrifugation and aspiration steps. Cells were washed once with PBS via centrifugation at 300×g for 5 minutes before being resuspended in 100 µL of a 1:500 dilution of Zombie Violet dye in PBS. Cells were incubated in the live/dead stain for 10-15 minutes at room temperature in the dark and subsequently washed twice with PBS with 1% BSA (PBSA from diluted 10% BSA stock, Miltenyi). If antibody staining was used in the experiment, cells were incubated in 100 µL of the diluted antibody cocktail for 20 minutes at room temperature, and washed twice with 1% PBSA. Cells were resuspended in 200 µL of 1% PBSA, and immediately analyzed on a MacsQuant Analyzer flow cytometer (Miltenyi) where at least 10,000 events in the "Live Cells" gate were collected.

Data analysis was performed using FlowJo software (FlowJo, LLC), with serial gating (Supplemental Figure 4.3). Transfection efficiency was measured as the percentage of live cells expressing GFP fluorescence.

4.2.9 *Statistical analyses*

Results are given as mean value ± standard deviation (SD). Multiple t tests, or one-way ANOVA with either Tukey's or Dunnett's multiple comparisons posthoc analysis were performed in GraphPad Prism software (Graph Pad Software).

4.3 Results and Discussion

4.3.1 *Polymer panel screening in Jurkat cell line*

Suspension cell lines and primary white blood cells are notoriously challenging to transfect, with no commercially available chemical reagent able to achieve high gene delivery efficiency. A panel of polymers were screened for transfection efficiency and cytotoxicity in the Jurkat human T cell line. This polymer panel included commercially available branched polyethylenimine (bPEI), as well as four distinct polymer architectures synthesized in our lab (Figure 4.1). VIPER (virus-inspired polymer for endosomal release) is a diblock copolymer that contains a hydrophilic cationic block for nucleic acid loading and colloidal stability, and a pH sensitive membrane lytic block for endosomal release. This polymer is the best-performing polymer our lab has developed to date, with 80% transfection of HeLa cells with low cytotoxicity (>90% viability).[31] Sunflower and comb polymers with a core size of 25 ($pHEMA_{25}$-g-$pDMAEMA_n$) also showed high efficiency in HeLas (50 and 40%, respectively) with low cytotoxicity (>75% viability), whereas the linear pDMAEMA polymer showed gene transfer efficiencies similar to bPEI (10%) in HeLas.[30] One polymer from each architecture was screened for transfection efficiency to Jurkat cells in both serum-containing and serum-free media using a range of polymer to DNA ratios (Supplemental Figure 4.4). The optimal N/P ratios for serum-containing and serum-free medium conditions were determined to be N/P 15 and N/P 5, respectively, such that the viability of cells stayed over 80% while maximizing transfection efficiency (Figure 4.2). The higher N/P ratio required in serum-containing media is likely due to the interaction of free polymer with serum proteins; free polymer has been reported to assist in intracellular trafficking.[32–34]

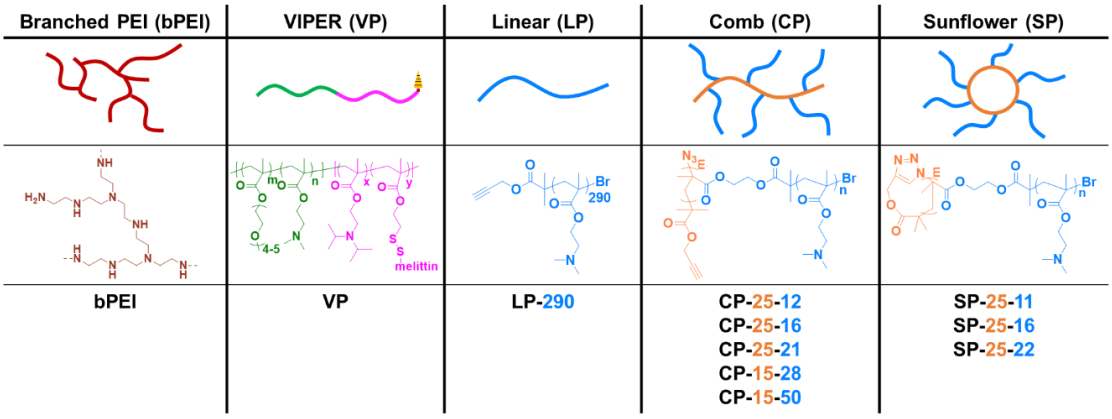

Figure 4.1. Schematic and chemical structures of polymers evaluated in gene delivery studies. Abbreviated polymer names denote degrees of polymerization (DP) for each block.

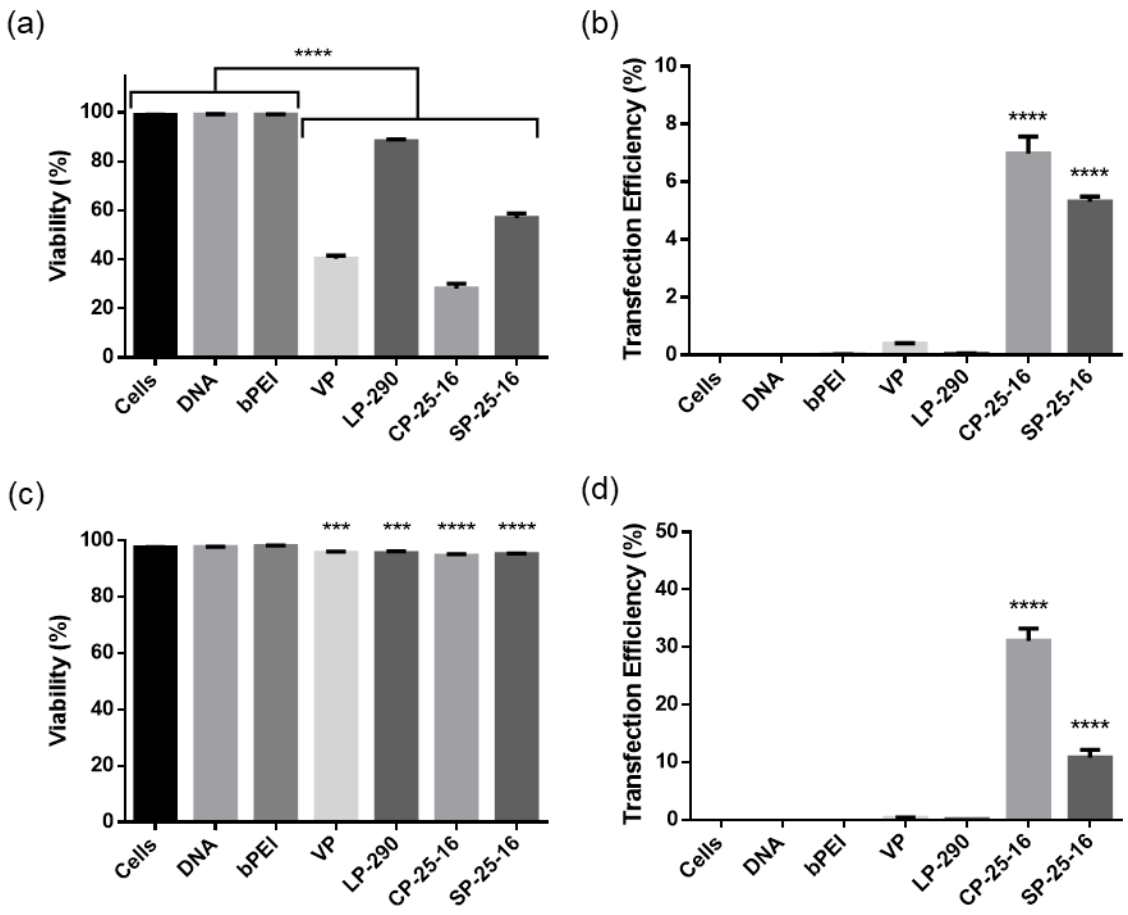

Figure 4.2. Polymer transfections of pmaxGFP plasmid in serum and serum-free medium to Jurkat T cell line. Toxicity (a) and transfection efficiency (b) of cationic polymers in Jurkat human T cell line in serum containing medium at N/P 15. Toxicity (c) and transfection efficiency (d) in serum-free medium at N/P 5. Transfection efficiencies are expressed as percentage of GFP-positive cells. Data are shown as mean ± SD (n=3; 1-way ANOVA with Tukey's multiple comparisons, * $p<0.05$, *** $p<0.001$, ****$p<0.0001$).

Surprisingly, the trends in polymer performance in adherent cell lines was not recapitulated in Jurkat cells. Comb and sunflower polymers were the only architectures that showed appreciable transfection efficiency in serum-containing or serum-free conditions. We speculate that these differences could be due to variations in uptake and intracellular trafficking mechanisms in suspension cells compared to adherent cells, resulting in different polymer characteristics required for successful gene delivery. A 5-fold increase in transfection efficiency in serum-free media compared to serum-containing media was observed for both the comb and sunflower polymers. These results are expected, as negatively charged serum proteins can nonspecifically bind and disrupt polyplexes prior to endocytosis.[35] In addition, the cell viability was improved for

transfections performed in serum-free medium, most likely due to the lower polymer concentration (N/P ratio) required for polyplex delivery. We chose to further evaluate the comb and sunflower polymers in serum-free transfection conditions for all additional Jurkat transfection studies, as the future utility of these polymers will be in well-defined *ex vivo* transfection protocols.

4.3.2 *Optimization of pDMAEMA polymer architecture for transfection of Jurkat cells*

Due to the promising T cell transfection efficiencies mediated by comb and sunflower polymers, we expanded this panel by synthesizing polymers with two core sizes and varying branch lengths per core size (Table 4.1). The impact of molecular weight and polymer geometry on gene transfer was then explored. Polymers with the same core size of DP 25 had similar transfection efficiencies and cytotoxicities in Jurkat cells (Figure 4.3 a & b). There were statistically significant differences between core geometries (linear vs. circular) at the two lower branch lengths, with comb polymers outperforming sunflower. Branch length was only significantly different within the same core geometry for the smallest molecular weight sunflower polymer (SP-25-11).

Table 4.1. Characterization of synthesized polymers.

Composition[a]	Code	M_n [kDa][a]	M_n [kDa][b]	PDI[b]
l-pDMAEMA$_{290}$	LP-290	46	53.5	1.09
l-pHEMA$_{25}$-g-(pDMAEMA$_{12}$)$_{25}$	CP-25-12	54	192	1.48
l-pHEMA$_{25}$-g-(pDMAEMA$_{16}$)$_{25}$	CP-25-16	70	263	1.67
l-pHEMA$_{25}$-g-(pDMAEMA$_{21}$)$_{25}$	CP-25-21	89	371	1.75
l-pHEMA$_{15}$-g-(pDMAEMA$_{28}$)$_{15}$	CP-15-28	70	209	1.43
l-pHEMA$_{15}$-g-(pDMAEMA$_{50}$)$_{15}$	CP-15-50	122	481	1.62
c-pHEMA$_{25}$-g-(pDMAEMA$_{11}$)$_{25}$	SP-25-11	50	176	1.44
c-pHEMA$_{25}$-g-(pDMAEMA$_{16}$)$_{25}$	SP-25-16	70	287	1.81
c-pHEMA$_{25}$-g-(pDMAEMA$_{22}$)$_{25}$	SP-25-22	93	413	1.88
p(OEGMA$_{11}$-DMAEMA$_{56}$)-*b*-p(DIPAMA$_{33}$-(PDSEMA-*g*-melittin)$_1$)	VP-67-34	23	25	1.03

[a] Determined by ^{1}H NMR; [b] Obtained by GPC.

We observed a larger significant difference in transfection efficiencies of comb polymers with varying core sizes (DP 15 vs. 25), with the DP 15 core polymers exhibiting significantly reduced transfection efficiency and greater cytotoxicity (Figure 4.3 c & d, Supplemental Figure 4.5). While we did not investigate the mechanism underlying this difference in performance between the two core sizes, we hypothesize that this difference may be due to increased branching on the DP25 polymers. This hypothesis would be consistent with the results from the Müller group, where they

have previously shown that star pDMAEMA with a higher number of arms were less toxic and resulted in higher transfection efficiency than polymers with fewer arms at equivalent molecular weights.[36] With these results, we chose to use comb polymers with a core size of DP 25 to optimize transfection conditions for primary human T cells, as they consistently showed the highest transfection efficiencies and viabilities across transfection studies in the Jurkat cell line.

Prior to moving into primary T cell studies, a tighter range of N/P ratios (3, 5, & 7) were evaluated around the highest performing N/P in serum-free transfection conditions. The size and zeta potential of polyplexes formed at these N/P ratios were similar (Supplemental Figure 4.2). N/P ratios of 5 and 7 resulted in similar viabilities and transfection efficiencies in Jurkat cells and were used for primary T cell studies (Supplemental Figure 4.6).

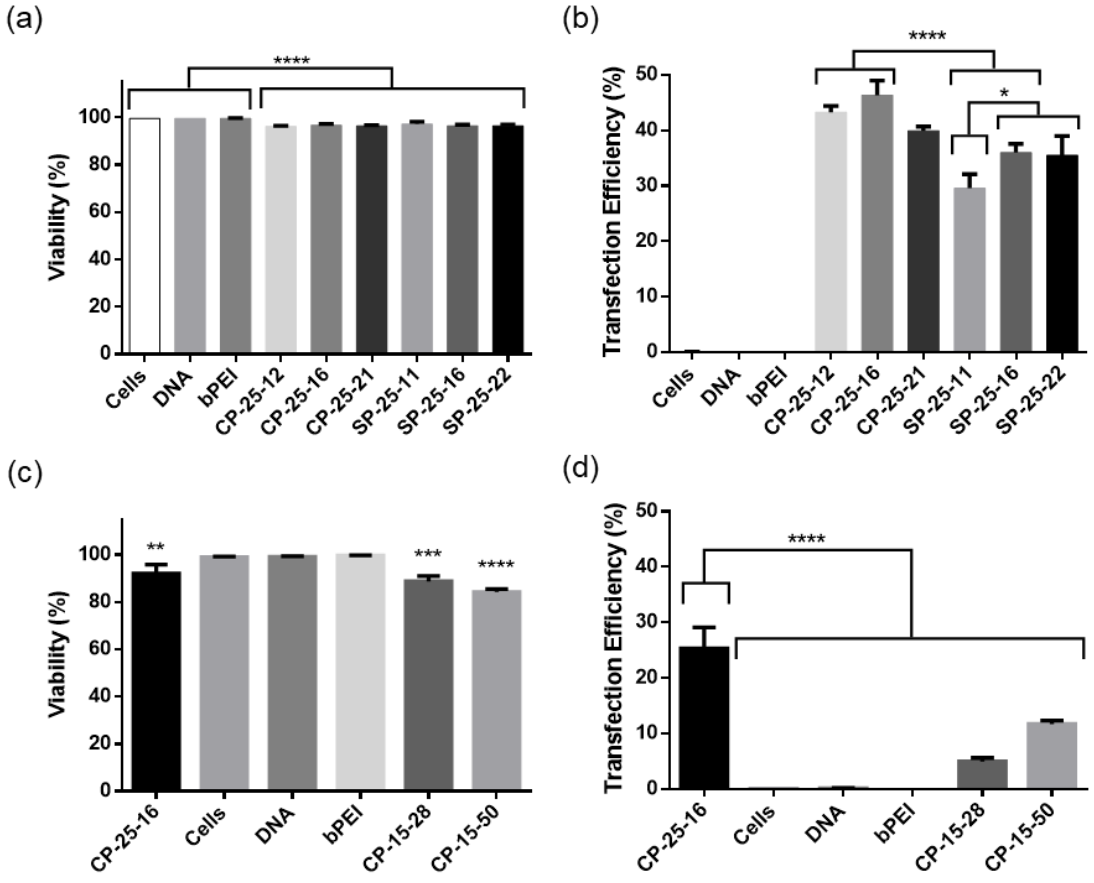

Figure 4.3. Polymer transfections of pmaxGFP plasmid in serum and serum-free medium to Jurkat T cell line. Toxicity (a) and transfection efficiency (b) of cationic polymers in Jurkat human T cell line in serum containing medium at N/P 15. Toxicity (c) and transfection efficiency (d) in serum-free medium at N/P 5. Transfection efficiencies are expressed as percentage of GFP-positive cells. Data are shown as mean ± SD (n=3; 1-way ANOVA with Tukey's multiple comparisons, * $p<0.05$, *** $p<0.001$, ****$p<0.0001$).

4.3.3 *Impact of activation time on primary T cell transfection*

Unlike viruses, cationic polymers do not have an active mechanism for transporting DNA into the nucleus of cells. Therefore, transfection efficiency is highly dependent on cell cycling and is most efficient during the G2/M phase of mitosis.[37] Unsurprisingly, transfections to quiescent, unactivated primary human T cells resulted in negligible gene expression (data not shown). To determine the optimal timing for transfections, primary T cells were transfected at various timepoints from 0-72 hours post-activation (Figure 4.4). In this study, cells were seeded at 250 K cells/well in OptiMEM and transfected with 1 μg of pDNA at N/P ratio of 5 with CP-25-16. The complete T cell medium was supplemented with 200 IU/mL IL-2. Untransfected cells went through the same manipulation steps as transfected cells, but were not treated with polyplexes.

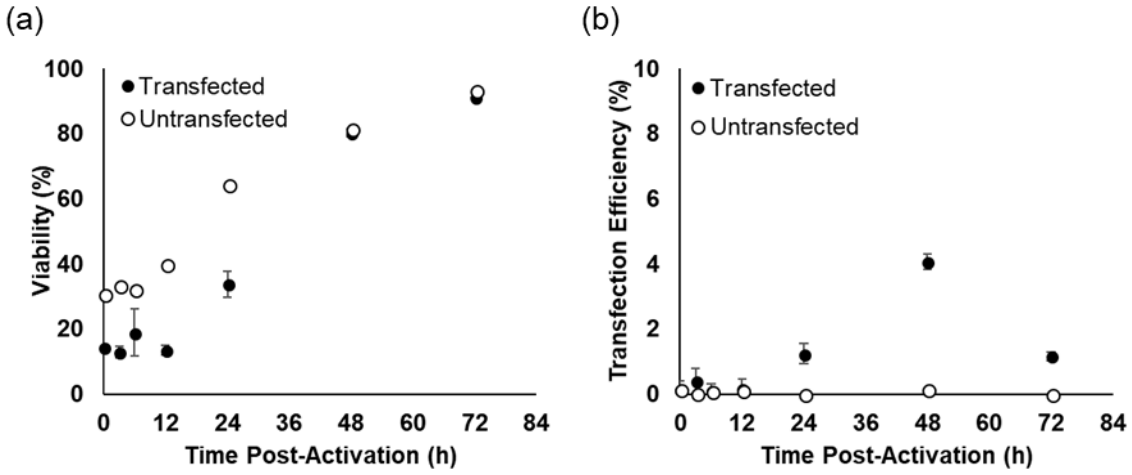

Figure 4.4. Impact of activation time prior to transfection on primary T cell viability (a) and transfection efficiency (b). Cells were transfected with 1 μg of pmaxGFP pDNA at N/P ratio of 5 using CP-25-16. Transfection efficiencies are expressed as percentage of GFP-positive cells. Data are shown as mean ± SD (n=3).

Significant cell death (>50%) was observed in transfected and control groups manipulated prior to 24-hours. These results are consistent with common *in vitro* T cell culture practices of leaving T cells untouched for the first 2-3 days after bead-based activation, as cells are more prone to activation-induced apoptosis.[38] Maximum transfection efficiency was reached when performed 48-hours after activation, however, transfection efficiencies were 10-fold lower than those observed in Jurkat cells. We therefore sought to improve transfection efficiencies by optimizing other parameters of the transfection protocol.

4.3.4 *Optimization of transfection conditions for primary T cells*

We performed two design of experiment (DOE)-style screening experiments to identify which variables impacted primary T cell transfection and viability. In the first experiment, we screened cell density (125 K, 250 K, or 500 K cells/well), total mass of DNA delivered (1 or 2 µg), and transfection medium (OptiMEM or complete T cell medium with IL-2) (Figure 4.5 a & b). Higher cell densities and lower DNA doses both improved viability of cells. Transfection efficiency with CP-25-16 was slightly higher when OptiMEM was used as the transfection medium, and was highest for the highest cell density (500 K cells/well) and highest DNA dose (2 µg).

We hypothesized that higher DNA doses could be tolerated at higher cell densities, and perhaps result in even greater transfection efficiencies. In the second optimization experiment we screened cell density (500 K or 750 K cells/well), DNA dose (2 or 3 µg), and cytokine supplement (IL-2 or IL-21). We chose to include cytokine supplement to T cell culture medium as a variable because cytokines can significantly impact the phenotype and differentiation programs of cultured T cells. While IL-2 is the most common cytokine used for outgrowth of T cells, it has been shown that T cells cultured in IL-21 supplemented media can better mediate tumor regression after adoptive transfer.[39]

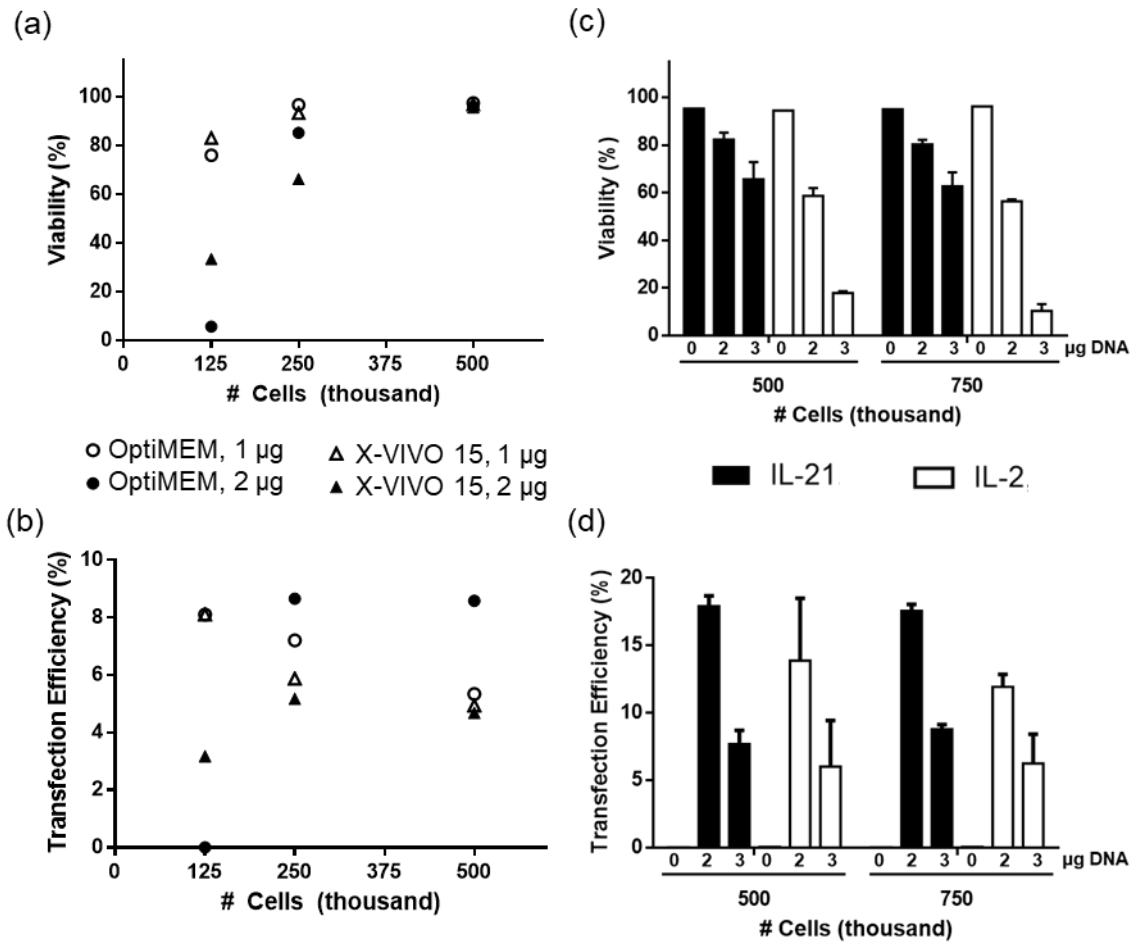

Figure 4.5. Design of Experiments (DOE) optimization of primary T cell transfection conditions. (a & b) Screening effects of transfection medium, cell density, and DNA dose on viability and transfection efficiency (n=1). (c & d) Screening effects of cytokine supplement in culture medium, cell density, and DNA dose (n=3). Cells were transfected with pmaxGFP pDNA at N/P ratio of 7 using CP-25-16. Transfection efficiencies are expressed as percentage of GFP-positive cells. Data are shown as mean ± SD.

Cells cultured in IL-21 showed an overall higher cell viability and comparable or higher transfection efficiency by CP-25-16 for all cell densities and DNA doses tested (Figure 4.5 c & d). Increasing the DNA dose to 3 µg significantly reduced the viability of cells cultured in IL-2 and reduced the viability of IL-21 cultured cells. Increasing the DNA dose to 3 µg did not have the desired effect of increasing transfection efficiency. Instead, cells treated with this higher dose showed lower transfection efficiencies for all conditions tested.

The maximum transfection efficiency achieved for delivery of plasmid DNA to primary T cells was 18%. Optimal conditions were 500-750K cells per well in a 24-well-plate format in complete

T cell medium supplemented with IL-21, and transfecting cells in OptiMEM with a total dose of 2 µg of DNA 48-hours after activation. These transfection parameters were used to probe the initial utility of these comb polymers for applications relevant to adoptive T cell therapy.

4.3.5 *Delivery of various nucleic acid cargoes to primary T cells*

Many future applications of cationic polymers as gene transfer agents for T cell-based therapies will require the use of an integrating technology like transposon/transposase for stable gene expression or CRISPR/Cas9 systems for gene editing.[40,41] The Sleeping Beauty transposon/transposase system has already been used with electroporation to generate stably expressing CAR T cells.[11,42,43] These systems require the parallel delivery of two nucleic acid cargoes: a plasmid or mRNA to express the editing enzyme (Cas9 or transposase) and a plasmid with the gene for insertion (transposon or DNA template). The delivery platform with the best safety profile delivers the editing enzyme gene via mRNA and the gene for insertion by plasmid DNA.[44] The transient expression of the enzyme nearly eliminates the possibility of repeat template excision/re-integration genotoxicities, and prevents the enzyme from integrating itself into the host genome.

To show the utility of cationic polymers for this application, we successfully delivered mRNA and pDNA to primary T cells using the optimized transfection protocol (Figure 4.6 a & b). We observed a higher level of gene expression from cells transfected with mRNA compared to plasmid DNA, suggesting that nuclear transport is a contributing barrier to higher gene expression with this reagent.

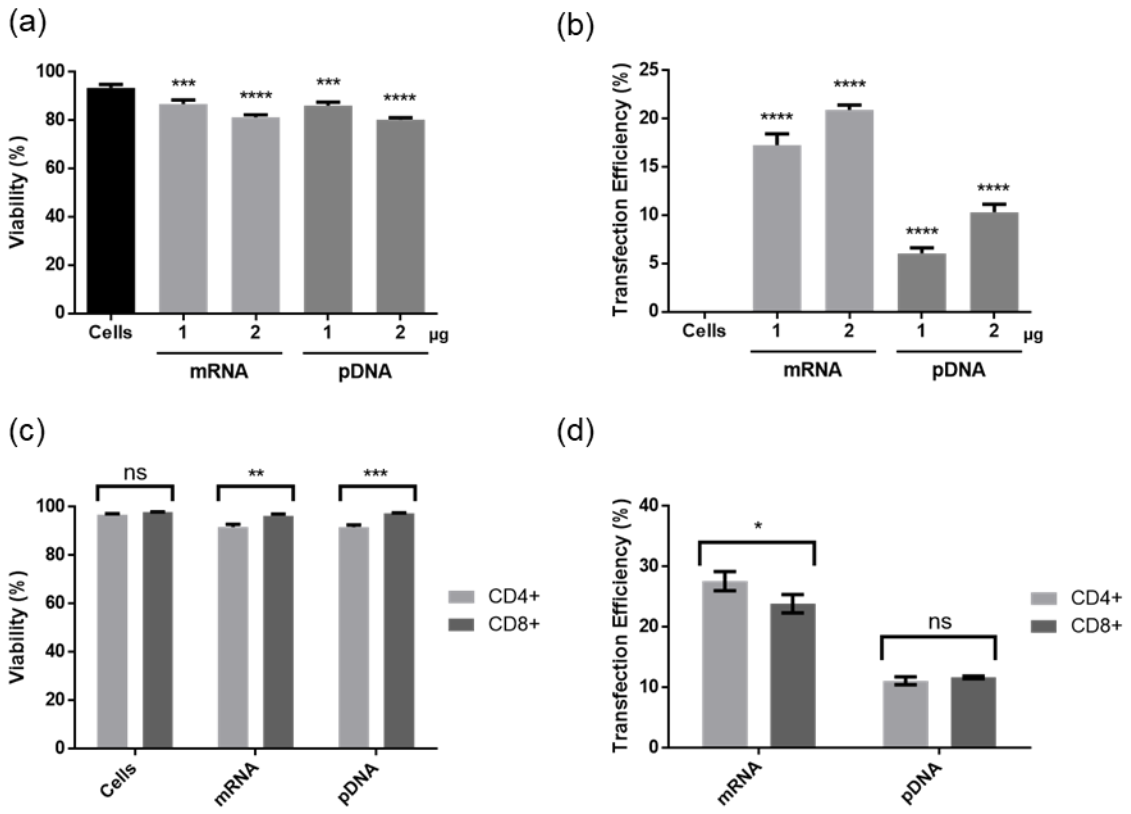

Figure 4.6. Viability (a) and transfection efficiency (b) of eGFP expressing pDNA and mRNA to a mixture of $CD4^+$ and $CD8^+$ T cells at optimized conditions. Viability (c) and transfection efficiency (d) in $CD4^+$ and $CD8^+$ T cells. Cells were transfected with pDNA at N/P ratio of 7 using CP-25-16. Transfection efficiencies are expressed as percentage of GFP-positive cells. Data are shown as mean ± SD (n=3; (a & b) 1-way ANOVA with Tukey's multiple comparisons, (c & d) multiple t tests, * $p<0.05$, ** $p<0.01$, *** $p<0.001$, ****$p<0.0001$).

4.3.6 *Delivery to both $CD4^+$ and $CD8^+$ primary T cells*

We wanted to ensure that these comb polymers could transfect both $CD4^+$ "helper" and $CD8^+$ "cytotoxic" T cells, as both subtypes are used in CAR T cell therapy, and initial polymer screening was performed on the $CD4^+$ Jurkat cell line. We stained transfected T cells with fluorescently tagged antibodies for CD4 and CD8 and observed an equivalent proportion of transfected cells in each subset (Figure 4.6 c & d). There was no difference in transfection efficiency of pDNA and only a small statistical difference in transfection efficiency of mRNA between $CD4^+$ and $CD8^+$ T cells, with a slightly higher level of gene delivery to $CD4^+$ T cells.

These results support the continued development of comb polymers for *ex vivo* non-viral genetic reprogramming of primary human T cells for the application of CAR T cell manufacturing.

Additional polymer and polyplex engineering would be required to create a gene delivery platform for *in vivo* delivery to prevent non-specific interactions and toxicities caused by the positive charges on the surface of the polyplex. However, the flexible cargo loading of this polymer system makes it attractive for *ex vivo* gene delivery applications.

4.4 CONCLUSION

One of the major opportunities for cost reduction and safety improvement in CAR T cell manufacturing is moving from viral to non-viral methods of genetically reprogramming patient T cells. These studies begin to evaluate shelf-stable, easy to manufacture, untargeted cationic polymers as alternative non-viral gene delivery vehicles for CAR T cell manufacturing. We identified a class of pHEMA-*g*-pDMAEMA comb and sunflower polymers that can transfect the Jurkat T cell line at high efficiencies of 25-50% in serum-free medium. This could be a very useful tool for the screening experiments performed in the development of new chimeric antigen receptors. Extensive and iterative protein engineering is required for developing new chimeric antigen receptors.[45,46] Having a quick and efficient method to screen expression and binding affinity of various CARs in a T cell line, instead of creating a new viral vector for each one, could significantly reduce the time it takes to develop and perform early validation studies on new CAR constructs. Jurkat cells, like all suspension cell lines, are notoriously challenging to transfect. Though untested, these comb and sunflower polymers may also be able to transfect other suspension cell lines with high efficiency.

Our data demonstrate that these polymers can also transfect primary human T cells with pDNA and mRNA at modest efficiencies up to 18 and 25%, respectively, while maintaining high cell viability (>75%). These efficiencies were reached through DOE-style optimization experiments that yielded a 4-fold increase over initial transfection values. These results support the continued development of comb polymers for non-viral genetic reprogramming of primary human T cells for the application of CAR T cell manufacturing. Future studies will seek to understand the additional barriers to non-viral gene delivery in primary T cells and identify alternative protocol changes that will further increase transfection efficiency to a level approaching those achieved by viral gene delivery methods.

4.5 ACKNOWLEDGEMENTS

We thank Dr. Joshua Gustafson (Seattle Children's Research Institute) for helpful discussions on primary T cell culture. We thank David Peeler, Albert Yen, and the lab of Dr. Shaoyi Jiang for assistance in zeta potential and DLS measurements. This work was supported by the National Institutes of Health [1R01CA177272, 2R01NS064404]. B.R.O. was supported by a National Science Foundation Graduate Research Fellowship [DGE-1256082].

4.6 DECLARATION OF INTEREST

A patent application has been filed on the sunflower and comb polymers by the University of Washington.

4.7 REFERENCES

1. Strausberg, R. L. Tumor microenvironments, the immune system and cancer survival. *Genome Biol.* **6,** 211 (2005).
2. Gajewski, T., Meng, Y. & Harlin, H. Immune suppression in the tumor microenvironment. *J Immunother* **29,** 233–240 (2006).
3. Banchereau, J. & Palucka, A. K. Dendritic cells as therapeutic vaccines against cancer. *Nat. Rev. Immunol.* **5,** 296–306 (2005).
4. Kalos, M. *et al.* T cells with chimeric antigen receptors have potent antitumor effects and can establish memory in patients with advanced leukemia. *Sci. Transl. Med.* **3,** 95ra73 (2011).
5. Hay, K. A. & Turtle, C. J. Chimeric Antigen Receptor (CAR) T Cells: Lessons Learned from Targeting of CD19 in B-Cell Malignancies. *Drugs* **77,** 237–245 (2017).
6. Barrett, D. M., Singh, N., Porter, D. L., Grupp, S. a & June, C. H. Chimeric antigen receptor therapy for cancer. *Annu. Rev. Med.* **65,** 333–47 (2014).
7. Holzinger, A., Barden, M. & Abken, H. The growing world of CAR T cell trials: a systematic review. *Cancer Immunol. Immunother.* **65,** 1–18 (2016).
8. Gill, S. & June, C. H. Going viral: Chimeric antigen receptor T-cell therapy for hematological malignancies. *Immunol. Rev.* **263,** 68–89 (2015).
9. Wang, X. & Rivière, I. Clinical manufacturing of CAR T cells: foundation of a promising therapy. *Mol. Ther. oncolytics* **3,** 16015 (2016).
10. Jaspers, J. E. & Brentjens, R. J. Development of CAR T cells designed to improve antitumor efficacy and safety. *Pharmacol. Ther.* **178,** 83–91 (2017).
11. Singh, H. *et al.* Manufacture of Clinical-Grade CD19-Specific T Cells Stably Expressing Chimeric Antigen Receptor Using Sleeping Beauty System and Artificial Antigen Presenting Cells. *PLoS One* **8,** 1–11 (2013).
12. Zhao, Y. *et al.* High-efficiency transfection of primary human and mouse T lymphocytes using RNA electroporation. *Mol. Ther.* **13,** 151–159 (2006).
13. Yin, H. *et al.* Non-viral vectors for gene-based therapy. *Nat. Rev. Genet.* **15,** 541–555 (2014).
14. Pack, D. W., Hoffman, A. S., Pun, S. & Stayton, P. S. Design and development of polymers for gene delivery. *Nat. Rev. Drug Discov.* **4,** 581–93 (2005).
15. Boussif, O. *et al.* A versatile vector for gene and oligonucleotide transfer into cells in culture and in vivo: polyethylenimine. *Proc. Natl. Acad. Sci.* **92,** 7297–7301 (1995).
16. Jiang, X., Lok, M. C. & Hennink, W. E. Degradable-Brushed pHEMA – pDMAEMA Synthesized via ATRP and Click Chemistry for Gene Delivery. *Bioconjug. Chem.* 2077–2084 (2007). doi:10.1021/bc0701186
17. Khalil, I. a, Kogure, K., Akita, H. & Harashima, H. Uptake pathways and subsequent intracellular trafficking in nonviral gene delivery. *Pharmacol. Rev.* **58,** 32–45 (2006).
18. Mislick, K. a & Baldeschwieler, J. D. Evidence for the role of proteoglycans in cation-mediated gene transfer. *Proc. Natl. Acad. Sci. U. S. A.* **93,** 12349–12354 (1996).
19. Xie, Y. *et al.* Targeted delivery of siRNA to activated T cells via transferrin-polyethylenimine (Tf-PEI) as a potential therapy of asthma. *J. Control. Release* 120–129 (2016). doi:10.1016/j.jconrel.2016.03.029
20. Xie, Y., Killinger, B., Moszczynska, A. & Merkel, O. Targeted Delivery of siRNA to Transferrin Receptor Overexpressing Tumor Cells via Peptide Modified

Polyethylenimine. *Molecules* **21,** 1334 (2016).
21. Schallon, A., Synatschke, C. V., Jérôme, V., Müller, A. H. E. & Freitag, R. Nanoparticulate nonviral agent for the effective delivery of pDNA and siRNA to differentiated cells and primary human T lymphocytes. *Biomacromolecules* **13,** 3463–3474 (2012).
22. Raup, A. *et al.* Influence of polyplex formation on the performance of star-shaped polycationic transfection agents for mammalian cells. *Polymers (Basel).* **8,** (2016).
23. Smith, T. T. *et al.* In situ programming of leukaemia-specific T cells using synthetic DNA nanocarriers. *Nat. Nanotechnol.* (2017). doi:10.1038/nnano.2017.57
24. Moffett, H. F. *et al.* Hit-and-run programming of therapeutic cytoreagents using mRNA nanocarriers. *Nat. Commun.* **8,** 389 (2017).
25. Ahmed, M. & Narain, R. Progress of RAFT based polymers in gene delivery. *Prog. Polym. Sci.* **38,** 767–790 (2013).
26. Agarwal, S., Zhang, Y., Maji, S. & Greiner, A. PDMAEMA based gene delivery materials. *Mater. Today* **15,** 388–393 (2012).
27. Chu, D. S. H. *et al.* Application of living free radical polymerization for nucleic acid delivery. *Acc. Chem. Res.* **45,** 1089–1099 (2012).
28. York, A. W., Kirkland, S. E. & McCormick, C. L. Advances in the synthesis of amphiphilic block copolymers via RAFT polymerization: Stimuli-responsive drug and gene delivery. *Adv. Drug Deliv. Rev.* **60,** 1018–1036 (2008).
29. Qiu, L. Y. & Bae, Y. H. Polymer architecture and drug delivery. *Pharm. Res.* **23,** 1–30 (2006).
30. Cheng, Y. *et al.* Nano-Sized Sunflower Polycations As Effective Gene Transfer Vehicles. *Small* **12,** 2750–2758 (2016).
31. Cheng, Y., Yumul, R. C. & Pun, S. H. Virus-Inspired Polymer for Efficient In Vitro and In Vivo Gene Delivery. *Angew. Chemie - Int. Ed.* **55,** 12013–12017 (2016).
32. Boeckle, S. *et al.* Purification of polyethylenimine polyplexes highlights the role of free polycations in gene transfer. *J. Gene Med.* **6,** 1102–1111 (2004).
33. Saul, J. M., Wang, C. H. K., Ng, C. P. & Pun, S. H. Multilayer nanocomplexes of polymer and DNA exhibit enhanced gene delivery. *Adv. Mater.* **20,** 19–25 (2008).
34. Cai, J. *et al.* Quantitative study of effects of free cationic chains on gene transfection in different intracellular stages. *J. Control. Release* **238,** 71–79 (2016).
35. Buyens, K. *et al.* A fast and sensitive method for measuring the integrity of siRNA-carrier complexes in full human serum. *J. Control. Release* **126,** 67–76 (2008).
36. Synatschke, C. V., Schallon, A., Jérôme, V., Freitag, R. & Müller, A. H. E. Influence of polymer architecture and molecular weight of poly(2-(dimethylamino)ethyl methacrylate) polycations on transfection efficiency and cell viability in gene delivery. *Biomacromolecules* **12,** 4247–4255 (2011).
37. Tseng, W. C., Haselton, F. R. & Giorgio, T. D. Mitosis enhances transgene expression of plasmid delivered by cationic liposomes. *Biochim. Biophys. Acta - Gene Struct. Expr.* **1445,** 53–64 (1999).
38. Kalamasz, D. *et al.* Optimization of human T-cell expansion ex vivo using magnetic beads conjugated with anti-CD3 and Anti-CD28 antibodies. *J. Immunother.* **27,** 405–418 (2004).
39. Hinrichs, C. S. *et al.* IL-2 and IL-21 confer opposing differentiation programs to CD8+ T cells for adoptive immunotherapy. *Blood* **111,** 5326–5333 (2008).
40. Aronovich, E. L., McIvor, R. S. & Hackett, P. B. The Sleeping Beauty transposon system:

A non-viral vector for gene therapy. *Hum. Mol. Genet.* **20,** 14–20 (2011).
41. Eyquem, J. *et al.* Targeting a CAR to the TRAC locus with CRISPR/Cas9 enhances tumour rejection. *Nature* **543,** 113–117 (2017).
42. Singh, H., Huls, H. & Cooper, L. J. N. A new approach to gene therapy using Sleeping Beauty to genetically modify clinical-grade T cells to target CD19. *Immunol. Rev.* **257,** 181–190 (2014).
43. Monjezi, R. *et al.* Enhanced CAR T-cell engineering using non-viral Sleeping Beauty transposition from minicircle vectors. *Leukemia* **31,** 1–9 (2016).
44. Wilber, A. *et al.* RNA as a source of transposase for Sleeping Beauty-mediated gene insertion and expression in somatic cells and tissues. *Mol. Ther.* **13,** 625–630 (2006).
45. Hudecek, M. *et al.* Receptor affinity and extracellular domain modifications affect tumor recognition by ROR1-specific chimeric antigen receptor T cells. *Clin. Cancer Res.* **19,** 3153–3164 (2013).
46. Hudecek, M. *et al.* The Nonsignaling Extracellular Spacer Domain of Chimeric Antigen Receptors Is Decisive for In Vivo Antitumor Activity. *Cancer Immunol. Res.* **3,** 125–135 (2015).

4.8 SUPPLEMENTARY INFORMATION

4.8.1 *Synthesis of pHEMA$_{15}$-g-pDMAEMA*

pHEMA$_{15}$-*g*-pDMAEMA with different degrees of polymerization (DP) of DMAEMA was synthesized by three steps:

Synthesis of pHEMA$_{15}$. First, poly(2-hydroxyethyl methacrylate) (pHEMA) was synthesized by atom transfer radical polymerization (ATRP) using propargyl 2-bromoisobutyrate (PBrIB) as initiator. HEMA (0.76 g, 5.86 mmol), PBrIB (80 mg, 0.39 mmol) and PMDETA (85 μL) were dissolved in DMF and 2-propanol (v/v, 9/1, 1.0 mL), and the solution was purged with argon for 5 min. Then, CuBr (57 mg, 0.39 mmol) was added quickly under the protection of argon flow. The reaction was placed in an oil bath (60 ^{o}C). After 30 min, the polymerization was stopped through the exposure of the reaction solution to air for 1 h. The solution was diluted with DMF, and then directly subjected to dialysis against distilled water to remove the copper catalyst and unreacted monomer. pHEMA$_{15}$ was obtained after lyophilization with yield of 69%.

Bromination of pHEMA$_{15}$. pHEMA$_{15}$ (0.1 g, 0.77 mmol) and TEA (386 μL, 2.77 mmol) were dissolved in 5 mL of DMF, and the mixture was stirred in an ice bath for 0.5 h. Then α-bromoisobutyryl bromide (285 μL, 2.31 mmol) was added dropwise over 15 minutes. The mixture was kept stirring in an ice bath for an additional 30 min followed by 24 h at room temperature. The reaction was stopped by pouring into cold water, and the precipitate was collected by centrifuging for 10 min at 5000 rpm. The solid was washed three times with water followed by lyophilization, with a yield of 71%.

Synthesis of pHEMA$_{15}$-*g*-pDMAEMA. pHEMA$_{15}$-Br (10 mg, 0.036 mmol –Br), DMAEMA (302 μL, 1.8 mmol), $CuBr_2$ (0.8 mg, 0.0036 mmol), DMF (40 μL, used as internal reference) were dissolved in anisole (3.6 mL), and the mixture was degassed with argon for 10 min, followed by the addition of CuBr (5.2 mg, 0.036 mmol) under the protection of insert atmosphere. Then the reaction was placed in an oil bath at 60 ^{o}C for 20 h. The polymerization was quenched by exposing the solution to air, and the mixture was precipitated in to cold hexane. After centrifuging, the product was dissolved in methanol, and dialyzed against distilled water for 2 days.

4.8.2 *Supplementary Figures*

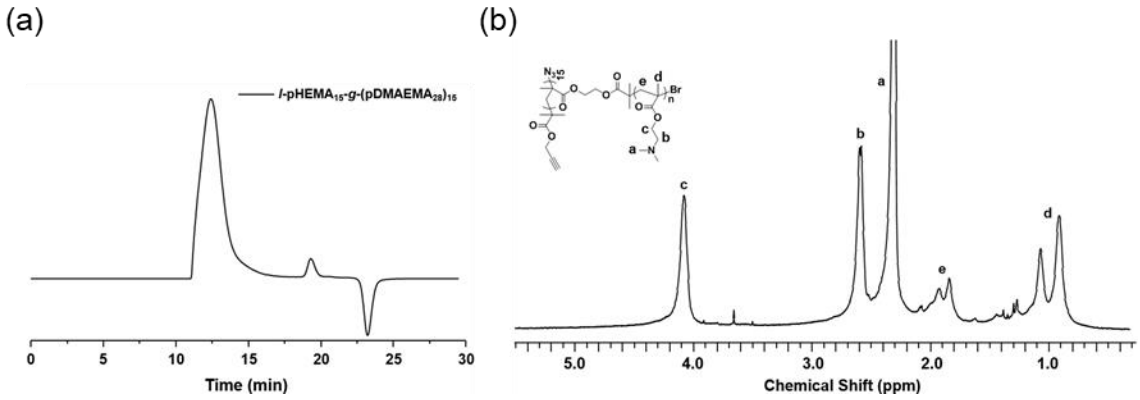

Supplemental Figure 4.1. Representative (a) GPC and (b) 1H NMR trace for l-pHEMA15-g-(pDMAEMA28)15 shown. Similar traces were obtained for l-pHEMA15-g-(pDMAEMA50)15.

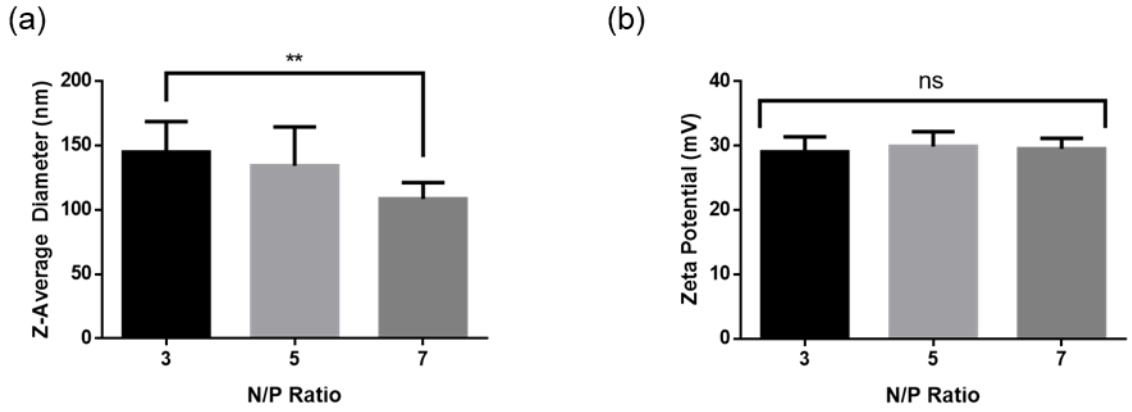

Supplemental Figure 4.2. Size (a) and zeta potential (b) of DNA polyplexes formed with CP-25-16 at various N/P ratios. Data are shown as mean ± SD (n=3; 1-way ANOVA with Tukey's multiple comparisons, ** $p<0.01$)

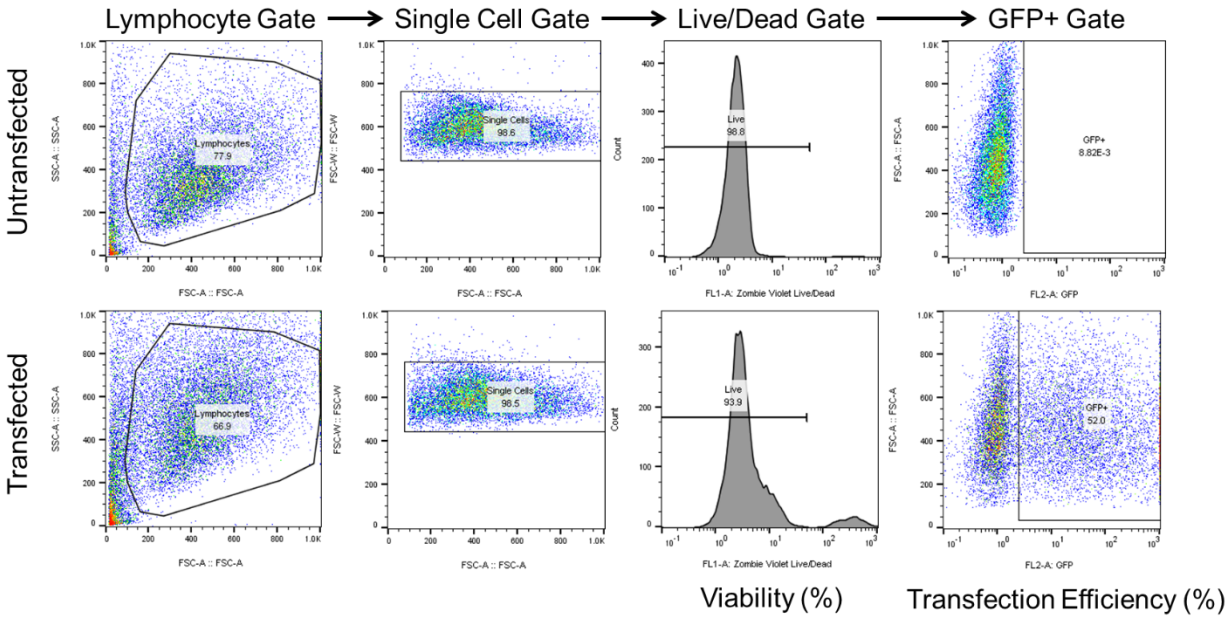

Supplemental Figure 4.3. Representative gating strategy for flow cytometry analysis. When included, additional gating of $CD4^+$ and $CD8^+$ T cell subsets was performed on single cells prior to applying additional gates.

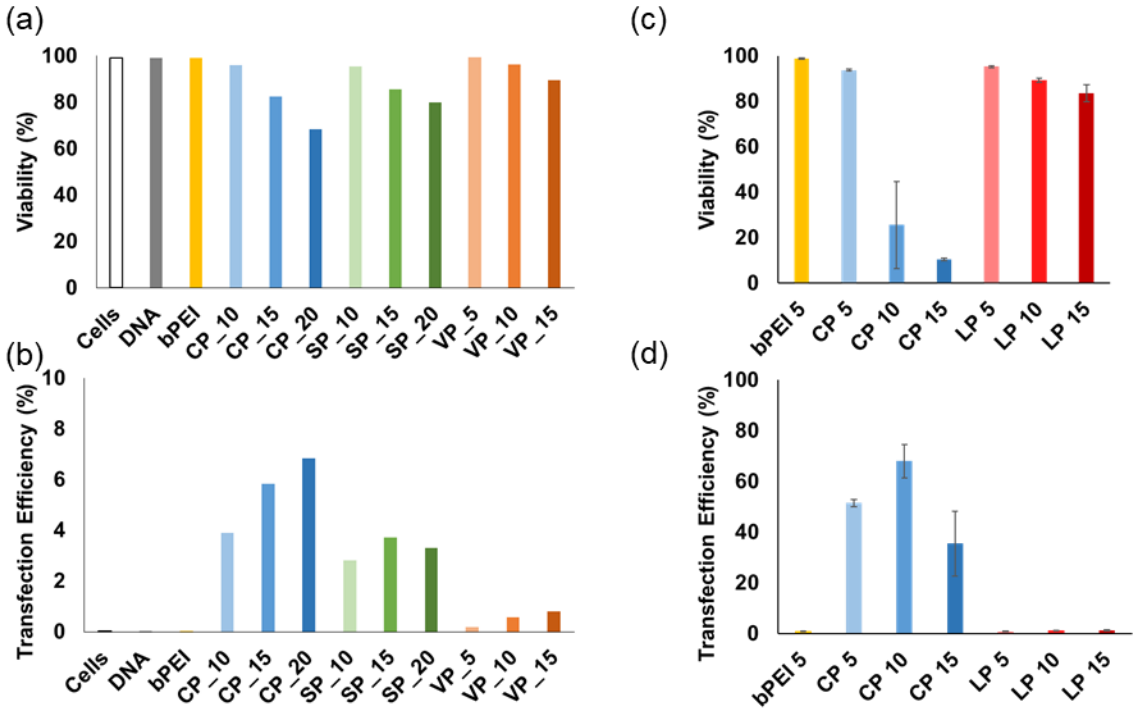

Supplemental Figure 4.4. Optimizing N/P ratio for (a & b) serum (n=1) & (c & d) serum free (n=3) Jurkat transfection conditions with subset of polymers. Data are shown as mean ± SD.

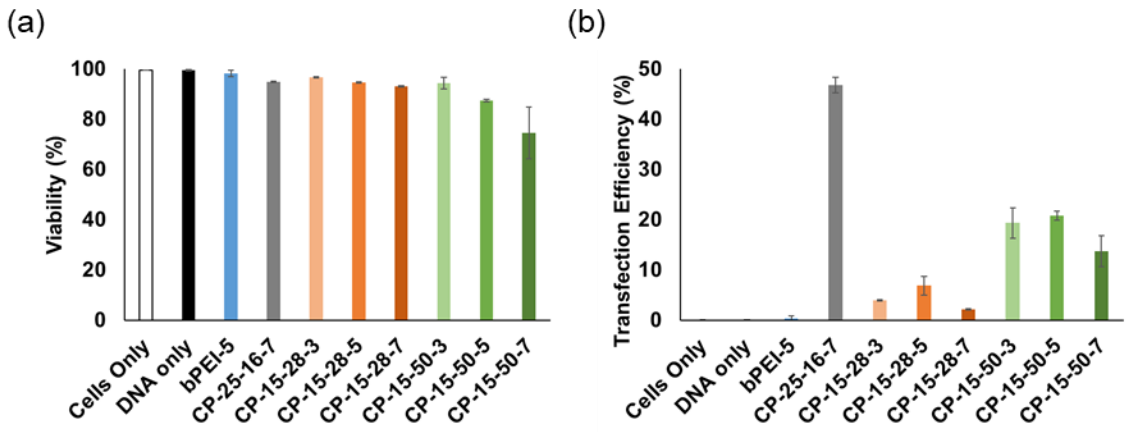

Supplemental Figure 4.5. Optimizing N/P ratio of DP 15 core size comb polymers for Jurkat transfection conditions (n=2). Data are shown as mean ± SD.

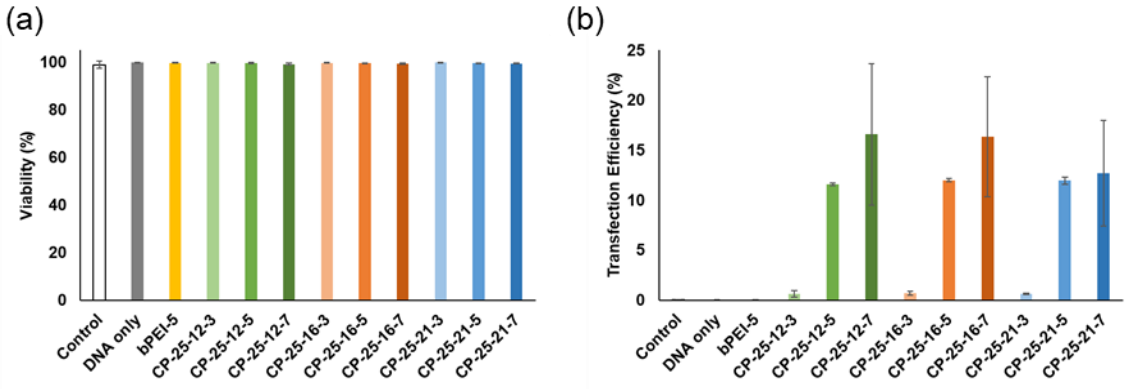

Supplemental Figure 4.6. Optimizing N/P ratio of DP 25 core size comb polymers with Jurkats prior to Primary T cell studies (n=2). Data are shown as mean ± SD.

Chapter 5. IDENTIFYING KEY BARRIERS IN CATIONIC POLYMER GENE DELIVERY TO HUMAN T CELLS

Brynn R. Olden, Yilong Cheng, Suzie H. Pun

Abstract

T cells have emerged as a therapeutically-relevant target for *ex vivo* gene delivery and editing. However, most commercially available reagents cannot transfect T cells and designing cationic polymers for non-viral gene delivery to T cells has resulted in moderate success. Here, we assess various barriers to successful gene transfer in the Jurkat human T cell line and primary human T cells. Using two polymers previously developed in our group, we show that uptake is one barrier to gene delivery in primary human T cells but is not predictive of successful gene delivery. We then probe intracellular pathways for barriers to gene transfer including endosomal acidification, autophagy, and immune sensing pathways. We find that endosomal acidification is slower and not as robust in human T cells compared to the model HeLa human cell line commonly used to evaluate cationic polymers for gene delivery. These studies inform the future design of cationic polymers for non-viral gene delivery to T cells, specifically, to rely on alternative endosomal release mechanisms than pH-triggered release.

5.1 INTRODUCTION

Genetically engineered T cells have recently gained FDA approval for treatment of various leukemias and lymphomas and additional subsets of T cells are being developed as therapeutics for autoimmune diseases.[1–4] The manufacturing of genetically modified patient T cells creates a need for a flexible, inexpensive system that can deliver multiple cargoes *in vitro*, especially as combinatorial gene editing techniques are emerging as important tools for improving safety and therapeutic efficacy.[5,6] Currently, the two FDA approved engineered T cell therapies rely on lentiviral transduction of cells during production. However, lentiviral vectors are very costly to produce at GMP scale for clinical use and can be a barrier to broad translation.

Cationic polymers, which are used routinely in laboratory settings for gene transfer, can be manufactured readily at clinical scale and formulated with various types of nucleic acid cargo. However, T cells and other blood cells are notoriously difficult to transfect using non-viral vectors, and recent attempts to design cationic polymer gene carriers for T cells has resulted in moderate *in vitro* efficiency.[7–10] In order to design better synthetic gene carriers specifically for T cells, more needs to be known about the current barriers leading to low gene transfer.

Successful non-viral gene delivery formulations must be internalized in cells, typically by some endocytosis mechanism, escape endosomal vesicles, traffic to the desired subcellular location and release protected nucleic acid cargo (Figure 5.1). In addition, polyplexes must overcome multiple cellular defense mechanisms to deliver their genetic cargo to target cells. The most widely studied trafficking path of polyplexes through cells starts with endocytosis into an early endosome.[11,12] This is followed by either endosomal escape or degradation from fusion to an acidic lysosome. The success of transfection reagents such as polyethylenimine (PEI) and poly(2-dimethylaminoethyl methacrylate) (pDMAEMA) is credited to their buffering capacity and "proton sponge effect" in early endosomes, promoting endosomal lysis before acidification.[13,14]

There is also the potential that polyplexes could be recognized by immune sensing pathways like the family of interferon-induced transmembrane (IFITM) proteins that inhibit viral entry and endosomal escape by promoting cholesterol accumulation and endosomal stiffening.[15,16] Additionally, polyplexes can be sequestered in tubulovesicular autophagosomes that accumulate near the nucleus.[17]

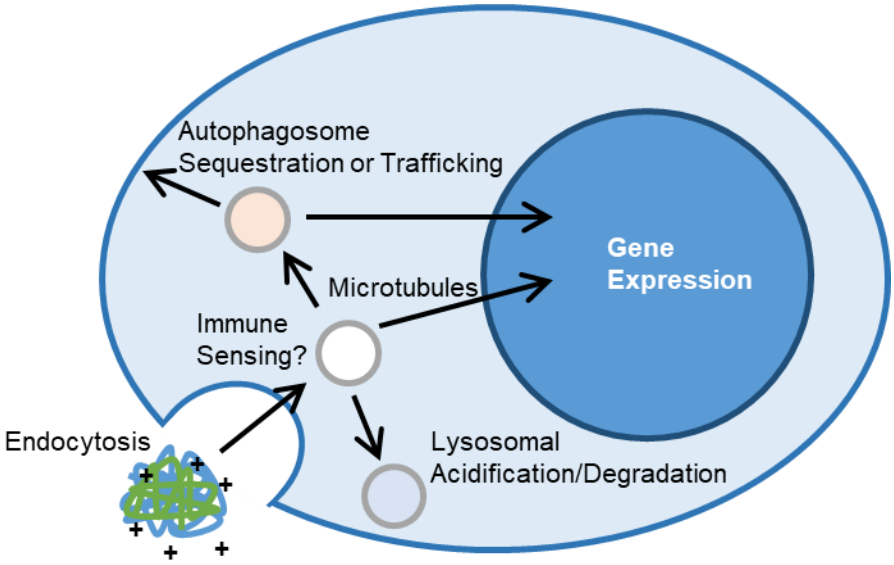

Figure 5.1. Schematic of barriers and intracellular trafficking steps for cationic polymer gene complexes.

Recently, we developed two cationic polymers that can successfully transfect several adherent cell lines as well as primary cells like human macrophage and neural progenitor cells (unpublished data).[18,19] These two polymers contain the same DNA-condensing monomer unit 2-dimethylaminoethyl methacrylate (DMAEMA) but vary in polymer architecture (linear vs. comb) and designed endosomal release mechanism (pH-triggered release vs. proton sponge effect) (Supplemental Figure 5.1). The virus-inspired polymer for endosomal release (VIPER) has a linear di-block polymer design that shields a membrane lytic peptide, melittin, in a stable micelle that disassembles at pH 6.4, promoting endosomal escape. The comb polymer (Comb) has a poly(2-hydroxyethyl methacrylate) back-bone with pDMAEMA branches, resulting in the comb architecture. Unexpectedly, VIPER, the polymer that exhibited less toxicity and higher gene transfer efficiencies compared to Comb in all other cell types tested, exhibited poor transfection efficiency in the Jurkat T cell line and in primary T cells.[9]

Here, we probe multiple potential barriers to successful gene delivery in T cells from a polymer design and biological perspective. From a polymer design perspective, we investigate the importance of uptake efficiency and kinetics of intracellular pH to identify key parameters in polymer design for gene delivery to T cells. From a biological perspective, we explore the roles of immune sensing pathways and autophagy as potential barriers to cationic polymer gene delivery to T cells. We find that uptake of polyplexes is reduced and intracellular acidification of endocytic

compartments is slowed in primary T cells, which indicate cell type-specific barriers to non-viral gene delivery.

5.2 Materials and Methods

5.2.1 *Materials*

Rapamycin, 3-methyladenine, polyclonal goat anti-rabbit IgG HRP antibody, and polyclonal goat anti-mouse IgG HRP antibody were purchased from Sigma Aldrich. YOYO-1 iodide, pHrodo red dextran 10,000 MW, pHrodo green dextran 10,000 MW, and intracellular pH calibration buffer kit, were purchased from ThermoFisher. Monoclonal mouse anti-human IFITM1 antibody (clone: 5B5E2), polyclonal rabbit anti-human IFITM2 antibody, and polyclonal rabbit anti-human IFITM3 antibody were purchased from Proteintech. Polyclonal rabbit anti-human IC3B antibody was purchased from Cell Signaling Technology. Alexa Fluor 488 donkey anti-rabbit antibody purchased from Jackson ImmunoResearch. Zombie Violet and Zombie NIR fixable viability stains were purchased from Biolegend.

PmaxGFP plasmid (Lonza) was transformed into XL10 Gold ultracompetent cells (Stratagene) and a single colony was grown up in an overnight culture. Plasmid was purified using the NucleoBond Xtra Maxi Endotoxin Free kit (Macherey-Nagel), purity and concentration were quantified by Nanodrop and a diagnostic gel.

5.2.2 *Cell culture conditions*

Jurkat cells (human T lymphocyte line) were a kind gift from Prof. Michael Jensen (Seattle Children's Research Institute). Jurkat cell lines overexpressing IFITM 1, 2, or 3, and backbone vector were a generous gift from Prof. Shan-Lu Liu (Ohio State University). All Jurkat cell lines were maintained in RPMI-1640 media supplemented with 10% fetal bovine serum (v/v). Cells were passaged 18-24 hours prior to transfection.

HeLa cells were maintained in DMEM media supplemented with 10% fetal bovine serum and 1% penicillin-streptomycin (v/v). Cells were seeded at 50,000 cells in 500 μL of media in a 24 well-plate 18-24 hours prior to transfection.

Cryopreserved vials of healthy donor primary human T lymphocytes, isolated by magnetic activated cell sorting, were generously provided by Juno Therapeutics. T cells were cultured at 1.5×10^6 cells/mL in X-VIVO 15 media (Lonza) supplemented with 2% KnockOut serum

replacement (ThermoFisher) and premium grade recombinant human IL-21 at 10 ng/mL (Miltenyi). Cells were activated with CD3/CD28 Human T Activator beads (DynaBeads, Gibco) 40-48 hours prior to transfection. All cells were maintained in a 37 °C and 5% CO_2 humidified incubator.

5.2.3 *Western blotting*

Cells (5-10×10^6) were washed twice in PBS via centrifugation at 500 ×g for 3 minutes. Cell pellets were flash frozen in dry ice and stored at -80 °C prior to use. Cell pellets were thawed and resuspended in cell lysis buffer (20 mM Tris-HCl pH 8.0, 137 mM NaCl, 10% glycerol, 1% NP-40, 2 mM EDTA, cOmplete Protease Inhibitor from 25× stock, and 1 mM PMSF) and incubated at 4 °C with intermittent vortexing for 1 hour. Supernatant from samples centrifuged at 15,000 ×g for 20 minutes at 4 °C were quantitated via micro BCA protein assay kit (ThermoFisher).

Equivalent masses of protein extract (40 μg) from each cell line were mixed with 2× Laemmli sample buffer and run on a 4-20% Mini-PROTEAN TGX precast protein gel (Bio-Rad). Proteins were transferred to Immobilon-P PVDF membrane (Millipore Sigma) and subjected to standard immunoblotting with primary IFITM 1, 2, or 3 antibodies at a 1:5000, 1:1000, or 1:1000 dilution, respectively. Goat anti-mouse or goat anti-rabbit HRP-labeled secondary antibodies were used at a 1:5000 dilution. Immunoblots were developed with SuperSignal West Pico Chemiluminescent Substrate kit (Pierce) and imaged using a Xenogen IVIS imager (PerkinElmer).

5.2.4 *Polymer and polyplex preparation*

Comb-shaped $pHEMA_{25}$-g-$pDMAEMA_{16}$ polymer (Comb) and virus-inspired polymer for endosomal release (VIPER) were synthesized as reported previously by controlled living radical polymerization.[18,19] Polymers were diluted from protonated stocks into sterile molecular grade H_2O to desired amine concentration for transfection studies.

For uptake studies, plasmid DNA was labeled with YOYO-1 iodide nucleic acid stain. DNA and YOYO-1 were mixed at a dye to base pair ratio of 1:50 and incubated for 1 hour at room temperature prior to polyplex formation.

Polyplexes were formed immediately before use in uptake and transfection studies. Plasmid was diluted from a stock solution to 0.1 μg/μL with sterile molecular grade H_2O or 150 mM NaCl. Polymer solution was added to plasmid in an equivalent volume at an amine-to-phosphate ratio (N/P) of 5, vortexed briefly, and allowed to complex for 20-30 minutes at room temperature.

5.2.5 *Polyplex uptake and transfection*

Jurkat and primary human T cells were washed once with sterile phosphate buffered saline (PBS) via centrifugation at 500×g for 3 minutes and resuspended in Opti-MEM media (Gibco). Jurkats were plated at 1×10^6 cells/mL in 250 μL (2.5×10^5 cells) and primary T cells were plated at 3×10^6 cells/mL in 250 μL (7.5×10^5 cells). HeLa cells were washed once with sterile PBS before the addition of 250 μL of Opti-MEM media. All cells were stored in a 37 °C and 5% CO_2 humidified incubator during polyplex formation.

YOYO-1 labeled plasmid DNA was used for polyplex formation in uptake studies and unlabeled plasmid DNA was used in transfection studies. Polyplexes were added dropwise to wells, with 1, 1.5, and 2 μg equivalent of DNA (20, 30, and 40 μL of polyplex) added to HeLa, Jurkat, and primary T cells, respectively. Cells were incubated with polyplexes for 4 hours prior to flow cytometry analysis for uptake studies, or 700 μL complete media addition and additional 48-hour culture period for transfection studies.

5.2.6 *Autophagy regulation treatments*

Autophagy regulators 3-methyladenine (3-MA) and rapamycin were used in transfection studies as previously described.[20] Briefly, 3-MA was supplemented to Opti-MEM medium at 5 or 10 mM during the 4 hour transfection period. The complete media added after transfection did not contain 3-MA. In rapamycin transfection studies, rapamycin at 10 or 100 nM was added to the complete culture media of cells 2 hours prior to transfection. Rapamycin was removed from cells during the 4-hour transfection period, and supplemented in the complete media at the same concentrations for the 48-hour culture period prior to flow cytometry analysis.

5.2.7 *pH-sensitive dextran uptake*

HeLa cells were seeded the same for dextran uptake studies as transfection studies, detailed above, washed once in PBS, and maintained in 180 μL of live cell imaging solution (LCIS, 140 mM NaCl, 2.5 mM KCl, 1.8 mM $CaCl_2$ 1 mM $MgCl_2$, 20 mM HEPES, pH 7.4) during uptake studies. Jurkats and primary T cells were washed once in PBS and seeded at 2.22×10^6 cells/mL in 90 μL in a 96 well plate (2×10^5 cells per well) in LCIS.

At designated times (15, 30, 60, 120, or 240 minutes prior to analysis), pHrodo labeled dextran was added to designated wells to a final concentration of 20 μg/mL and cells were incubated at 37 °C. Prior to flow cytometry analysis, HeLa cells were lifted using 0.05% trypsin (ThermoFisher)

and Jurkat and Primary T cells were washed once with 0.05% trypsin. Cells were washed twice with LCIS and resuspended in either LCIS or pH clamping buffers (pH 5.5, 6.5, and 7.5) supplemented with the ionophores valinomycin and nigericin. After a 5-minute incubation at 37 °C, cells were analyzed by flow cytometry (Supplemental Figure 5.3).

5.2.8 *LC3B staining and confocal microscopy*

Cells were plated and treated with polyplexes as described above. 30-60 minutes after transfection, cells were resuspended in culture medium and transferred to poly-D-lysine coated glass slides. Cells adhered for 1 hour prior to being fixed in 4% paraformaldehyde for 15 minutes at room temperature. Cells were stained with rabbit anti-human LC3B antibody at 1:200 dilution followed by staining with Alexa Fluor 488 donkey anti-rabbit secondary antibody at 1:400 dilution and DAPI. Coverslips were mounted using PVA/DABCO mounting medium and imaged the on a Leica SP8X scanning confocal microscope.

5.2.9 *Flow cytometry*

Cells were transferred to a U-bottom 96-well plate. In transfection studies, cells were washed once with PBS and stained with a 1:500 dilution of Zombie Violet or Zombie NIR fixable viability stain. For both transfection and uptake studies, cells were washed twice with PBS with 1% bovine serum albumin (BSA, Miltenyi) via centrifugation 500×g for 3 minutes. For transfection studies, cells were resuspended in 200 μL of PBS with 1% BSA. In uptake studies, cells were resuspended in 200 μL of 0.04% trypan blue in PBS to quench extracellular fluorescence. Cells were immediately analyzed on either a MacsQuant Analyzer (Miltenyi) or Attune NxT (ThermoFisher) flow cytometer. At least 1×10^4 events were collected for each sample.

FlowJo software (FlowJo, LLC) was used for data analysis, with serial gating (Supplemental Figure 5.2). Transfection efficiency was measured as the percentage of live cells expressing GFP fluorescence.

5.2.10 *Statistical analyses*

Results are given as mean value ± standard deviation (SD). Two-way ANOVA with Dunnett's multiple comparisons posthoc analysis were performed in GraphPad Prism software (Graph Pad Software).

5.3 Results and Discussion

5.3.1 *Polyplex uptake and transfection reduced in primary T cells*

Cell binding and uptake of cationic polyplexes by endocytosis is the initial step in successful transfection.[21] To quantify polyplex uptake in cells, we used the fluorescent dimeric cyanine dye YOYO-1 to label plasmid DNA prior to polyplex formation with Comb or VIPER. The percentage of HeLa, Jurkat, or activated primary human T cells that had taken up polyplexes after a 4-hour incubation was quantified by flow cytometry (Figure 5.2 a). Extracellular fluorescence of associated, but not internalized, polyplexes was quenched with trypan blue.[21] In all cells tested, VIPER polyplexes were detected in a higher percentage of cells. The uptake efficiency for Comb and VIPER polyplexes was consistent between HeLa and Jurkat cell lines, but significantly lower in primary human T cells. As we previously reported, Comb and VIPER polyplexes transfect HeLa cells, while VIPER polyplexes showed very low transfection levels (1.5% and 3.5%) in Jurkat and primary T cells respectively (Figure 5.2 b).[9] Overall transfection levels were also lower in primary T cells.

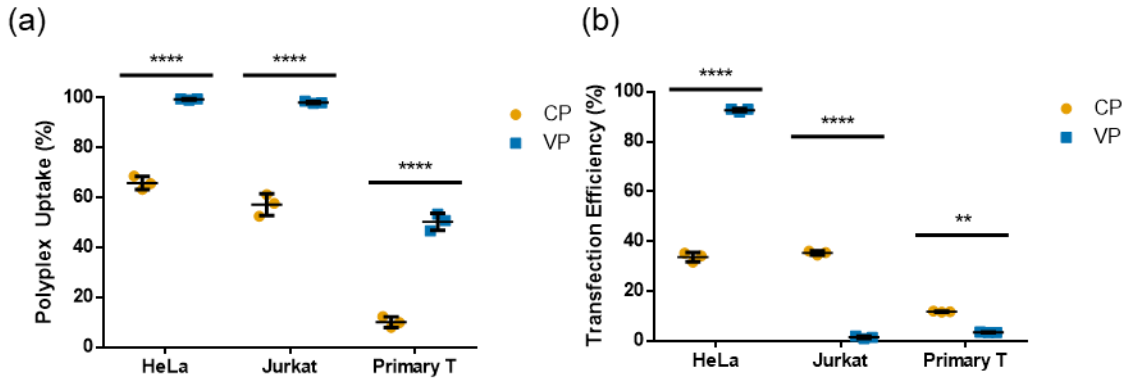

Figure 5.2. (a) Uptake and (b) transfection efficiency of Comb and VIPER polyplexes in HeLa, Jurkat, and primary T cells. Transfection efficiencies are expressed as percentage of GFP-positive cells. Data are shown as mean ± SD (n=3; 2-way ANOVA with Dunnett's multiple comparisons, **p<0.01, ****p<0.0001).

These results indicate that overall lower uptake of polyplexes into primary T cells may contribute to low transfection efficiencies compared to other cell types. Future polymers designed for T cell delivery should be screened and optimized for uptake efficiency. However, it is clear that intracellular trafficking represents a significant challenge for polyplex mediated gene delivery to T cells, as VIPER polyplexes had greater accumulation in Jurkat and primary T cells but still had lower transfection efficiency.

5.3.2 *Endosomal acidification is delayed in T cells*

VIPER's potent pH-selective membrane-lytic activity is responsible for its high transfection efficiency in most cultured cells.[19,22] Since uptake was not a barrier to successful gene delivery with VIPER, we hypothesized that the acidification of endosomal compartments in Jurkat and primary T cells may be delayed compared to the cell lines that VIPER efficiently transfects. To test this hypothesis, we measured the average endosomal pH of HeLa, Jurkat, and primary human T cells over a 4-hour period to understand the intracellular environment during transfection studies. We used 10 kDa dextran labeled with the pH-sensitive pHrodo dye (ThermoFisher) for these studies. Dextran is a well-established molecule used to study fluid-phase endocytosis pathways, as well as endosomal and lysosomal trafficking and pH.[23–25] In addition, dextran does not have buffering capacity like pDMAEMA polymers, resulting in more accurate intracellular pH measurements.[26]

Standard curves were created for each cell type by fixing the intracellular pH at 5.5, 6.5, or 7.5 using buffers supplemented with ionophores and measuring the fluorescent intensity of internalized dextran at that pH (Supplemental Figure 5.4). The experimental intracellular pH was calculated using a linear regression at each time point, which accounts for the variation in total dextran uptake over time. The intracellular pH of HeLa cells rapidly dropped to 6 within 30 minutes (Figure 5.3). However, the intracellular pH of primary T cells was much higher than HeLa cells at every time point tested, except for 60 minutes, and did not get below pH 6 even 4 hours after initial uptake. The intracellular pH of Jurkat cells was only significantly higher than HeLas at the 2 hour time point ($p<0.05$), and only significantly lower than primary T cells at 4 hours ($p<0.01$). The pH-sensitive monomer in VIPER has a pKa of 6.4 and therefore the micelle core of the polyplex may not reach a low enough pH to dissociate within primary human T cells.[27]

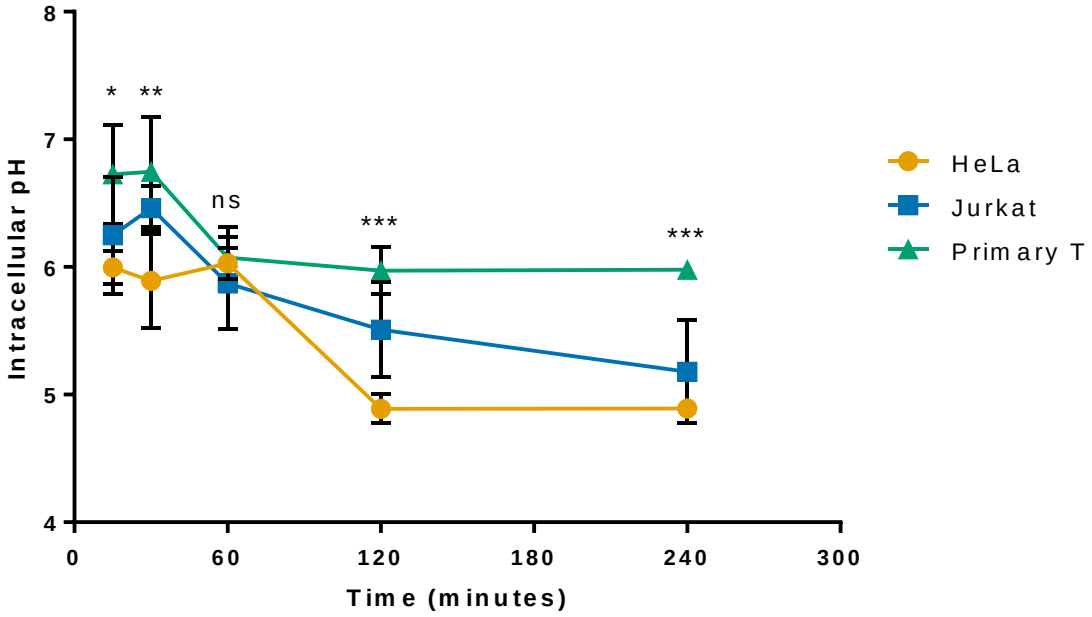

Figure 5.3. Intracellular pH of HeLa, Jurkat, and primary human T cells over time. Intracellular pH at various incubation times as measured using pHrodo labeled dextran and flow cytometry. Data are shown as mean ± SD (n=3; 2-way ANOVA with Dunnett's multiple comparisons, *p<0.05, **p<0.01, ***p<0.001).

This study suggests that the future design of polymer gene delivery systems for human T cells should include endosomal release mechanisms that can be effective without relying on rapid acificiation to lower pH (below 6). For example, a pH-sensitive monomer with a higher pKa value could be used in place of the diisopropylaminoethyl methacrylate (DIPAMA) and potentially be triggered in the endosomal compartment of T cells.[28,29]

5.3.3 *Immune sensing IFITM proteins play minor role in modulating transfection*

Polyplexes and viruses take similar intracellular paths through cells. The interferon induced transmembrane (IFITM) family of proteins (IFITM 1, 2, and 3) has been implicated as a sensing pathway that reduces viral uptake and escape from endosomes.[16] IFITM3 specifically recruits cholesterol to the endosomal membrane, increasing membrane stiffness and reducing endosomal escape. While these proteins are not solely expressed in immune cells, they have been shown to play a role in the viral infectivity of T cell lines. We used IFITM overexpressing Jurkat T cell lines developed by Shan-Lu Liu's laboratory to evaluate the impact of these proteins on non-viral gene delivery.[15] Expected overexpression in each cell line was confirmed by western blot (Figure 5.4

a). The antibodies for IFITM2 and IFITM3 have known cross-reactivity and stained both the IFITM2 overexpressing and IFITM3 overexpressing Jurkat cell lines. Important to note, when we performed western blots for all three IFITM proteins on cell extracts from HeLa cells and three Jurkat cell lines, the HeLa cell extracts had the highest IFITM expression (Figure 5.4 b). This data alone suggests that IFITM proteins do not significantly inhibit polymer-mediated gene delivery, as both Comb and VIPER can efficiently transfect HeLa cells.

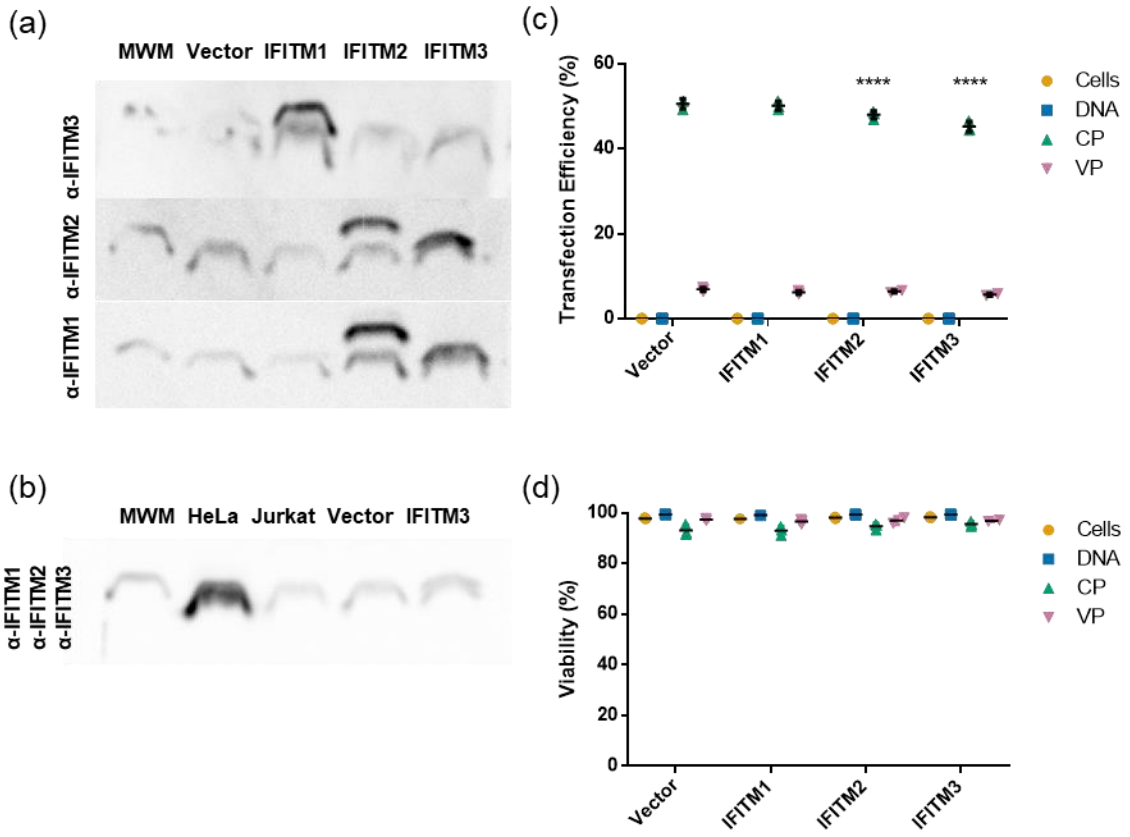

Figure 5.4. IFITM protein expresison analysis and polymer transfections of pmaxGFP plasmid in IFITM overexpressing Jurkat T cell lines. (a) Protein expression of individual IFITM 1, 2, and 3 proteins in Jurkat cell lines visualized by western blot. (b) Protein expression of IFITM 1, 2, and 3 in HeLa, parental Jurkat, vector only, and IFITM3 overexpressing Jurkat cells. (c) Transfection efficiency and (d) viability of cationic polymers in Jurkat human T cell lines overexpressing IFITM 1, 2, or 3. Transfection efficiencies are expressed as percentage of GFP-positive cells. Data are shown as mean ± SD (n=3; 2-way ANOVA with Dunnett's multiple comparisons, ****p<0.0001).

Transfection efficiency and viability were compared to the vector transduced Jurkat cell line that does not overexpress any of the IFITM proteins (Figure 5.4 c). Jurkat cell lines overexpressing

IFITM 2 and IFITM 3 did have a slight (~5-10%), but statistically significant, reduction in transfection efficiency when Comb was used as the gene delivery agent. Similar percent reductions of 5-10% were observed in IFITM 2 and IFITM 3 overexpressing cells when VIPER was used as the gene deliver agent. Additional mechanistic studies would be needed to understand the interactions between IFITM proteins and cationic polymer gene carriers. From this study, IFITM proteins were ruled out as a critical barrier to improving gene delivery in T cells.

5.3.4 *Enhancing autophagy reduces transfection efficiency in T cells*

Autophagy is a conserved process within mammalian cells that plays the important role of sequestering and degrading proteins aggregates, damaged organelles, and intracellular pathogens.[30] Autophagy is an integral process in T cells, tied to homeostasis, mitochondrial clearance, memory formation, proliferation, and survival.[31–35] Studies have shown that polyplex uptake can increase autophagosome formation in cells, and that polyplexes are sequestered in autophagosomes, a suspected non-productive destination that prevents nuclear transport.[17,36,37] We fixed primary human T cells 30 or 60 minutes after transfection, stained with an anti-LC3B antibody that labels autophagosomes, and imaged by confocal microscopy (Supplemental Figure 5.5). Widespread punctate staining was observed, confirming the presence of significant autophagosomes in T cells during transfection.

Small molecule inhibitors and activators of autophagy have been investigated as tools to modulate *in vitro* non-viral gene delivery. The Wang group evaluated the mTOR-dependent autophagy inhibitor 3-methyladenine (3-MA) and activator rapamycin in PEI mediated gene delivery to murine fibroblasts.[20] They found that increasing mTOR-dependent autophagy with rapamycin improved transfection efficiency by 20%, whereas inhibiting autophagy with 3-MA reduced transfection efficiency by 80%. The same trends held for the Yang group who evaluated the impact of mTOR-dependent and -independent regulators of autophagy on siRNA knockdown efficiency using chitosan as a gene carrier to a human lung cancer cell line.[38] While the mechanism for this phenomenon has not been determined, the Yang group proposes that mTOR-independent autophagosomes, rather than mTOR-dependent, are responsible for polyplex sequestration and reduced transfection efficiency. They posit the “LC3 competing” hypothesis, that by increasing mTOR-dependent autophagy with Rapamycin, mTOR-independent autophagosome formation and polyplex sequestering is reduced.

We evaluated these two small molecule regulators of autophagy in the Jurkat human T cell line and the HeLa human cervical endothelial cell line using VIPER and Comb as gene carriers. Rapamycin, an autophagy activator, increased transfection efficiency of VIPER delivered plasmid DNA in HeLa cells at the highest concentration tested (100 nM) (Figure 4.5). However, rapamycin treatment reduced transfection efficiency and viability in Jurkat cells transfected using Comb. These results are opposite of what has been observed in many adherent cell lines tested, but is likely due to the mTOR pathway regulating many different facets of T cell function outside of autophagy activation.[39] The potential benefits of rapamycin treatment on autophagosome cycling during transfection were most likely offset by the G1 arrest and anergy induction also caused by mTOR signaling in T cells.[11,40]

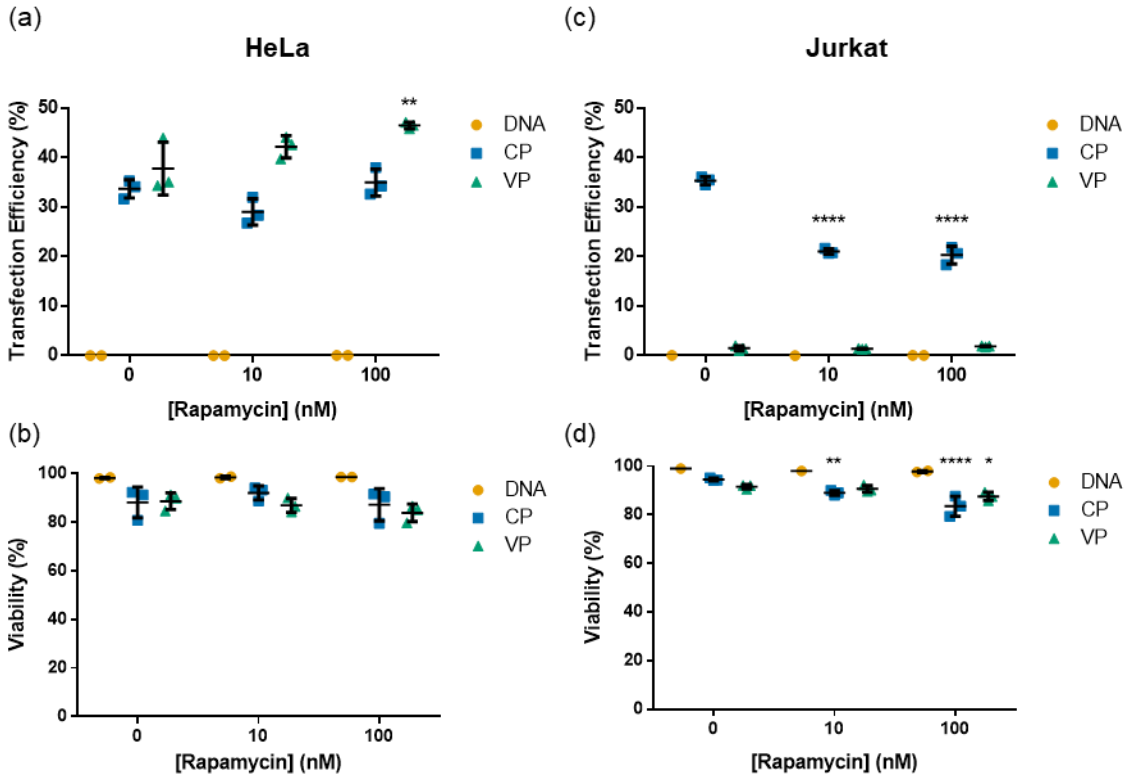

Figure 5.5. Transfection of HeLa and Jurkat cells with rapamycin treatment. (a & b) Transfection efficiency and viability of HeLa cells transfected with Comb or VIPER at varying rapamycin concentrations. (c & d) Transfection efficiency and viability of Jurkat cells transfected with Comb or VIPER polymer at varying rapamycin concentrations. Transfection efficiencies are expressed as percentage of GFP-positive cells. Data are shown as mean ± SD (n=3, 2-way ANOVA with Dunnett's multiple comparisons test, * $p<0.05$, ** $p<0.01$, **** $p<0.001$).

We then tested the autophagy inhibitor 3-MA in Jurkat T cell transfections with Comb to test if inhibiting autophagy would increase transfection efficiency (Figure 5.6). Treatment with 3-MA did increase transfection efficiency as measured by percent of cells expressing GFP and had only a slight impact on the viability of cells. When expressed in terms of total number of cells, treatment with 3-MA significantly reduced the number of live cells, with or without polyplex treatment, and reduced the total number of transfected cells. This potential gain in transfection efficiency is negated by the total reduction in cell number also caused by 3-MA treatment. These results are corroborated by previous studies that report a reduction in murine $CD4^+$ T cell proliferation with 3-MA treatment.[41]

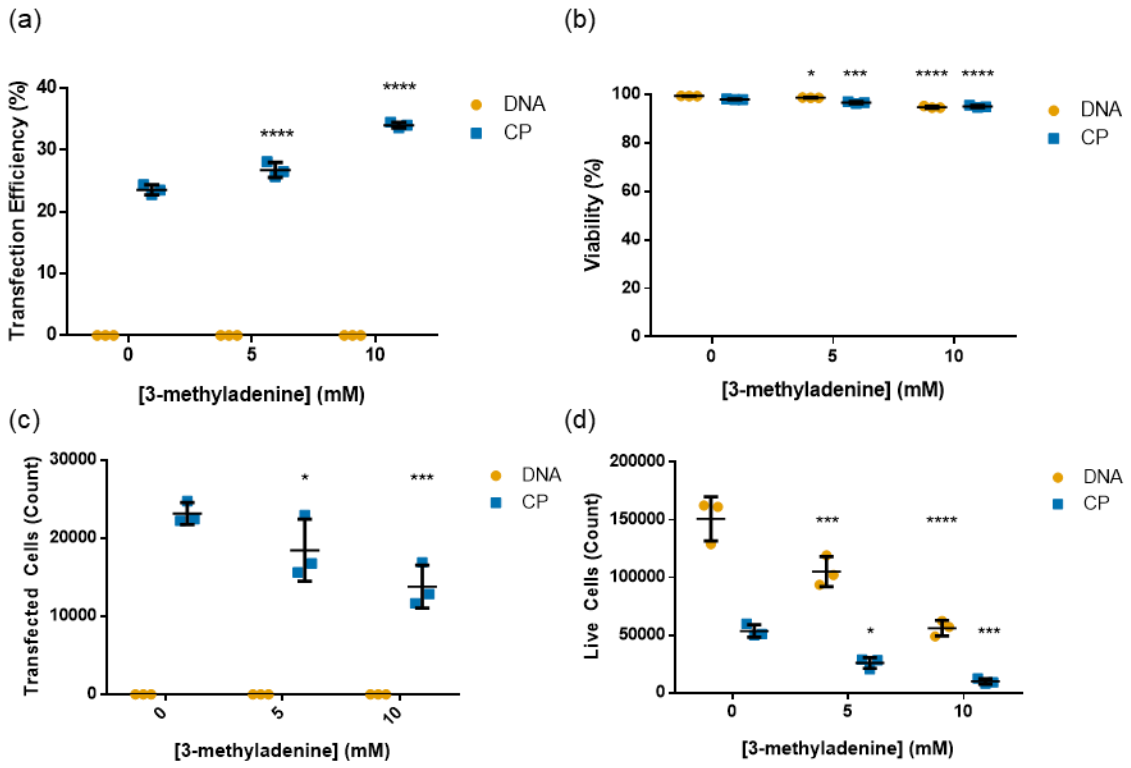

Figure 5.6. Transfection of Jurkats with 3-MA treatment. (a) Transfection efficiency, (b) viability, (c) transfected cell count, and (d) live cell count of Jurkat cells transfected with Comb at varying 3-methyladenine concentrations. Transfection efficiencies are expressed as percentage of GFP-positive cells. Data are shown as mean ± SD (n=3; 2-way ANOVA with Dunnett's multiple comparisons, * $p<0.05$, *** $p<0.001$, ****$p<0.0001$).

These results demonstrate that T cells have autophagosomes during the early stages of polyplex transfections and that manipulating autophagy does impact polyplex gene delivery in the Jurkat T cell line. However, the mTOR and PI3K pathways that these small molecules inhibit also control other important pathways key to T cell function and survival. Small molecule regulators of autophagy are likely not a viable method for improving polyplex gene delivery to T cells.

5.4 CONCLUSION

Developing efficient non-viral gene delivery platforms specifically for T cells is an emerging area of interest. The current nature of manufacturing genetically modified T cells lends itself well to non-viral gene delivery agents. The genetic modification process happens *ex vivo*, removing the need to design gene carriers for *in vivo* stability or organ specificity. The transfection conditions can be specifically tuned in the *ex vivo* environment to promote successful delivery, like brief culture periods in serum-free media. In addition, chemically defined polymer transfection agents have reduced lot-to-lot variability compared to viruses yielding a more predictable gene transfer process. In order to design more efficient gene carriers specifically for T cells, there is a need to better understand the unique barriers to gene delivery in T cells.

These studies begin to identify key barriers to efficient gene delivery with cationic polymers in T cells. Our data indicate that the family of interferon induced transmembrane (IFITM) proteins do not play as significant of a role in preventing polyplex endosomal escape as they do in preventing viral escape. We do observe that autophagosomes are present in T cells during transfection. However, applying previously developed methods for modulating autophagy with small molecules to increase transfection efficiency had a deleterious effect on T cell growth and viability.

Both the poor polyplex uptake efficiency and higher endosomal pH of primary T cells dictated the success of the two polymer gene carriers tested. Primary T cells take up polyplexes less efficiently than HeLa or Jurkat cell lines. In addition, the acidification of endosomes in primary T cells is slower and less severe than HeLa cells, reducing the gene transfer efficiency of polymers designed for pH-triggered endosomal escape. These finding motivate the design of new gene carrier systems that can be tailored to these biological traits of T cells.

5.5 ACKNOWLEDGEMENTS

We thank Dr. Heather Gustafson for helpful suggestions and discussion. Confocal microscopy images were taken at the W.M.Keck Center for Advanced Studies in Neural Signaling at the University of Washington with the help of Dr. Heather Gustafson and Dr. Nathaniel Peters. We thank Prof. Shan-Lu Liu for providing the IFITM overexpressing Jurkat cell lines and Prof. Michael Jensen for providing the parental Jurkat cell line. This work was supported by the National Institutes of Health [1R01CA177272, 2R01NS064404]. B.R.O. was supported by a National Science Foundation Graduate Research Fellowship [DGE-1256082].

5.6 REFERENCES

1. FDA. Food and Drug Administration approval for Kymriah - tisagenlecleucel. (2017).
2. U.S. Food and Drug Administration. Yescarta BL 125643/0 Approval Letter. (2017).
3. McGovern, J. L., Wright, G. P. & Stauss, H. J. Engineering specificity and function of therapeutic regulatory T cells. *Front. Immunol.* **8,** 1–6 (2017).
4. Arellano, B., Graber, D. J. & Sentman, C. L. Regulatory T cell-based therapies for autoimmunity. *Discov. Med.* **22,** 73–80 (2016).
5. Eyquem, J. *et al.* Targeting a CAR to the TRAC locus with CRISPR/Cas9 enhances tumour rejection. *Nature* **543,** 113–117 (2017).
6. Morsut, L. *et al.* Engineering Customized Cell Sensing and Response Behaviors Using Synthetic Notch Receptors. *Cell* **164,** 780–791 (2016).
7. Smith, T. T. *et al.* In situ programming of leukaemia-specific T cells using synthetic DNA nanocarriers. *Nat. Nanotechnol.* (2017). doi:10.1038/nnano.2017.57
8. Moffett, H. F. *et al.* Hit-and-run programming of therapeutic cytoreagents using mRNA nanocarriers. *Nat. Commun.* **8,** 389 (2017).
9. Olden, B. R., Cheng, Y., Yu, J. L. & Pun, S. H. Cationic polymers for non-viral gene delivery to human T cells. *J. Control. Release* **282,** 140–147 (2018).
10. Schallon, A., Synatschke, C. V., Jérôme, V., Müller, A. H. E. & Freitag, R. Nanoparticulate nonviral agent for the effective delivery of pDNA and siRNA to differentiated cells and primary human T lymphocytes. *Biomacromolecules* (2012). doi:10.1021/bm3012055
11. Kamiya, H., Tsuchiya, H., Yamazaki, J. & Harashima, H. Intracellular trafficking and transgene expression of viral and non-viral gene vectors. *Adv. Drug Deliv. Rev.* **52,** 153–164 (2001).
12. Lechardeur, D., Verkman, A. S. & Lukacs, G. L. Intracellular routing of plasmid DNA during non-viral gene transfer. *Adv. Drug Deliv. Rev.* **57,** 755–767 (2005).
13. Akinc, A., Thomas, M., Klibanov, A. M. & Langer, R. Exploring polyethylenimine-mediated DNA transfection and the proton sponge hypothesis. *J. Gene Med.* **7,** 657–663 (2005).
14. Amin, Z. R., Rahimizadeh, M., Eshghi, H., Dehshahri, A. & Ramezani, M. The effect of cationic charge density change on transfection efficiency of Polyethylenimine. *Iran. J. Basic Med. Sci.* **16,** 150–156 (2013).
15. Yu, J. *et al.* IFITM Proteins Restrict HIV-1 Infection by Antagonizing the Envelope Glycoprotein. *Cell Rep.* **13,** 145–156 (2015).
16. Amini-Bavil-Olyaee, S. *et al.* The antiviral effector IFITM3 disrupts intracellular cholesterol homeostasis to block viral entry. *Cell Host Microbe* **13,** 452–464 (2013).
17. Roberts, R. *et al.* Autophagy and formation of tubulovesicular autophagosomes provide a barrier against nonviral gene delivery. *Autophagy* **9,** 667–682 (2013).
18. Cheng, Y. *et al.* Nano-Sized Sunflower Polycations As Effective Gene Transfer Vehicles. *Small* **12,** 2750–2758 (2016).
19. Cheng, Y., Yumul, R. C. & Pun, S. H. Virus-Inspired Polymer for Efficient In Vitro and In Vivo Gene Delivery. *Angew. Chemie - Int. Ed.* **55,** 12013–12017 (2016).
20. Zhong, X., Panus, D., Ji, W. & Wang, C. Modulating polyplex-mediated gene transfection by small-molecule regulators of autophagy. *Mol. Pharm.* **12,** 932–940 (2015).
21. Rejman, J., Bragonzi, A. & Conese, M. Role of clathrin- and caveolae-mediated

endocytosis in gene transfer mediated by lipo- and polyplexes. *Mol. Ther.* **12,** 468–474 (2005).
22. Feldmann, D. P. *et al.* In vitro and in vivo delivery of siRNA via VIPER polymer system to lung cells. *J. Control. Release* **276,** 50–58 (2018).
23. Bayer, N. *et al.* Effect of Bafilomycin A1 and Nocodazole on Endocytic Transport in HeLa Cells : Implications for Viral Uncoating and Infection. **72,** 9645–9655 (1998).
24. Deriy, L. V. *et al.* Disease-causing mutations in the cystic fibrosis transmembrane conductance regulator determine the functional responses of alveolar macrophages. *J. Biol. Chem.* **284,** 35926–35938 (2009).
25. Li, L. *et al.* The effect of the size of fluorescent dextran on its endocytic pathway. *Cell Biol. Int.* **39,** 531–539 (2015).
26. Lee, H., Son, S. H., Sharma, R. & Won, Y. A Discussion of the pH-Dependent Protonation Behaviors of Poly (2- (dimethylamino) ethyl methacrylate) (PDMAEMA) and Poly (ethylenimine- ran -2-ethyl-2-oxazoline) (P (EI- r -EOz)). 844–860 (2011). doi:10.1021/jp109151s
27. Zhu, L., Powell, S. & Boyes, S. G. Synthesis of tertiary amine-based pH-responsive polymers by RAFT Polymerization. *J. Polym. Sci. Part A Polym. Chem.* **53,** 1010–1022 (2015).
28. Wang, C. *et al.* A nanobuffer reporter library for fine-scale imaging and perturbation of endocytic organelles. *Nat. Commun.* **6,** 1–11 (2015).
29. Luo, M. *et al.* A STING-activating nanovaccine for cancer immunotherapy. *Nat. Nanotechnol.* **12,** 1–13 (2017).
30. Bento, C. F. *et al.* Mammalian Autophagy: How Does It Work? *Annu. Rev. Biochem.* **85,** 685–713 (2016).
31. Jia, W., Pua, H. H., Li, Q.-J. & He, Y.-W. Autophagy regulates endoplasmic reticulum homeostasis and calcium mobilization in T lymphocytes. *J. Immunol.* **186,** 1564–74 (2011).
32. Xu, X. *et al.* Autophagy is essential for effector CD8+ T cell survival and memory formation. *Nat. Immunol.* **15,** 1152–1161 (2014).
33. Pua, H. H., Dzhagalov, I., Chuck, M., Mizushima, N. & He, Y.-W. A critical role for the autophagy gene Atg5 in T cell survival and proliferation. *J. Exp. Med.* **204,** 25–31 (2007).
34. Walsh, C. M. & Edinger, A. L. The complex interplay between autophagy, apoptosis, and necrotic signals promotes T-cell homeostasis. *Immunol. Rev.* **236,** 95–109 (2010).
35. Pua, H. H., Guo, J., Komatsu, M. & He, Y.-W. Autophagy is essential for mitochondrial clearance in mature T lymphocytes. *J. Immunol.* **182,** 4046–55 (2009).
36. Man, N., Chen, Y., Zheng, F., Zhou, W. & Wen, L. P. Induction of genuine autophagy by cationic lipids in mammalian cells. *Autophagy* **6,** 449–454 (2010).
37. Remaut, K., Oorschot, V., Braeckmans, K., Klumperman, J. & De Smedt, S. C. Lysosomal capturing of cytoplasmic injected nanoparticles by autophagy: An additional barrier to non viral gene delivery. *J. Control. Release* **195,** 29–36 (2014).
38. Song, W., Ma, Z., Zhang, Y. & Yang, C. Autophagy plays a dual role during intracellular siRNA delivery by lipoplex and polyplex nanoparticles. *Acta Biomater.* 1–9 (2017). doi:10.1016/j.actbio.2017.05.038
39. Powell, J. D. & Delgoffe, G. M. The Mammalian Target of Rapamycin : Linking T Cell Differentiation , Function , and Metabolism. *Immunity* **33,** 301–311 (2010).
40. Golzio, M., Teissié, J. & Rols, M. P. Cell synchronization effect on mammalian cell

permeabilization and gene delivery by electric field. *Biochim. Biophys. Acta - Biomembr.* **1563,** 23–28 (2002).
41. Whang, M. I. *et al.* The Ubiquitin Binding Protein TAX1BP1 Mediates Autophagosome Induction and the Metabolic Transition of Activated T Cells Article The Ubiquitin Binding Protein TAX1BP1 Mediates Autophagosome Induction and the Metabolic Transition of Activated T Cells. *Immunity* **46,** 405–420 (2017).

5.7 SUPPLEMENTARY INFORMATION

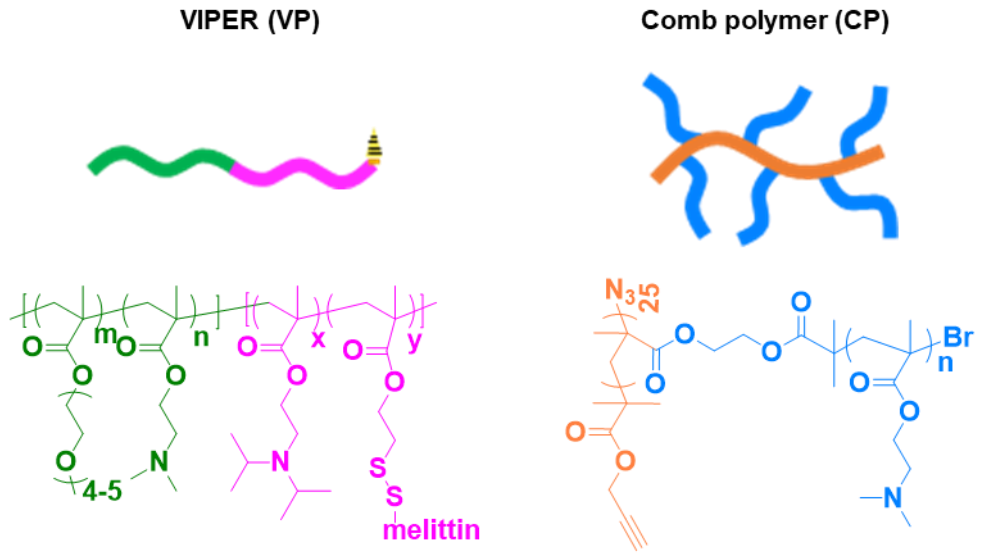

Supplemental Figure 5.1. Schematic and chemical structures of virus-inspired polymer for endosomal release (VIPER) and comb polymer (Comb).

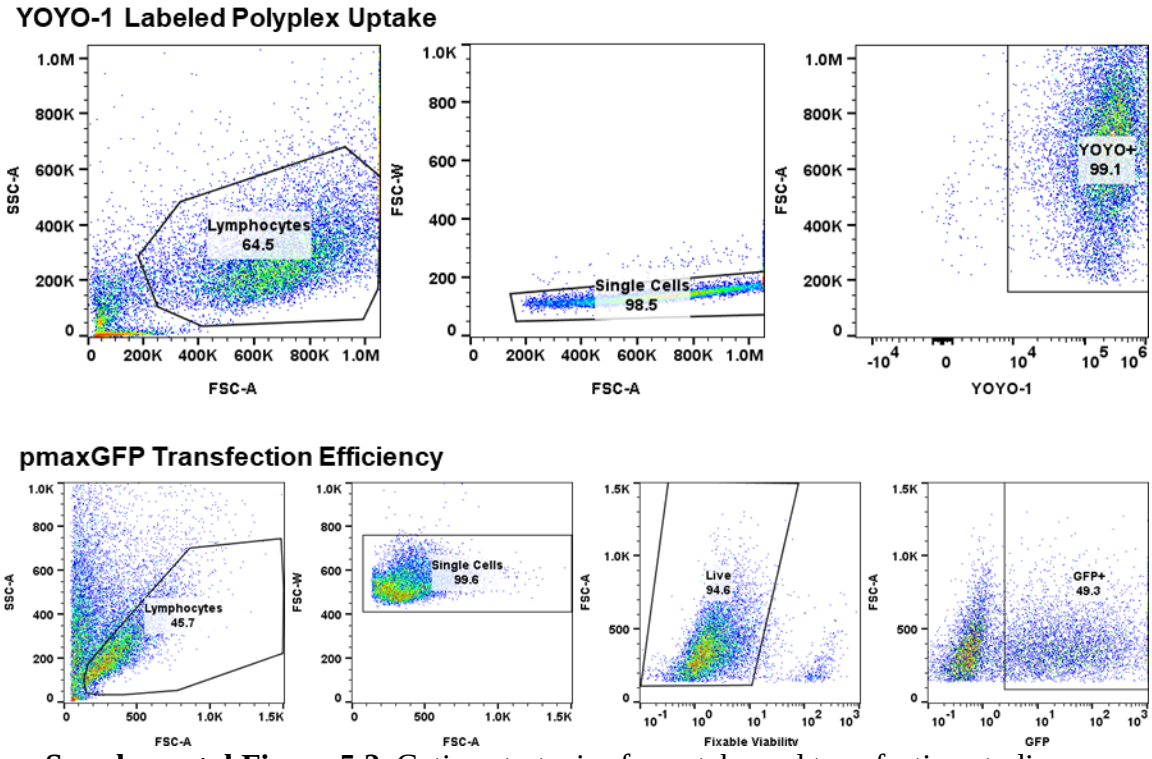

Supplemental Figure 5.2. Gating strategies for uptake and transfection studies.

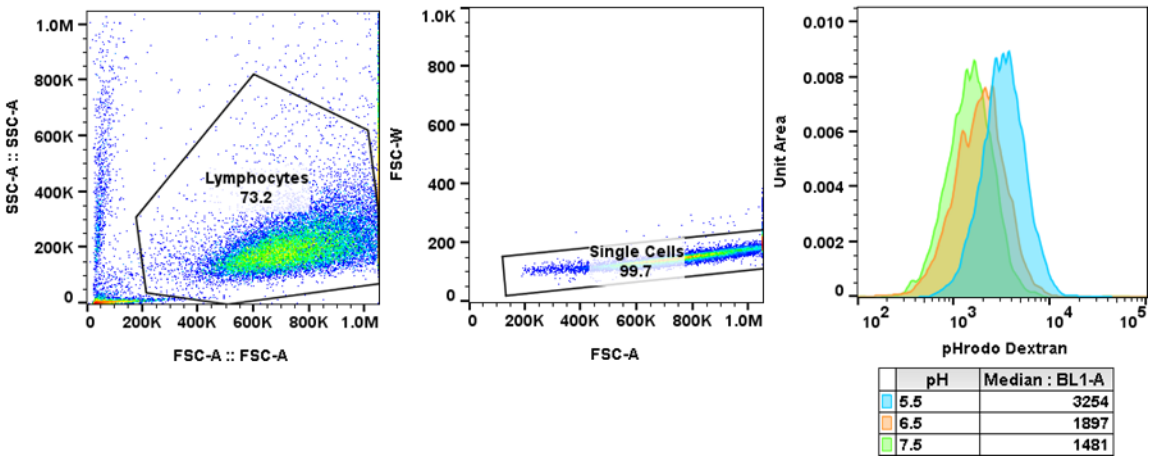

Supplemental Figure 5.3. Gating strategies for pHrodo dextran uptake studies.

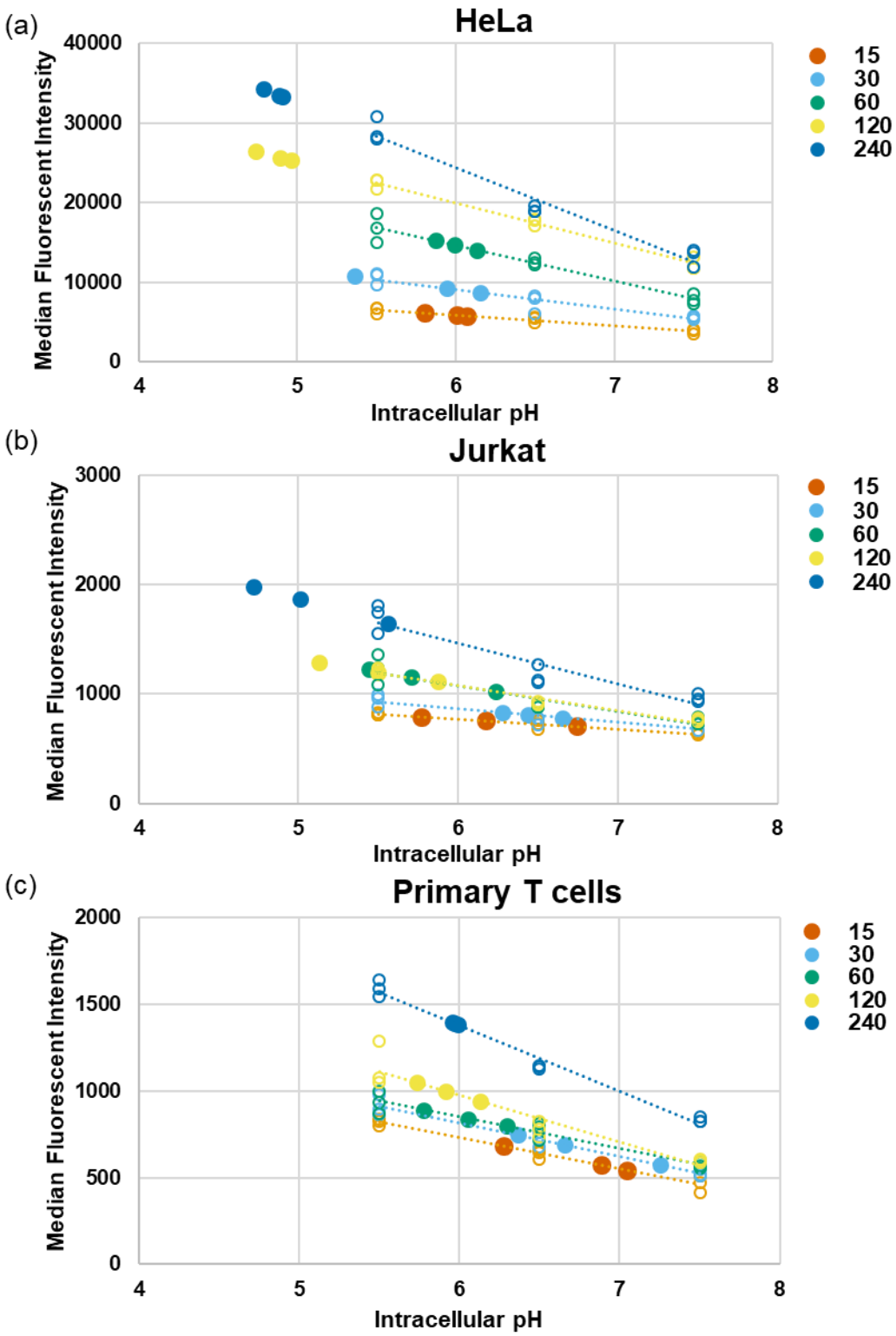

Supplemental Figure 5.4. Calibration curves (open circles with dotted trendline) used for experimental intracellular pH calculations (filled circles) for (a) HeLa, (b) Jurkat, and (c) primary human T cells using pHrodo labeled 10 kDa MW dextran.

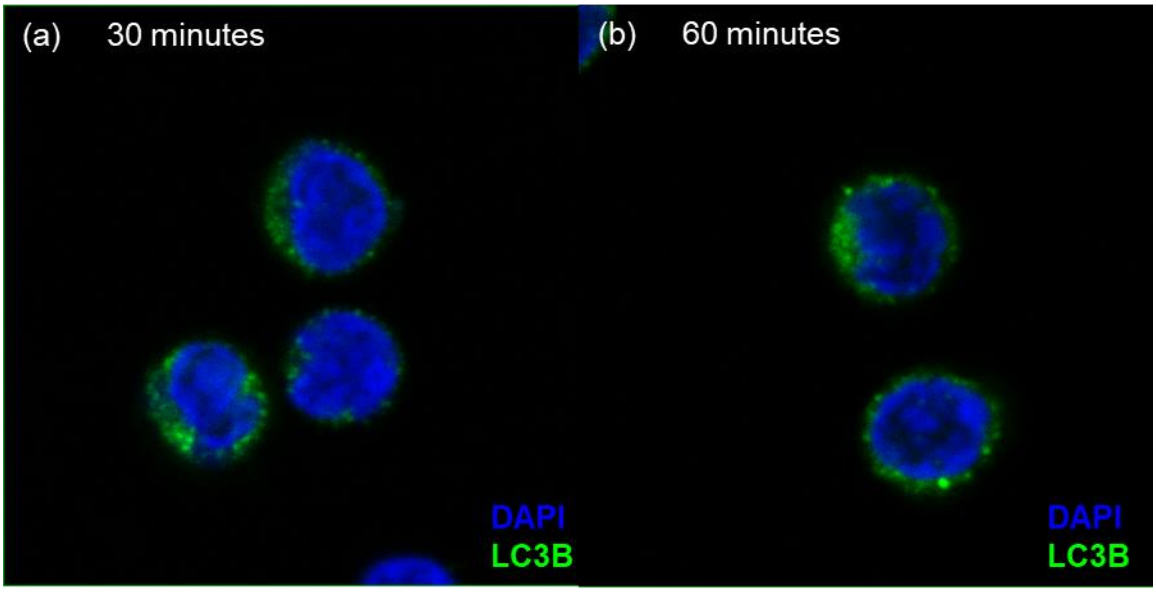

Supplemental Figure 5.5. Confocal microscopy images of autophagy in primary human T cells. T cells transfected with VIPER polyplexes for (a) 30 minutes or (b) 60 minutes stained with LC3B antibody that labels autophagosomes.

Chapter 6. SUMMARY OF MAJOR FINDINGS AND RECOMMENDATIONS FOR FUTURE WORK

6.1 SUMMARY OF MAJOR FINDINGS

6.1.1 *Supported lipid bilayer platform for T cell growth and activation*

Cell-templated silica microparticles can be used as a platform for supported lipid bilayers and T cell activation. In Chapter 2, a panel of 18 artificial antigen presenting cells (aAPCs) were synthesized with varying size, shape, membrane fluidity, and antigen density. These particles were able to initiate T cell growth at similar rates, but significantly increased the ratio of outgrowth of $CD8^+$ T cells over $CD4^+$ T cells, as compared to commercially available DynaBeads. However, no statistical trends were observed across particle shape, membrane fluidity, or antigen density in either fold-expansion or $CD4^+$:$CD8^+$, largely due to donor-to-donor variability across treatments. Particle shape had an impact on $CD8^+$ T cell differentiation state after outgrowth, with HeLa and red blood cell templated particles resulting in larger populations of less-differentiated cells ($CD45RA^+$/$CD62L^+$) compared to microsphere aAPCs at the same membrane fluidity and antigen loading.

6.1.2 *Synthetic targeting ligands for T cell activation remain elusive*

Synthetic ligands like peptides and aptamers are an attractive alternative to antibodies in the application of T cell activation due to the ease of chemical synthesis, reduced lot-to-lot variability, and reduced cost. In Chapter 3, both peptide phage display and aptamer SELEX were used to screen for novel ligands with affinity and specificity to the T cell receptor CD3ε and costimulatory receptor CD28. Phage display experiments using recombinant proteins and target expressing cell lines did not yield any peptides with high affinity to either receptor. Modified RNA and ssDNA aptamer libraries were used in protein-SELEX experiments that did not yield highly specific aptamer sequences or enrich for aptamers that bind to human T cells. Despite these experiments not meeting the primary objective of finding ligands for T cell activation, the methods developed for next-generation sequencing and analysis of selected libraries is applicable to future library screening experiments. Future work should focus on developing selection experiments for ssDNA aptamers that incorporate complex selection strategies that rely on multiple target display

platforms (cells and recombinant proteins) as well as specific elution strategies using known ligands against the receptors of interest.

6.1.3 *Cationic polymers for non-viral gene delivery to T cells*

Cationic polymers were investigated as non-viral gene delivery agents for T cells. Comb-shaped polymers with a hydrophilic hydroxyethyl methacrylate (HEMA) backbone and branches of the tertiary amine 2-dimethylaminoethyl methacrylate (DMAEMA) were able to achieve moderate gene expression from the delivery of plasmid DNA and messenger RNA to the human Jurkat T cell line and primary human T cells. Activation time prior to transfection, cytokine supplements in cell culture media, DNA dose, and cell density were all important parameters to optimize for increasing gene expression in primary T cells. Mechanistic studies revealed that primary T cells uptake fewer polyplexes compared to HeLa and Jurkat cell lines, and slower acidification of endosomes in T cells likely requires cell-specific considerations for designing polymers for endosomal escape in T cells.

6.2 RECOMMENDATIONS FOR FUTURE WORK

6.2.1 *Totally synthetic targeted gene carriers for human T cells*

Background and significance

The extensive *ex vivo* manipulation steps required in CAR T cell manufacturing make the therapy cost prohibitive for widespread patient access. A recently explored alternative is to reprogram circulating T cells *in vivo*.[1] In Chapter 4 of this thesis, a cationic polymer system was developed to deliver nucleic acid cargo to T cells *in vitro*. This system relies on non-specific charge interactions between the net-positively charged polyplex and negatively charged cell membrane for intracellular cargo delivery which limits its utility to *in vitro* applications. A layer-by-layer nanoparticle synthesis technique previously used by the Stephan group for *in vivo* gene delivery to T cells could be combined with aptamers as targeting ligands to create a completely synthetic gene carrier for *in vivo* CAR T production.

Aim 1: Synthesis of aptamer-targeted nanoparticles for gene delivery

Our group recently identified a ssDNA aptamer sequence via cell-SELEX (denoted JBA) that binds to and internalizes into the Jurkat human T cell line (data not shown) and activated primary

human T cells (Figure 6.1). We hypothesize that this aptamer can facilitate specific uptake of polyplexes into activated T cells. The truncated version of this aptamer (tJBA) will be synthesized with a 6-PEG spacer and terminal amine on the 3' end (IDT). The aptamer will be conjugated to 15 kDa polyglutamic acid (PGA, Alamanda Polymers) at a 1:1 target molar ratio via standard EDC/NHS chemistry. To facilitate binding studies, a parallel conjugation reaction will dope in amine-PEG_2-biotin (ThermoFisher) for detection using a secondary fluorescent stain. Conjugation efficiency will be monitored with a ninhydrin test to confirm the loss of terminal primary amines after aptamer and biotin conjugation. PGA-aptamer conjugates will be purified via PAGE gel purification. PGA-conjugated aptamers will be annealed at 95 °C for 5 minutes before being snap-cooled on ice to ensure proper aptamer conformation for binding. Conserved binding of PGA-aptamer conjugates to the Jurkat cell line and activated primary human T cells will be confirmed by flow cytometry binding studies using the biotinylated PGA-aptamer conjugates and streptavidin-PE.

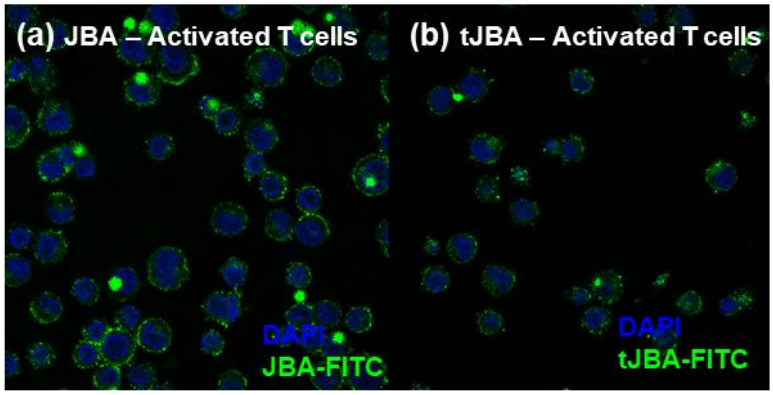

Figure 6.1. JBA aptamer internalization into primary human T cells. (a) JBA and (b) tJBA aptamers internalizes into activated human T cells.

Aptamer-targeted polyplexes will be formulated using a layer-by-layer synthesis approach. First, cationic polyplexes will be formed using plasmid DNA and comb polymer DP-25-16 as described in Chapter 5 at an amine-to-phospate ratio of 8. Aptamer-PGA conjugates will then be added at a carboxylate-to-phosphate ratio of 6. This ratio has previously been used for coating cationic polyplexes with γ-PGA.[2] Nanoparticle size and surface charge will be monitored after each step of synthesis by DLS and Zeta Potential measurements. We expect the surface charge and size of untargeted polyplexes to be +30-40 mV and 100-120 nm as observed previously

(Supplemental Figure 4.2) and targeted polyplexes to be <0 mV and slightly larger than untargeted polyplexes (~150 nm).

Aim 2: In vitro evaluation of aptamer-targeted polyplexes

Receptor-specific uptake of aptamer-targeted polyplexes will be confirmed by monitoring uptake of targeted polyplexes formulated withYOYO-1 labeled plasmid DNA by flow cytometry and confocal microscopy. We expect to see uptake in receptor positive cells (Jurkat and activated primary T cells) but not in receptor negative cells (HeLa). Selectivity will further be confirmed by performing uptake studies in a mixed human peripheral blood mononuclear cell (PBMC) culture spiked with either Jurkat cells or activated primary human T cells. Selectivity will be confirmed by co-staining with a fluorescent CD3 antibody.

Conserved transfection efficiency of aptamer-targeted polyplexes will be confirmed using pmaxGFP, evaluating GFP fluorescence 2 days post-transfection as described in Chapter 4. Ability to elicit stable integration of genes using the Sleeping Beauty Transposon system will be evaluated using genetic constructs previously designed by our group.[3]

Aim 3: In vivo evaluation of aptamer-targeted polyplexes

Aptamer-targeted polyplexes will be tested *in vivo* in a humanized mouse model (Hu-CD34$^+$ NSG mice, The Jackson Laboratory) that has circulating human T cells.[4] Initial proof-of-concept studies will be performed using pmaxGFP plasmid as the cargo. Transient gene expression will be monitored in circulating T cells collected from a retro-orbital bleed via flow cytometry. Successful transient gene expression would warrant further studies in humanized mouse models using a CD19-CAR Sleeping Beauty construct for stable integration of a CAR into circulating T cells, and subsequent antitumor activity against a CD19$^+$ Raji flank tumor.[5]

6.2.2 *On- target, off-tumor screening of CAR T cells using supported lipid bilayers*

Background and significance

In chapter 2, we report the development of a facile supported lipid bilayer system for T cell activation. The flexibility of antigen loading, in both type of antigen and density of surface coverage, lends this platform well to additional applications in CAR T cell manufacturing and development, as well as expansion of antigen-specific T cells. A key challenge in CAR construct design is to maximize on-tumor killing while minimizing on-target/off-tumor toxicities. This

challenge is especially important to overcome for transitioning CAR T cells into a treatment for solid tumors, as most cell surface markers on solid tumors are expressed at lower levels in healthy tissue.[6] One current approach is to design lower-affinity CARs that are only triggered to kill by high antigen expressing cells. A qualitative approach to this technique has been successful in screening CARs against $CD38^+$ for multiple myeloma treatment, and ICAM-1 for carcinoma treatment.[7,8] A supported lipid bilayer system could be used to quantitatively assess CAR T cell reactivity to variable antigen expression levels in a biologically relevant system. Using a fluid-phase lipid bilayer mimics the antigen fluidity of cells which more accurately recapitulates receptor expression on cells than solid-support beads. Using cytokine expression as a functional marker of activity in an intracellular cytokine assay allows for rapid, quantitative, and high-throughput screening of many CAR constructs. This assay could be used to determine the "goldilocks" region of CAR affinity that results in robust tumor killing while preventing on-target/off-tumor side effects.

Aim 1: Manufacturing ICAM-1 and CD38 displaying spherical supported lipid bilayers

Liposomes composed of 80 mol% DOPC and 20 mol% cholesterol will be formulated as described for DOPC liposomes in Chapter 2. Target proteins (human ICAM-1 or human CD38, AcroBiosystems) will be conjugated to DSPE-PEG(2000)-NHS using standard NHS chemistry. Micelles of 18:1 PEG-2000-PE and DSPE-PEG(2000)-protein will be incorporated into the liposomes in half-log steps and a total molar composition of 2.5 mol% to achieve varying levels of antigen display (molar protein loading from 2.5%-0.0025%). Protein-loaded liposomes will be fused to ~8 μm diameter silica microspheres to form supported lipid bilayers (SLBs) as reported in Chapter 2. Molar protein-lipid loading will be correlated to average ligand density via SDS-PAGE as reported previously.[9]

Aim 2: ICAM-1 training set for intracellular cytokine staining (ICCS) assay for CAR efficacy

CAR T cells against ICAM-1 of varying affinities will be generated from healthy human donor T cells as reported previously.[8] CAR^+ T cells will be incubated at various effector-to-target (E:T) ratios (0:1, 1:10, 1:3, 1:1, 3:1, 10:1), with ICAM-1 SLB particles as the target (2.5×10^{-3}-2.5×10^{0} mol% ICAM-1 loading in half-log steps), with PMA (phorbol 12-myristate-13-acetate) and ionomycin used as a positive control. 4-hour co-culture assays will be performed, with Brefeldin

A treatment to prevent cytokine release as described in Chapter 2. Cells will be fixed and permeabilized before staining for IL-2, IFN-γ, and TNF-α, and CD3, and CAR. Samples will be analyzed for cytokine production by flow cytometry.

A limit-of-detection (LOD) and minimum threshold cytokine production (C_{min}) will be calculated for each CAR T cell at each E:T ratio and for each cytokine, where the LOD represents the lowest amount of protein that triggers cytokine production in CAR T cells and the C_{min} is the cytokine production value that delineates between CAR T cells that can and cannot control tumor growth. This will provide a heat-map for each CAR receptor at various target ligand densities. We hypothesize that CAR T cells with a higher LOD will have less on-target/off-tumor killing and that *in vivo* tumor killing will correlate with a minimum threshold of cytokine expression (C_{min}) at high target concentrations. The LOD and C_{min} obtained in this study, combined with the previously published *in vitro* and *in vivo* data on the panel of ICAM-1 CAR T cells will be used to determine a range of LOD and C_{min} values that result in safe and effective CAR T cell constructs.

Aim 3: Predicting CD38 CAR selectivity with ICCS LOD assay

Previously developed CAR T cells against CD38 with high (CAR028) and medium (CARA4) and low (CARB3) affinities will be used to evaluate the robustness of the ICCS assay for CAR efficacy. These three CD38-targeted CAR constructs will be used to determine if the ICCS assay for CAR efficacy is target agnostic and predictive of on-target/off-tumor activity and affinity requirements for tumor killing. In previous animal studies, the tumor killing of high (CAR028) and medium (CARA4) affinity CAR T cells was equivalent, while only CAR028 showed on-target/off-tumor killing of $CD34^+/CD38^+$ hematopoietic progenitor cells.[7] CAR T cells transduced with these three constructs will be generated and used in the ICCS assay as described above. We would expect CAR028 and CARA4, but not CARB3 to have C_{min} values above the threshold cytokine expression value. We would also expect CARA4 to have a higher LOD than CAR028, and be the only construct within the "safe and effective" range. Results that corroborate the LOD and C_{min} values obtained in Aim 2 would motivate testing this assay with additional libraries of *in vivo* validated CAR receptors to suggest the usefulness of this assay in screening novel CAR receptors prior to *in vivo* studies.

6.3 REFERENCES

1. Smith, T. T. *et al.* In situ programming of leukaemia-specific T cells using synthetic DNA nanocarriers. *Nat. Nanotechnol.* (2017). doi:10.1038/nnano.2017.57
2. Kurosaki, T. *et al.* γ-Polyglutamic acid-coated vectors for effective and safe gene therapy. *J. Control. Release* **142,** 404–410 (2010).
3. Kacherovsky, N., Liu, G. W., Jensen, M. C. & Pun, S. H. Multiplexed gene transfer to a human T-cell line by combining Sleeping Beauty transposon system with methotrexate selection. *Biotechnol. Bioeng.* **112,** 1429–1436 (2015).
4. Shultz, L. D. *et al.* Human Lymphoid and Myeloid Cell Development in NOD/LtSz-scid IL2R null Mice Engrafted with Mobilized Human Hemopoietic Stem Cells. *J. Immunol.* **174,** 6477–6489 (2005).
5. Hudecek, M. *et al.* The Nonsignaling Extracellular Spacer Domain of Chimeric Antigen Receptors Is Decisive for In Vivo Antitumor Activity. *Cancer Immunol. Res.* **3,** 125–135 (2015).
6. Fesnak, A. D., June, C. H. & Levine, B. L. in *Nat Rev Cancer* **16,** 566–581 (2016).
7. Drent, E. *et al.* A Rational Strategy for Reducing On-Target Off-Tumor Effects of CD38-Chimeric Antigen Receptors by Affinity Optimization. *Mol. Ther.* **25,** 1946–1958 (2017).
8. Park, S. *et al.* Micromolar affinity CAR T cells to ICAM-1 achieves rapid tumor elimination while avoiding systemic toxicity. *Sci. Rep.* **7,** 1–15 (2017).
9. Ashley, C. E. *et al.* The targeted delivery of multicomponent cargos to cancer cells by nanoporous particle-supported lipid bilayers. *Nat. Mater.* **10,** 389–397 (2011).